Doctoral Thesis

Solution Self-Assembly of Block Copolymers into Inverse Bicontinuous Cubic Mesophases and Their Applications

Arah Cho

Department of Chemistry

Graduate School of UNIST

2019

Solution Self-Assembly of Block Copolymers into Inverse Bicontinuous Cubic Mesophases and Their Applications

Arah Cho

Department of Chemistry

Graduate School of UNIST

Solution Self-Assembly of Block Copolymers into Inverse Bicontinuous Cubic Mesophases and Their Applications

A thesis/dissertation
submitted to the Graduate School of UNIST
in partial fulfillment of the
requirements for the degree of
Doctor of Philosophy

Arah Cho

11/28/2018 of submission

Approved by

Advisor
Ja-Hyoung Ryu

Solution Self-Assembly of Block Copolymers into Inverse Bicontinuous Cubic Mesophases and Their Applications

Arah Cho

This certifies that the thesis/dissertation of Arah Cho is approved.

11/28/2018 of submission

Advisor: Prof. Ja-Hyoung Ryu

Kyoung Taek Kim: Thesis Committee Member #1

Sung You Hong: Thesis Committee Member #2

Bongsoo Kim: Thesis Committee Member #3

Min Sang Kwon: Thesis Committee Member #4

Abstract

The self-assembly of amphiphilic block copolymers (BCPs) into inverse bicontinuous cubic (IBC) mesophases in dilute solution is an emerging phenomenon that facilitates the direct synthesis of three-dimensionally well-defined periodic porous nanostructures composed of self-assembled bilayers of BCPs with minimal surfaces. We recently reported that diblock copolymers composed of branched hydrophilic blocks with peripheral poly(ethylene glycol) (PEG) chains and linear polystyrene (PS) blocks preferentially self-assemble into IBC mesophases in dilute solution. This process results in the formation of colloidal particles (polymer cubosomes) and large mesoporous films consisting of triply periodic minimal surfaces (TPMSs) of BCP bilayers.

With the aim of directly controlling molecular packing parameters (P), such as molecular interfacial areas (a_0) and the critical lengths of hydrophobic blocks (l_c), we synthesized amphiphilic block copolymers composed of branched polymer blocks in this study. The resulting branched−branched block copolymers (bb-BCPs) preferentially self-assemble into inverse bicontinuous cubic mesophases of BCP bilayers in dilute solution, resulting in the formation of colloidal polymer cubosomes.

In addition, we show that binary blends of BCPs self-assemble into desired nanostructures in solution by adjusting the compositions of the two BCPs associated with the smaller and larger packing parameters (P values). By modifying the P value of a binary BCP blend through compositional control, two BCPs that share repeating units in both polymer blocks coassemble into desired structures, ranging from spherical micelles to inverse cubic and hexagonal mesophases. We demonstrate that these BCP blends directly form complex periodic mesoporous structures of desired periodicity and pore size, and also provide nanostructures of unprecedented morphology by simple solution self-assembly without relying on the syntheses of correspondingly designed BCPs. These findings facilitate the design of BCPs that preferentially self-assemble into IBC structures with desired lattice and periodic structures in dilute solution. Our results contribute to expanding the availability of highly defined periodic nanostructures that are created by the simple solution self-assembly of BCPs, which are potentially valuable for applications such as separation and nanotemplating.

In addition, a variety of functional groups can be introduced into the polymer cubosome through the blending of polymers bearing desired functional groups. Using this method, we introduce amine functional groups into polymer cubosomes, after which Ni-NTA groups are introduced through post-modification. We show that the porous 3D structure of the polymer cubosomes bearing Ni-NTA functional groups can be used for the selective separation of histidine-tagged proteins by affinity chromatography.

Morphological control through blending mainly results in intermediate structures of blended polymers. However, when two polymers that differ in molecular weight by more than a certain amount are blended, unusual nonergodic structures, such as cylindrical micelles with junctions or colloidal particles of micellar aggregates, are observed.

Contents

List of Figures

Figure 2-5. Representative TEM images of self-assembled structures of PEG750$_3$-(*3,4*)-(PS$_n$)$_2$ at varying DP_n values of the PS chains. (a) flat lamella and polymer vesicles (n = 54, f_{PEG} = 20.0%); (b) polymer cubosomes (n = 68, f_{PEG} = 15.9%); (c) polymer hexasomes (n = 97, f_{PEG} = 11.2%). The insets are magnified views of the internal lattices (scale bars = 100 nm).

Figure 2-6. Simple phase diagram for solution self-assembly of bb-BCPs (1 wt% in dioxane) with an identical branched hydrophilic block (PEG750$_3$) and different numbers of PS chains of varying molecular weights in the hydrophobic block. (1: PEG750$_3$-PS$_n$, 2: PEG750$_3$-(*3,4*)-(PS$_n$)$_2$, 2': PEG750$_3$-(*3,5*)-(PS$_n$)$_2$, and 3: PEG750$_3$-(*3,4,5*)-(PS$_n$)$_3$). f_{PEG} is the ratio of the molecular weight of the PEG domain to that of the PS chain.

Figure 2-7. (a–d) TEM images of self-assembled structures of (a) PEG2000-PS$_{121}$ (f_{PEG} = 15.9 %), (b) PEG750$_3$-PS$_{120}$ (f_{PEG} = 18.0 %), (c) PEG750$_3$-(*3,4*)-(PS$_{60}$)$_2$ (f_{PEG} = 18.0 %), and (d) PEG750$_3$-(*3,4,5*)-(PS$_{40}$)$_3$ (f_{PEG} = 18.0 %). (e) A schematic representation of BCPs of different architectures at the fixed molecular weight and block ratio.

Figure 2-8. (a) SEM images showing the polymer cubosomes of PEG750$_3$-(*3,5*)-(PS$_{60}$)$_2$. The inset shows the surface morphology (scale bar = 100 nm). (b) SEM image of the internal IBC structures. (c) SAXS result obtained from dried polymer cubosomes indicating *Im3m* symmetry (a = 81.1 nm). (d−g) SEM images showing the P minimal surface (*Im3m*) viewed at the indicated directions.

Figure 2-9. (A and B) SEM image of the polymer cubosomes of (A) PEG750$_3$-(3,5)-(PS$_{60}$)$_2$ and (B) PEG750$_3$-(3,4)-(PS$_{60}$)$_2$. (C and D) Size distribution of polymer cubosomes of (C) PEG750$_3$-(3,5)-(PS$_{60}$)$_2$ (average = 10.3 μm) and (D) PEG750$_3$-(3,4)-(PS$_{60}$)$_2$ (average = 9.6 μm) obtained by SEM image analysis.

Figure 2-10. SAXS result of the polymer cubosomes of PEG750$_3$-(3,5)-(PS$_{65}$)$_2$ having mixed structures of Schwartz P and D surfaces (*Im3m* space group, lattice constant a = 42.5 nm, for *Pn3m* space group, a = 33.2 nm).

Figure 2-11. (a) SEM images showing the polymer cubosomes of PEG750$_3$-(*3,4*)-(PS$_{60}$)$_2$. The inset shows the surface morphology (scale bar = 100 nm). (b) A SEM image of the internal IBC structures. (c) SAXS result obtained from dried polymer cubosomes indicating *Pn3m* symmetry (a = 50.0 nm). (d–g) SEM images showing the D minimal surface (*Pn3m*) viewed at the indicated directions.

assembled structures.

Figure 3-2. Transition of morphology of the self-assembled structure of BCP blends. (a−h) Representative TEM images of the self-assembled structures of the BCP blends, $PEG550_3$-PS_{42}-$PEG550_3$-PS_{228} with varying compositions: (a) Spherical micelles ($PEG550_3$-PS_{42}: $PEG550_3$-PS_{228} = 100:0, w/w). (b) Cylindrical micelles (50:50). (c) Polymer vesicles (40:60). (d) Flat bilayers (25:75). (e) Sponge phase particles (20:80). (f) Polymer cubosomes of Schwarz P-surfaces (15:85). The inset shows a (100) plane of the P-surface (scale bar = 50 nm). (g) Polymer cubosomes of Schwarz D-surfaces (5:95). The inset shows a (100) of the D-surface (scale bar = 50 nm). (h) Polymer hexasomes (0:100). The inset shows a (110) plane of the HII phase (scale bar = 20 nm).

Figure 3-3. DLS results of micellar solution of $PEG550_3$-PS_{42}. (a) Size distributions and (b) autocorrelation functions of spherical micelle. The average diameters of $PEG550_3$-PS_{42} were 62.42 nm (dispersity 0.27).

Figure 3-4. Gel permeation chromatography (GPC) results of polymer blends of (a) $PEG550_3$-PS_{42} (M_n = 6800 g mol^{-1}, $Đ$ = 1.06) and $PEG550_3$-PS_{228} (M_n = 23000 g mol^{-1}, $Đ$ = 1.07); (b) $PEG550_3$-PS_{105} (M_n = 7700 g mol^{-1}, $Đ$ = 1.06) and $PEG550_3$-PS_{228} (M_n = 23000 g mol^{-1}, $Đ$ = 1.07). (m = $PEG550_3$-PS_{42}, micelle; v = $PEG550_3$-PS_{105}, vesicle; wt%).

Figure 3-5. SEM image of (a and b) polymer vesicles of the BCP blend of $PEG550_3$-PS_{42}–$PEG550_3$-PS_{228} (40:60, w/w) and (c and d) flat bilayers (25:75, w/w).

Figure 3-6. SEM and TEM images of irregular sponge (L_3) phase of the BCP blend of $PEG550_3$-PS_{42}–PEG 550_3-PS_{228} (20/80, w/w). (a) SEM image of internal structure of irregular sponge phase. TEM image of representative irregular sponge phase (b) and its internal structures (c and d).

Figure 3-7. Internal structures of polymer cubosomes and hexasomes of the BCP blends. (a−d) SEM images of the polymer cubosomes of the BCP blend of $PEG550_3$-PS_{42} and $PEG550_3$-PS_{228} (15:85, w/w), showing a Schwarz P-minimal surface of BCP bilayers viewed along the (b) [100], (c) [110], and (d) [211] directions. (e−h) SEM images of the polymer cubosomes of a $PEG550_3$-PS_{42}-$PEG550_3$-PS_{228} blend (5:95, w/w) showing a Schwarz D-minimal surface viewed along the (f) [100], (g) [110], and (h) [111] directions. (i−k) SEM images of the polymer hexasomes of $PEG550_3$-PS_{228} showing H_{II} phase. (l) SAXS result of the dried polymer cubosomes of a $PEG550_3$-PS_{42}-$PEG550_3$-PS_{228} (15:85, w/w) blend assigned to primitive cubic symmetry (*Im3m* space group, a = 60.4 nm). (m) SAXS result of the dried

polymer cubosomes of a $PEG550_3$-PS_{42}-$PEG550_3$-PS_{228} (5:95, w/w) blend assigned to double diamond symmetry (*Pn3m* space group, a = 42.8 nm). (n) SAXS result of the dried polymer hexasomes of $PEG550_3$-PS_{228} showing the H_{II} phase (*P6mm* space group, a = 30.2 nm).

Figure 3-8. Phase transition of inverse mesophases of block copolymer blends of $PEG550_3$-PS_{42} and PEG 550_3-PS_{228}. SEM image of (a and b) sponge phase particles, (c and d) polymer cubosomes with primitive cubic (*Im3m*) symmetry, and (e and f) polymer cubosomes with double diamond (*Pn3m*) symmetry.

Figure 3-9. (a) Schematic diagram illustrating another mix-and-match process between $PEG550_3$-PS_{56} and PEG 550_3-PS_{228}. (b–h) Representative TEM images of the self-assembled structures of the BCP blends, $PEG550_3$-PS_{56}–$PEG550_3$-PS_{228} with varying compositions. (b) cylindrical micelles ($PEG550_3$-PS_{56}–$PEG550_3$-PS_{228} = 100/0, w/w); (c) polymer vesicles (60/40, w/w); (d) flat bilayers (40/60, w/w); (e) sponge phase particles (30/70, w/w); (f) polymer cubosomes of Schwarz P-surfaces (20/80, w/w); (g) polymer cubosomes of Schwarz D-surfaces (10/90, w/w); (h) polymer hexasomes (0/100, w/w). The scale bars in the insets are 50 nm.

Figure 3-10. SAXS result of (a) polymer cubosomes of the BCP blend of $PEG550_3$-PS_{56}–$PEG550_3$-PS_{228} (20:80, w/w). The peaks were assigned to *Im3m* space group (a = 63.8 nm) and (b) polymer cubosomes of the BCP blend with a composition of 10:90 (w/w). The peaks were assigned to *Pn3m* space group (a = 47.0 nm).

Figure 3-11. Representative SEM images of polymer cubosomes of BCP blends of $PEG550_3$-PS_{105} and $PEG550_3$-PS_{228} with the ratio of (a and b) 15/85, w/w; (c and d) 23/77, w/w; and (e and f) 27/73, w/w.

Figure 3-12. Control of the periodicity and pore size of water channel networks among polymer cubosomes of BCP blends. (a−c) SEM images showing the (111) plane of the lattice of the Schwarz D-surface of polymer cubosomes of BCP blends of $PEG550_3$-PS_{105}-$PEG550_3$-PS_{228} with the composition of (a) 15:85, w/w, pore distance (d) = 36.4 nm; (b) 23:77, w/w, d = 51.0 nm; and (c) 27:73, w/w, d = 62.8 nm. (d) SAXS results of these polymer cubosomes showing double diamond symmetry (*Pn3m* space group). The a value of the polymer cubosomes was gradually increased from 32.6 nm for the blend of $PEG550_3$-PS_{105}-$PEG550_3$-PS_{228} with the composition of 15:85, w/w, to 58.4 nm with the composition of 27:73, w/w. (e) The BJH pore size distributions of the polymer cubosomes of the blends of $PEG550_3$-PS_{105}-$PEG550_3$-PS_{228} with different compositions. (f) SEM image of the silica replica of the internal water channels of the polymer cubosomes of the BCP blend of $PEG550_3$-PS_{105}-$PEG550_3$-

PS_{228} (23:77, w/w). (g) TEM image of the silica replica shows two noninterpenetrating single diamond networks (*Fd3m* space group), which are marked by red and blue arrows, respectively. The distance between 4-folded junctions of the diamond network was 43.5 nm (white line).

Figure 3-13. TEM images of the polymer cubosomes of BCP blends of $PEG550_3$-PS_{105} and $PEG550_3$-PS_{228} with a composition of (a) 23/77, w/w; (b) 15/85, w/w; (c) 23/77, w/w; (d) 27/73, w/w. (b–c) Arrows indicate the thickness of the bilayer shells of the polymer cubosomes (16.7 nm in b, 16.3 nm in c, 16.6 nm in d).

Figure 3-14. N_2 adsorption–desorption isotherms measured at 77 K of the polymer cubosomes of the BCP blends of $PEG550_3$-PS_{105}–$PEG550_3$-PS_{228} with a composition of (a) 15/85 (w/w); (b) 20/80 (w/w); (c) 23/77 (w/w); (d) 25/75 (w/w); (e) 27/73 (w/w). The BET surface area and pore volume are (a) 130 $m^2\ g^{-1}$ / 0.52 $cm^3\ g^{-1}$, (b) 138 $m^2\ g^{-1}$ / 0.64 $cm^3\ g^{-1}$ (c) 138 $m^2\ g^{-1}$, 0.66 $cm^3\ g^{-1}$, (d) 137 $m^2\ g^{-1}$, 0.75 $cm^3\ g^{-1}$, and (e) 136 $m^2\ g^{-1}$, 0.74 $cm^3\ g^{-1}$.

Figure 3-15. (a–c) SEM images of the silica replica of the polymer cubosomes of the BCP blend of $PEG550_3$-PS_{105} and $PEG550_3$-PS_{228} (23:77 w/w). The silica replica was synthesized by sol-gel reaction of TEOS under acidic condition using the polymer cubosome as a template.

Figure 3-16. Hexasome flowers of the BCP blends. (a, b) Low magnification (a) SEM and (b) TEM image of the hexasome flowers of the BCP blends of NH_2-PEG2000-PS_{184}-$PEG550_3$-PS_{251} at the composition of 30:70 (w/w). (c, d) High magnification images showed the vesicular petals tethered to the hexasome core. (e) TEM image of the hexasome flower of NH_2-PEG2000-PS_{184}-$PEG550_3$-PS_{251} (50:50, w/w) showing the inverse hexagonal phase of the core. (f) SEM image of collapsed silica cylinders synthesized by sol−gel reaction of TEOS using the hexasome flowers as templates, followed by removal of polymer templates. (g) SIM image of the rhodamine-labeled hexasome flowers of NH_2-PEG2000-PS_{184} and $PEG550_3$-PS_{251} at the composition of 50:50 (w/w). Surface amino groups were labeled with rhodamine−N-hydroxysuccinic anhydride. (h) Cross-sectional CLSM images of the rhodamine-labeled hexasome flower captured at different focal planes show the accessibility of the core.

Figure 3-17. (a and b) TEM images of the hexasome flower of the BCP blend of NH_2-PEG2000-PS_{184}–$PEG550_3$-PS_{251} (50/50, w/w). (c and d) Silica replica synthesized by sol-gel reaction of tetraethoxysilicate (TEOS) using the hexasome flower as a template. Silica cylinders were created from the crosslinking of TEOS within the hexagonally packed cylindrical channels within the hexasome flower. D shows the collapsed silica cylinders after removing the hexasome flower template in THF.

Figure 4-5. TEM images of fragments from BCP blends of $PEG2000_3$-PS_{2030}/$PEG1000_3$-*(3,4,5)*-$(PS_{54})_3$ with composition of (A) 80/20 w/w, (B) 78/22 w/w, (C) 76/24 w/w, (D) 74/26 w/w, (E) 72/28 w/w.

Figure 4-6. TEM images of self-assembled structures of BCP blends (A-D) $PEG2000_3$-PS_{2030}/ $PEG1000_3$- *(3,4,5)* - $(PS_{54})_3$ with varying composition, (A) bicontinuous structures ($PEG2000_3$-PS_{2030}: $PEG1000_3$- *(3,4,5)* - $(PS_{54})_3$ = 95:5), (B) cylindrical micelle aggregates ($PEG2000_3$-PS_{2030}: $PEG1000_3$- *(3,4,5)* - $(PS_{54})_3$ = 80:20), (C) cylindrical micelles ($PEG2000_3$-PS_{2030}: $PEG1000_3$- *(3,4,5)* - $(PS_{54})_3$ = 75:25), (D) spherical micelles ($PEG2000_3$-PS_{2030}: $PEG1000_3$- *(3,4,5)* - $(PS_{54})_3$ = 70:30), (E-H) $PEG2000_3$-PS_{2030}: $PEG1000_3$-PS_{118} with varying composition, (E) bicontinuous structures ($PEG2000_3$-PS_{2030}: $PEG1000_3$-PS_{118} = 95:5), (F) cylindrical micelle aggregates ($PEG2000_3$-PS_{2030}: : $PEG1000_3$-PS_{118} = 90:10), (G) cylindrical micelles and vesicles ($PEG2000_3$-PS_{2030}: $PEG1000_3$-PS_{118} = 75:25), (H) vesicles ($PEG2000_3$-PS_{2030}: $PEG1000_3$-PS_{118} = 50:50).

Figure 5-1. (a and b) Low magnification SEM images showing the polymer cubosomes of (a) $PEG750_3$-(3,4)-$(PS_{60})_2$ and (b) the BCP blend of $PEG750_3$-*(3,4)*-$(PS_{60})_2$ and NH_2-PEG2000-PS_{180} (9:1 w/w). (c) SAXS results showing the phase transition from the D surface of $PEG750_3$-*(3,4)*-$(PS_{60})_2$ (*Pn3m*, a =50.0 nm) to the P surface of the BCP blend (*Im3m*, a = 71.8 nm). (d) Distribution of the diameters of polymer cubosomes of $PEG750_3$-*(3,4)*-$(PS_{60})_2$ (blue bars, average = 11 μm) and the BCP blend (red bars, average = 6 μm).

Figure 5-2. (a and b) 3-D reconstructed images of CLSM of (a)the polymer cubosomes of the BCP blend with the surface amino groups labeled by fluorescamine and (b) His-tagged GFP complexed Ni-NTA functionalized polymer cubosomes. (c) CLSM images of His-tagged GFP on the polymer cubosomes at different focal depths (each step: 0.8 μm, scale bar = 10 μm).

Figure 5-3. CLSM images of the polymer cubosomes after removing GFP different focal depths (each step: 2 μm, scale bar = 10 μm). (a-c) Fluorescence images and (d-f) merged images.

List of Tables

List of Schemes

Nomenclature

3D	Three-dimensional
a	Lattice constant
a_0	Molecular area
ATRP	Atom transfer radical polymerization
bb-BCP	Branched-branched block copolymer
BCP	Block copolymer
BET	Brunauer-Emmett-Teller
BJH	Barrett-Joyner Halenda
CLSM	Confocal Laser Scanning Microscopy
D	Double diamond
$Đ$	Polydispersity index
DLS	Dynamic light scattering
DMF	Dimethylforamide
DMSO	Dimethyl sulfoxide
DOPE	Dioleylphosphatidylethanolamine
DP_n	Degree of polymerization
EDTA	Ethylenediaminetetraacetic acid
EM	Electron microscopy
f_{PEG}	The ratio of the molecular weight of the PEG block to that of the PS block
G	Gyroid
GFP	Green fluorescent protein
GPC	Gel permeation chromatography
H_{II}	Inverse hexagonal
IBC	Inverse bicontinuous cubic
IMAC	Immobilized metal affinity chromatography
IPECs	Interpolyelectrolyte complexes
l_c	critical length of the hydrophobic chain
MALDI-TOF-MS	Matrix-assisted laser desorption ionization time-of-flight mass spectroscopy
MC	Dichloromethane
MCAC	Metal chelate affinity chromatography
M_n	Number-averaage molecular weight
NMR	Nuclear magnetic resonance
NTA	Nitrotriacetic acid
P	Primitive cubic
P	Packing parameter
PAA	poly(acrylic acid)
PB	poly(butadiene)
PDMAEMA	poly(2-(dimethylamino)ethyl methacrylate)
PEG	poly(ethylene glycol)
PISA	Polymerization induced self-assembly

PODMA	poly(octadecyl methacrylate)
PS	Polystyrene
SAXS	Small-angle X-ray scattering
SEM	Scanning electron microscopy
SIM	Structured illumination microscopy
TEM	Transmission electron microscopy
THF	Tetrahydrofuran
TPMS	Triply periodic minimal surfaces
V	Volume of the hydrophobic domain

Chapter 1. Introduction

1.1 Overview

The formation of regular nanostructures using the self-assembly of amphiphiles, such as surfactants and lipids, has been studied extensively. Based on the theory of packing parameters summarized by Israelachvili in 1976, [1,2] studies have been conducted to control desired nanostructures by controlling the area of the hydrophilic blocks (a_0), the volume of the hydrophobic blocks (v), and the critical length (l_c) of the amphiphiles.[3-5] These nanostructures are applied in various fields according to their structures, but nanostructures of such small molecules are limited by their weak physical properties and small sizes. In recent years, large nanostructures with more robust and versatile functionality have been reported, which use self-assembly of similar amphiphilic block copolymers to overcome these limitations.[6,7]

Although the formation of various types of nanostructures has been reported by controlling the composition or architecture of the polymers, precise control of structure and size and methods for their mass production are required for their application in various fields.[8-11] These examples illustrate blending, [12] solubility control, [13] or new polymer synthesis methods,[14] but there remains a need for more precise control of the nanostructures.

Among these nanostructures, bicontinuous structures with large packing parameters (>1) can be applied in various fields, such as delivery vehicles, water purification, reactors, and separations as a 3D porous material. Previous studies have shown that hierarchical bicontinuous structures are formed via the self-assembly of poly(ethylene glycol)-*b*-polystyrene (PEG-*b*-PS) with branched hydrophilic groups.[15] However, this structure can only be applied to the self-assembly of polymers with a very limited range of molecular weights. Therefore, it is necessary to study the precise control of the mesostructures and particle sizes of bicontinuous structures by broadening their range and sufficiently increasing their reproducibility.

1.2 Synthesis of well-defined block copolymers

Atom transfer radical polymerization (ATRP) is a versatile and facile synthetic tool for preparing block copolymers with precisely controlled molecular weights, relatively low dispersities, compositions (block, graft, alternating, and gradient copolymers), architectures (stars, combs, cycles, brushes, and regular networks), and diverse functionalities.[16] (Figure 1-1)

By controlling the equilibrium between the propagating radical and the dormant species, ATRP maintains a constant low concentration of the propagating radical, with molecular weight increasing at a constant rate such that a polymer with a narrow molecular-weight distribution is formed. (Figure 1-2)

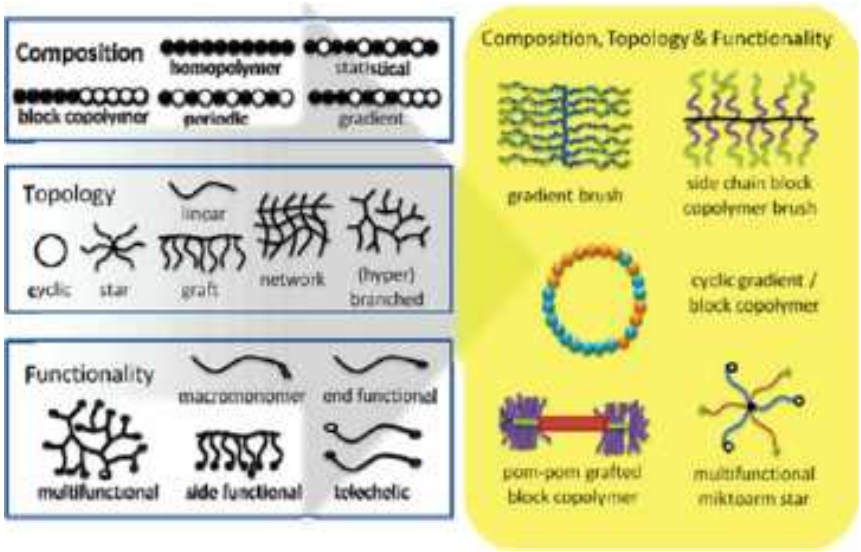

Figure 1-1. Synthetic method of block copolymers with complex architecture based on controlled radical polymerization.[16]

Reaction-equilibrium rates vary, depending on the type of ligand, initiator, and monomer, and can be adjusted as needed. In addition, chain extension is possible by maintaining end functionality even after completion of the reaction, and a variety of functional groups can be introduced through substitution reactions.

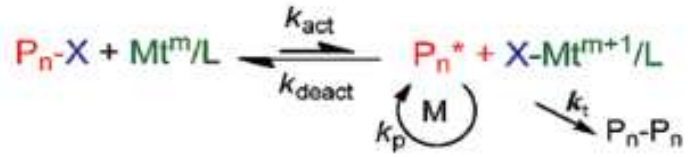

Figure 1-2. Atom transfer radical polymerization (ATRP)[16]

However, ATRP has some limitations associated with the use of copper catalysts; commercialization opportunities are also limited due to problems associated with the complete removal of the metal catalyst from the product. In addition, problems associated with metal-catalyst oxidation has led to the limited use of ATRP in electronics and biological fields; however, some studies aimed at reducing the amount of catalyst to 100 ppm or less, or using other catalysts, such as organic catalysts, have recently been conducted.[16,17]

Studies on the ATRP synthesis and behavior of precisely controlled macromolecules with various

composition and architectures are actively underway. For example, Kim and coworkers synthesized amphiphilic block copolymers with PS hydrophobic blocks through ATRP using an initiator with a dendrimer-type PEG block. These amphiphilic block copolymers assembled into hierarchical 3D porous nanostructures in dilute solution. In addition, a variety of other nanostructures were formed by controlling the length of the PS block.[15]

1.3 Self-assembly of block copolymers in solution

During bulk assembly, the phase separation of different blocks of a block copolymer induces the formation of nanostructures. [8] On the other hand, during solution self-assembly, hydrophobic interactions between a selective solvent and hydrophobic blocks induce the formation of nanostructures as the proportion of the selective solvent in the polymer solution increases. Therefore, more-complex and more-varied structures are observed during solution self-assembly. [8,9] These self-assembled structures are determined by the packing parameter (P, defined as $P=v/a_0l$, where V is the volume of the hydrophobic domains, a_0 is the molecular area per amphiphile, and l is the critical length of the hydrophobic chain). Spherical micelles are formed when $P < 1/3$, while cylindrical micelles are formed when $1/3 < P < 1/2$, vesicles are formed when $1/2 < P < 1$, lamella are formed at $P = 1$, and inverted structures are observed when $P > 1$. (Figure 1-3)

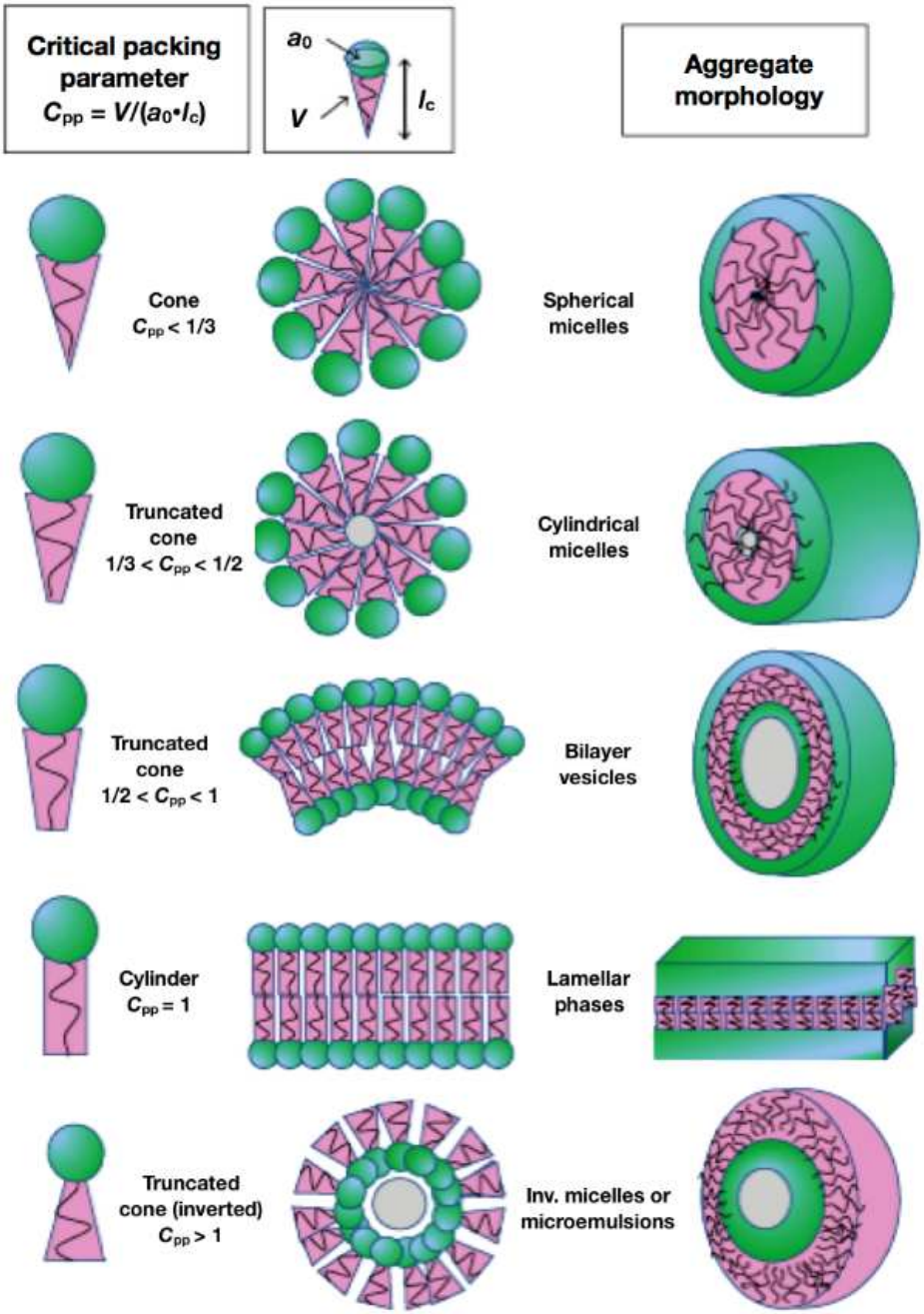

Figure 1-3. A summary of the packing shape of amphiphiles and its aggregated structure that can be predicted from critical packing parameter.[53]

Eisenberg and coworkers used asymmetric PS-*b*-PAA block copolymers with larger hydrophobic blocks than hydrophilic blocks, and observed morphological block-copolymer transitions resulting from changes in packing parameter controlled by the block ratio. [8,18] (Figure 1-4) A variety of morphologies were obtained with increasing hydrophobic-block length, such as simple spherical micelles, rods (cylindrical or wormlike micelles), bilayers (lamella and vesicles), and inverted structures (hexagonally packed hollow hoops and large compound micelles), which indicate that the packing parameter increases with hydrophobic-block length.

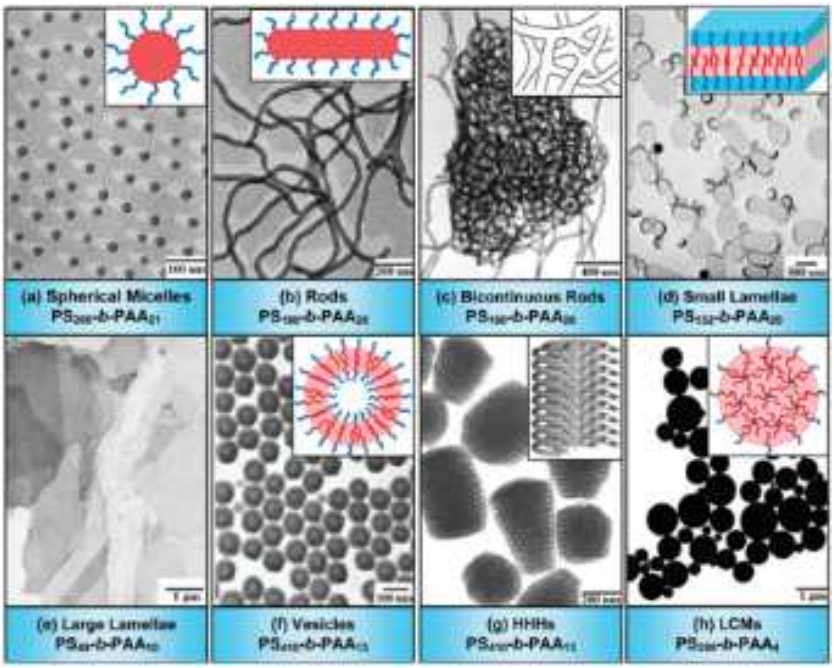

Figure 1-4. Transmission electron microscopy (TEM) images of various morphologies formed from PS_m-*b*-PAA_n having various composition.[8]

Controlled radical polymerizations in aqueous solution using macro-initiators composed of water-soluble polymer blocks were recently reported by Armes and coworker.[14] Aggregation resulting from decreasing solubility was observed with increasing molecular weight of the hydrophobic block. A variety of structures and intermediates involved in morphological transitions were observed with increasing block ratio. Such a polymerization induced self-assembly (PISA) has the advantage of enabling trace of a desired structure and mass-production.

1.4 Inverse bicontinuous structures

When the packing parameter (*P*) is greater than unity, amphiphiles form cubic lipid mesophases in solution, which are usually observed in highly ordered 3D periodic structures in nature, such as the endoplasmic reticulum, butterfly-wing scales, and the exoskeletons of insects.

Over the past few decades, complex topologies, such as mathematical minimal surfaces, have been studied along with simple structures, such as layers, tubes, and spheres, through the self-assembly of monoolein in solution.[3] In the case of wedge-shaped molecules such as DOPE (dioleyl phosphatidylethanolamine), negative-inverse or type-2 micelles, with curvatures toward the water region, are formed.

A bicontinuous cubic phase, also referred to as a "minimal surface", has intermediate curvature between that of a flat lamellar phase and a cylindrical hexagonal phase. Minimal surfaces have infinitely periodic structures with zero mean curvatures and negative Gaussian curvatures at any position.[3, 21-24](Figure 1-5)

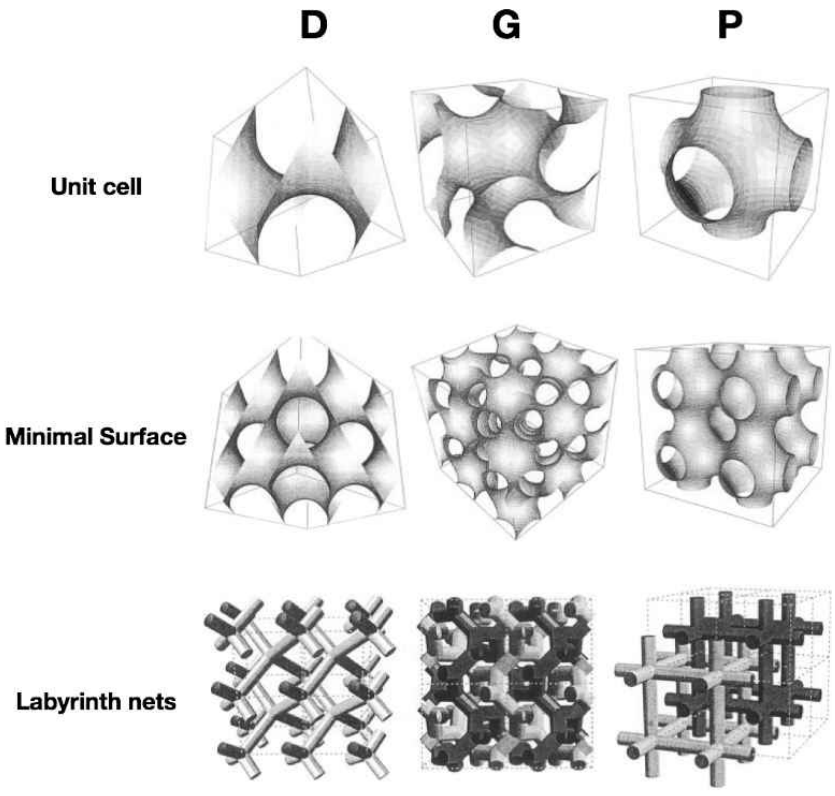

Figure 1-5. Representative triply periodic minimal surfaces (TPMS) – D, G, and P.[24]

Ever since the study of a double-diamond phase, which is a triply periodic minimal surfaces (TPMS), by Schwarz in 1865,[25,26] a variety of TPMS structures have been discovered and studied. Recently, the synthesis of TPMS structures and their structural analyses using tools such as small-angle X-ray scattering (SAXS) and electron microscopy (EM) have been undertaken. Martiel and coworkers[27] examined the internal network of *Im3m* by observing the structures of lipid cubosomes by cryo-EM. While these porous structures can be used in many biological applications, studies that synthesize inverse bicontinuous structures similar to lipids using amphiphilic block copolymers are underway, because of their low stabilities and small pore sizes.

Kim and coworkers[15] reported the synthesis of highly ordered polymer cubosomes by solution-phase self-assembly of PEG-*b*-PS with branched PEG blocks. These polymer cubosomes can be used as biochemical reactors, and templates, among others, through the introduction of functional groups by template polymerization. (Figure 1-6)

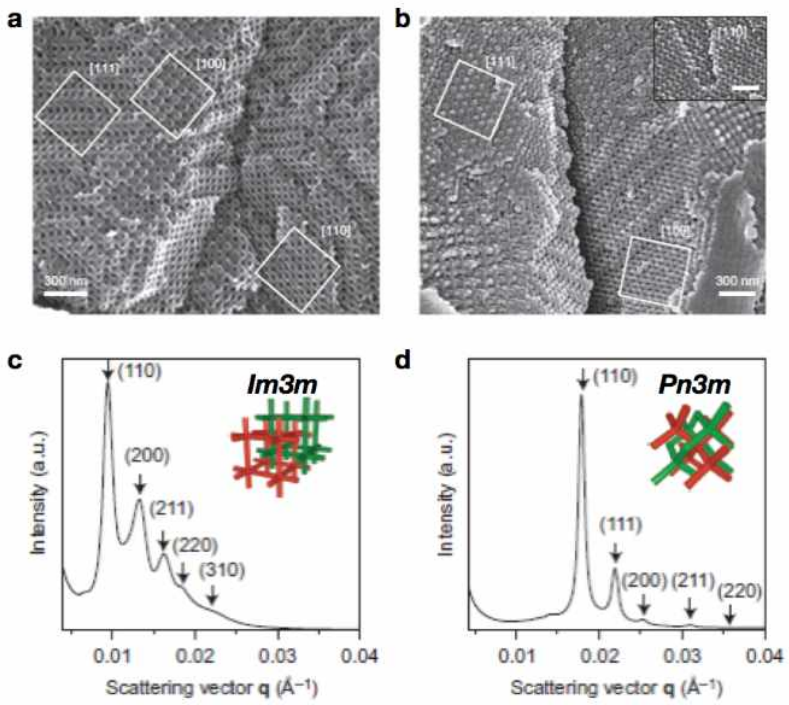

Figure 1-6. Structural analysis of (a,c) primitive cubic (*Im3m*) and (b,d) double diamond (*Pn3m*).[13]

Peinemann and coworkers[28] showed that microsphere particles containing highly porous internal structures can be synthesized by the self-assembly of PS-*b*-PAA. The internal porosities of these particles can be controlled by adjusting the pH; these structures enable high sorption capacities and the sustained release of molecules such as drugs, proteins, and peptides.

To date, studies on the synthesis of inverse bicontinuous structures using polymers with a variety of compositions and architectures have been reported, but further studies are needed in order to understand how to achieve the desired microstructure and lattice spacing.

1.5 Controlling the self-assembly of block copolymers through chemical architectures

The properties of a polymer depend on its composition as well as topology,[29] which also influence the self-assembly of a block polymer.[30,31] In early studies, simple structures, such as spheres and vesicles, were studied through morphological changes induced by compositional control or control of the block ratio of a block copolymer.[6-9] Recently, more-complex and novel structures have been studied by controlling block-copolymer topology with a variety of synthetic tools.[10,11,31-35]

Sommerdijk and coworker[32,33]s observed internally microphase-separated bicontinuous aggregates through the solution self-assembly of a polynorborene-based block copolymer with comb-like segments of oligo(ethylene glycol methyl ether) and a tri-peptide, namely glycine-leucine-phenylalanine. The structures of the branched water-channel networks inside the colloidal particles were determined by Cryo-ET (cryo-electron tomography). (Figure 1-7)

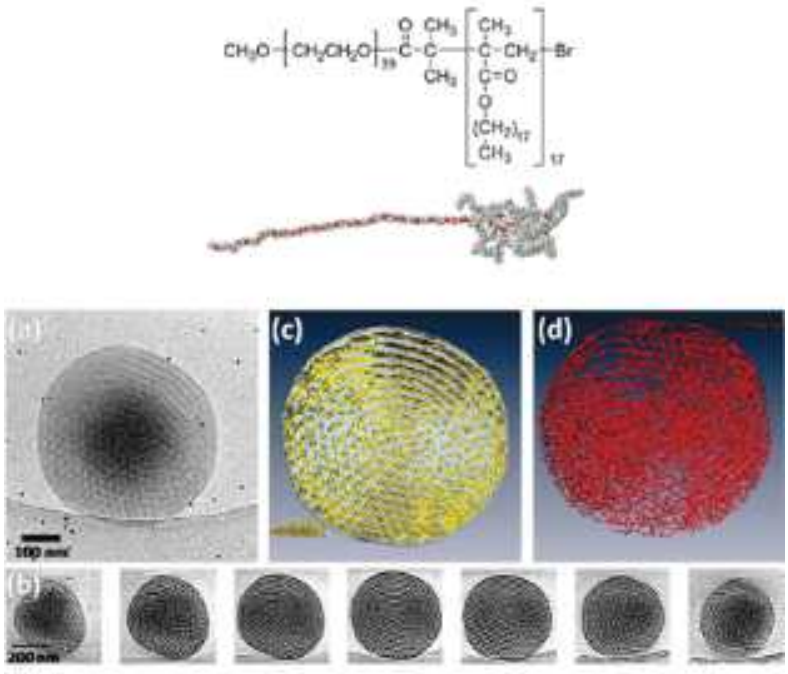

Figure 1-7. Chemical structure and cryoTEM analysis of PEG_{39}-*b*-$PODMA_{17}$ aggregate.

Percec and coworkers[34] synthesized amphiphilic Janus dendrimers with tailored hydrophilic and hydrophobic blocks using facile coupling reactions. The morphological screening of Janus dendrimers from solution self-assembly revealed various structures, including polygonal-dendrimersomal and bicontinuous-cubic structures, which were not previously observed. In addition, systematic tuning of molecular structure and the self-assembled architecture was demonstrated to be possible using this modular-synthesis strategy. (Figure 1-8)

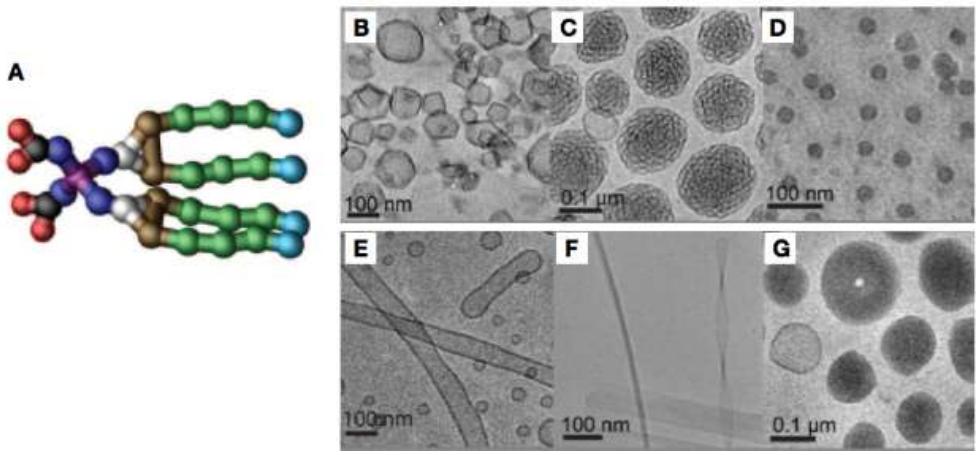

Figure 1-8. Molecular model of Janus dendrimer and cryoTEM images of (B) polygonal dendrimersomes, (C) bicontinuous cubic particles, (D) micelles, (E) tubular dendrimersomes, (F) rodlike, ribbon and helical micelles, (G) disklike micelles and toroids.[34]

Hillmyer and Lodge[35] observed the solution self-assembly of triblock copolymers composed of one hydrophilic block and two different hydrophobic blocks that are thermodynamically poorly compatible. In this study, the high thermodynamic incompatibility between two hydrophobic blocks with high Flory-Huggins interaction parameters led to the microsegregation of the micellar hydrophobic cores, which facilitated the observation of more-complex structures. More-complex interval morphologies were observed through the control of the block ratio of a block copolymer or its topology, including mictoarm-star-block, star, and graft-block copolymers.

Yin and coworker[30] compared different types of block copolymer with the same chain length but different chain architectures (cyclic AB and linear ABA). In this study, the self-assembled aggregate of a cyclic block copolymer has a compact and denser hydrophobic core, and is also more thermally stable than that formed from a linear polymer because of the entropic penalty associated with chain folding. The results demonstrate that the block-copolymer architecture plays an important role in self-assembly behavior.

The self-assembly of new polymers with controlled heterogeneity (MWD, topology, functionality, and composition) can contribute to the development of advanced nanostructured functional materials.

1.6 Controlling the self-assembly of block copolymers through polymer blending

Adjusting the block ratio is a method used to mainly control the morphology of a block copolymer; however, this method requires precise molecular weight control, which is often difficult in practice. In particular, to repeatedly synthesize a polymer until the desired molecular weight is obtained is troublesome.

One way to overcome this limitation is to assemble two or more polymers by mixing.[12, 36-39] The structures obtained by the blending method are hybrids of the polymers used, and a variety of nanostructures can be obtained by controlling the stoichiometric ratios of the polymers. In addition, the desired functionality can also easily be imparted to the nanostructure.

These blending methods are roughly classified into two types, namely pre-mixing and post-mixing. In the case of the pre-mixing method, in which the polymers are sufficiently mixed prior to the self-assembly process, an intermediate morphology, which is the average of each polymer, is observed. On the other hand, the post-mixing method, in which polymer solutions are mixed following the self-assembly process, affords interesting structures resulting from thermodynamic equilibria.

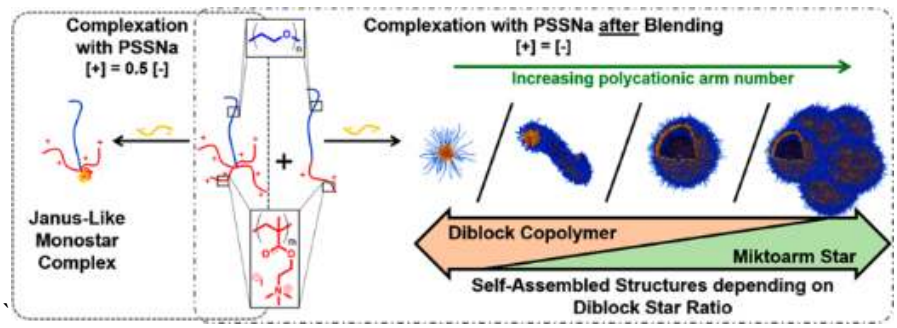

Figure 1-9. Schematic illustration of blending PEO-*b*-*q*PDMAEMA diblock copolymer and a PEO-(*q*PDMAEMA)$_{4.3}$ miktoarm star polymer.[12]

O'Reilly and coworkers[36] reported that the blending of two polymers with the same block length but with random hydrophobic monomer compositions formed micelles with properties that were hybrids of those of the two polymers. In addition, Plamper, Pergushov and coworkers[12] reported a versatile system for the formation of various types of Janus-like monostar interpolyelectrolyte complexes (IPECs) through the blending of linear diblock copolymers and mictoarm star polymers that can adjust their

average arm numbers. These simple blending protocols have shown that the characteristics of blended micelles can be tuned without requiring a synthesis approach. (Figure 1-9)

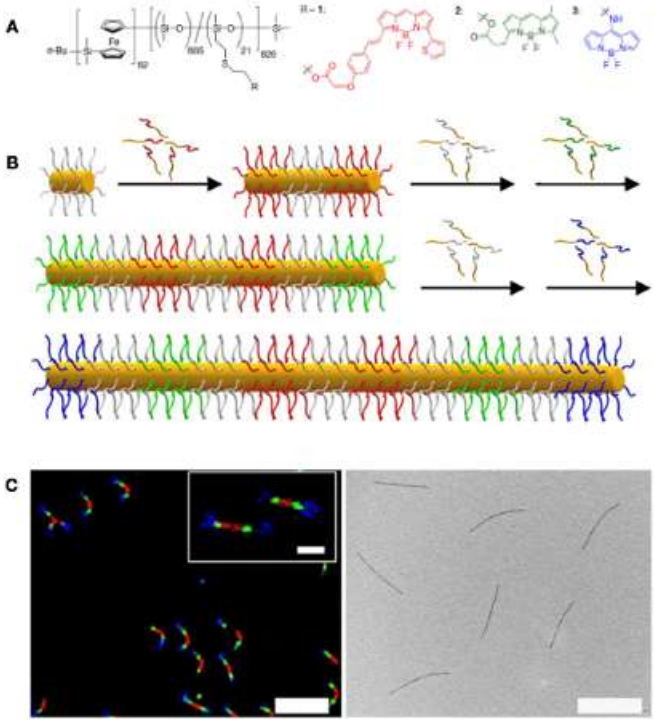

Figure 1-10. Fluorescent multiblock micelles. (A) structure of fluorescent BCPs, (B) schematic illustration of crystalline driven self-assembly of fluorescent BCPs (C) laser scanning confocal microscopy (LSCM) image of fluorescent multiblock micelles.[50]

In some studies, polymer chains were impossible to rearrange due to "frozen" amphiphilic-block-copolymer self-assemblies; consequently, unlike with the pre-mixing method, no structural changes are observed using the post-mixing method. However, Manners, Winnik, and coworkers[39, 50] proposed a new blending method for the synthesis of novel triblock co-micelles through the post-mixing of crystalline block-containing polymers. When the same block copolymer, or a different block copolymer, in a common solvent is added to a solution of pre-existing short cylindrical micelles that act as "seeds", continuous growth occurs from the seed through the epitaxial crystallization of the core-forming blocks. (Figure 1-10) Similarly, Zhu[37] and coworker observed novel mesh-like vesicles through the gradual addition of another type of block copolymer to a pre-generated micellar solution. This represents a post-mixing method for the preparation of flexible macromolecules with no crystalline coil blocks, which is the result of the kinetic trapping of intermediate micellar morphologies that can be adjusted to control

micellar structure and morphology.

Polymer self-assembly through the blending method allows the polymer structure to easily be adjusted without the hassle of new-polymer synthesis, while nanostructures with different properties, in whole or in part, can also be produced.

1.7 Nonergodic structures from binary blended systems with high molecular weight differences

Amphiphilic block copolymers are analogs of surfactants or lipids with large molecular weights. The slow chain dynamics and large chain lengths of these amphiphilic block copolymers affect and complicate micellization. Bates and coworker[40] observed a complicated cylindrical micelle structure with a Y-junction and a three-dimensional network, properties which have not been commonly found in block copolymers of PB-b-PEO with the above critical molecular weights. This is presumably due to the kinetic issue of the molecular weight of the polymer. (Figure 1-11)

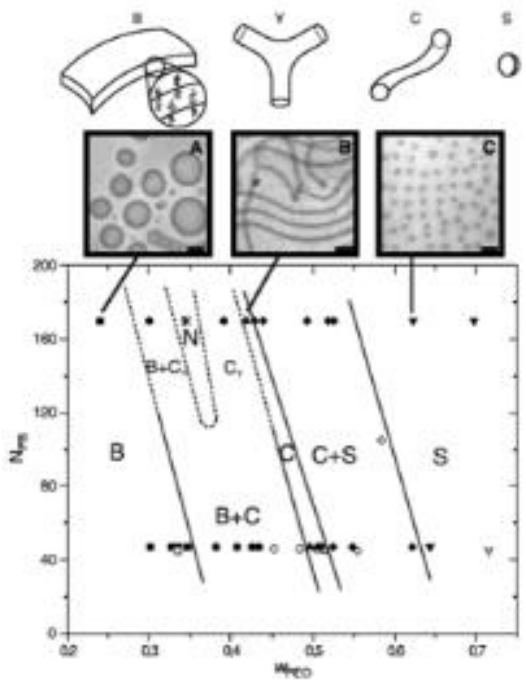

Figure 1-11. Mophology diagram for PB-PEO in water (1 wt%) as a function of molecular size and composition. B:bilayer,Y:Y-junctions, C:cylinder, S:spheres.[40]

These complex micellar structures can also be observed with molecular architecture control achieved via synthesis. Complex structures like multicompartment micelles were obtained from BCPs with complex structures, such as terpolymer and star terpolymer. For example, Hilmyer and Lodge[34,51] have

reported various complex micellar structures obtained by microphase separation through solution self-assembly of a triblock terpolymer with one hydrophilic block (O) and two hydrophobic blocks (E, F) with different solubilities. These multicompartment micelles can be morphologically controlled by controlling the length of each block, the architecture of the polymer, and the binary mixture system between the two polymers with different phobic blocks.

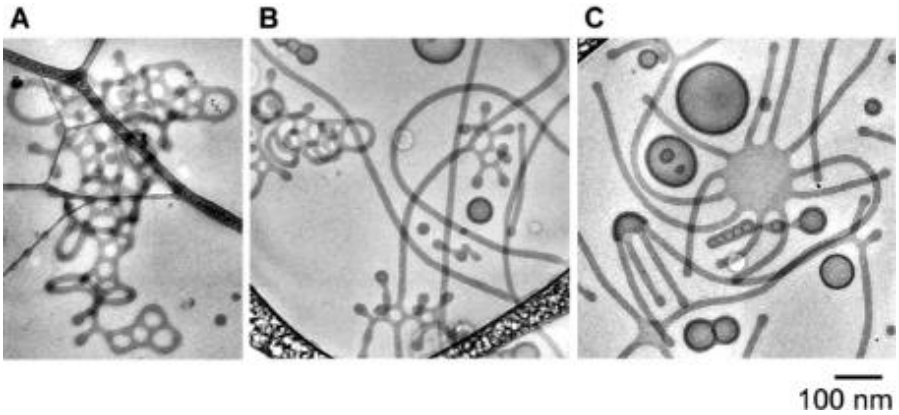

Figure 1-12. Cryo-TEM images of BCP blendingwith identical compositions (w_{PEO}=0.34); the molecular weight distribution broadens from A to B to C, (A,B) network, (C) vesicle, wormlike micelles, octopi.[41]

However, syntheses of complicated micelles with molecular weight control and architecture control are very limited and cumbersome. Bates and coworkers[41] used the binary blending method to solve these problems. By blending the two polymers of which average PEG franction (f_{PEG}) is fit to the target fraction (f_{peg}), the network micelles were observed without the hassle of synthesis. Further, with increasing molecular weight difference of the blending polymers by controlling the polydispersity, various structures were observed, and an interesting structure was also found. (Figure 1-12) Similarly, Danino, Dan, and coworkers[42] observed topological defect morphology changes in micelles with energetic penalties due to curvature changes with surfactants having relatively small molecular weights. The diverse topology of micelles plays an important role in bioscience and industry, including drug delivery (loading and delivery), catalysis, and cosmetics. Thus, controlling the size, shape, and structure of micelles is important for purposefully determining their properties.

1.8 Protein purification using affinity chromatography: Ni-NTA

Proteins vary in size, shape and properties, therefore, not all proteins can be purified in the same way. Proteins can be separated by exploiting their unique properties, and there are two main methods for their separation; they are based on protein size (electrophoresis, centrifugation, and gel-filtration chromatography) and properties (ion-exchange chromatography, affinity chromatography).[43]

The importance of affinity chromatography has been increasing since the 1980s, due to the development of recombinant DNA technology that can impart proteins with specific properties. Affinity chromatography is a method in which ligands are immobilized on an insoluble substrate, such as a resin or agarose gel; only specific proteins that have selective affinity for the ligand are separated through substrate binding as a mixture of proteins passes.[44,45,52] Typically, supramolecular interactions exist between a histidine tag and nickel-nitrotriacetic acid (NTA), which forms the basis of immobilized metal affinity chromatography (IMAC). NTA is a tetradentate ligand that binds divalent metal ions, such as Ni, Co, Cu, and Cu, with histidine binding to the two remaining binding sites. After protein separation, only proteins bound to the substrate can be obtained following treatment with a chelating (EDTA) or competitive (imidazole) agent.[46]

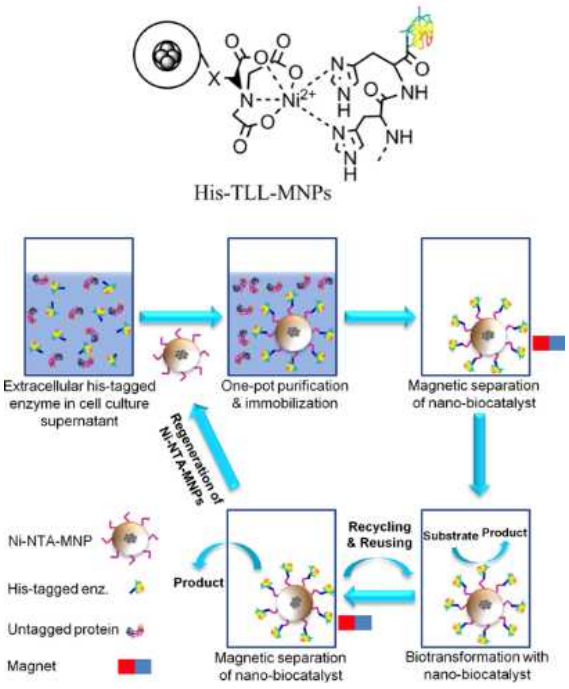

Figure 1-13. Illustration of immobilization of His-tagged enzyme directly from cell culture supernatant on magnetic nanoparticles, biotransformation with and recycling of the nanobiocatalyst, and regeneration of magnetic nanoparticles from the use catalyst.[52]

Ever since Porath and coworkers[47] demonstrated the selective separation of histidine-tagged proteins using agarose gels with metal ions, many studies have been carried out with the aim of improving efficiency. Various types of substrate have been proposed for selective immobilization, high loading capacity, and ease of separation, such as beads, nanoparticles, and glass. (Figure 1-13) For example, Xu and coworkers[48] synthesized magnetic nanoparticles with Ni-NTA on their surfaces to provide a large surface area and a method for the easy and hassle-free separation of proteins from cell debris. In addition, Martin and coworker[49] proposed a triazacyclononane (tacn)-ring-type Acbztacn (1-acetato-4-benzyl-triazacyclononane) ligand to reduce the limitations of NTA/metal/histidine-like metal leaching and protein dissociation. Ackztacn ligands stabilize ligand-metal interactions by the macrocyclic effect of the tacn ring, thereby reducing the complexities associated with metal leaching. (Figure 1-14) In a similar way, Zhao and coworker synthesized purification materials with high binding capacities by increasing the density of the bound nickel through the use of hollow nickel silicate nanospheres.

Inverse bicontinuous colloidal nanoparticles with such affinity moieties can be used as substrates for novel affinity-chromatography materials with wide hole sizes and surface areas, as well as physical stabilities.

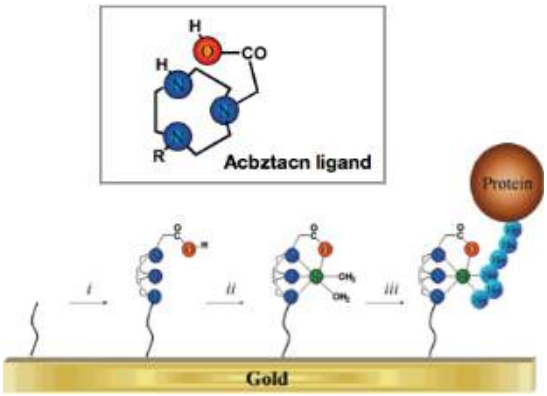

Figure 1-14. Modification of a gold surface for specific capture of histidine-tagged proteins using Acbztacn ligand.[49]

1.9 Summary

The synthesis of nanostructures having desired shapes and functions for specific purposes through the self-assembly of amphiphilic molecules is important in many fields. In order to adjust the self-assembled structure to the required purpose, it is necessary to adjust the block ratio or the block composition, and to synthesize molecules with unique architectures. Studies that control structure through simple methods, such as polymer blending or by exploiting solubility differences, have also been reported. In order to determine how to control microstructure and lattice size, we used these methods to investigate the inverse bicontinuous structures that were reported in our previous research.

Following the introduction in Chapter 1, Chapter 2 describes the structural requirements of block copolymers for self-assembly into inverse bicontinuous cubic structures. We suggest that the architectures of block copolymers play important roles as prerequisites for forming inverse bicontinuous structures. Various structures that depend on block-copolymer architecture are elucidated by electromagnetic microscopy and X-ray scattering experiments.

Chapter 3 discusses the mix-and-match assembly of block-copolymer blends required for obtaining desired nanostructures. This approach facilitates the preparation of nanostructures with structural and functional complexity without the precision synthesis of BCPs. Moreover, this method not only forms periodic mesoporous structures with desired periodicities and pore sizes, but also provides uncommon nanostructures.

Chapter 4 reports nonergodic structures from binary-blended systems with high molecular weight differences. The formation of cylindrical micelles with Y-junctions and their aggregates was observed at certain polymer-mixture compositions, resulting in a nonergodic binary-mixture state.

Finally, Chapter 5 concludes that three-dimensionally well-defined periodic porous structures from the self-assembly of dendritic-linear block copolymers are suitable large-surface-area substrates for imparting histidine-selective Ni-NTA functionality onto the surfaces of polymer cubosomes for use in affinity chromatography.

Portions of this thesis have been published.

Chapter 2: Cho, A.; La, Y.; Shin, T. J.; Park, C.; Kim, K. T., “Structural Requirements of Block Copolymers for Self-Assembly into Inverse Bicontinuous Cubic Mesophases in Solution” *Macromolecules* **2016**, *49*, 4510−4519.

Chapter 3: Cho, A.; La, Y.; Jeoung, S.; Moon, H. R.; Ryu, J. H.; Shin, T. J.; Kim, K. T., “Mix-and-Match Assembly of Block Copolymer Blends in Solution” *Macromolecules* **2017**, *50*, 3234−3243.

1.10 Reference

1. Israelachvili, J.; Mitchell, D. J.; Ninham, B. W. Theory of self-assembly of hydrocarbon amphiphiles into micelles and bilayers. *J. Chem. Soc., Faraday Trans. 2* **1976**, *72*, 1525-1568.
2. Israelachvili, J. N. *Intermolecular and Surface Forces*, 3rd ed.; Academic Press: Amsterdam, 1992.
3. Kulkarni, C. V.; Wachter, W.; Iglesias-Salto, G.; Engelskirchen, S.; Ahualli, S. Monoolein: a Magic Lipid? Phys. *Chem. Chem. Phys.* **2011**, *13*, 3004−3021
4. Kulkarni, C. V, Lipid crystallization: from self-assembly to hierarchical and biological ordering. *Nanoscale*, **2012**, *4*, 5779-5791
5. Fong, C.; Le, T.; Drummond, C. J., Lyotropic liquid crystal engineering-ordered nanostructured small molecule amphiphile self-assembly materials by design. *Chem. Soc. Rev.*, **2012**, *41*, 1297-1322.
6. Discher, D. E.; Eisenberg, A. Polymer Vesicle. *Science* **2002**, *297*, 967-973.
7. Bohdana M. Discher, B. M.; Won, Y. Y.; Ege, D. S.; Lee, J. C-M,; Bates, F. S.; Discher, D. E.; Hammer, D. A., Polymersomes: Tough Vesicles Made from Diblock Copolymers. *Science* **1999**, *284*,1143-1146.
8. Mai, Y.; Eisenberg, A. Self-assembly of Block Copolymers. *Chem. Soc. Rev.* **2012**, *41*, 5969−5985.
9. Blanazs, A.; Armes, S. P.; Ryan, A. J. Self-Assembled Block Copolymer Aggregates: From Micelles to Vesicles and their Biological Applications. *Macromol. Rapid Commun.* **2009**, *30*, 267−277.
10. Schacher, F. H.; Rupar, P. A.; Manners, I. Functional Block Copolymers: Nanostructured Materials with Emerging Applications. *Angew. Chem., Int. Ed.* **2012**, *51*, 7898−7921.
11. Holder, S. J.; Sommerdijk, N. A. J. M., New micellar morphologies from amphiphilic block copolymers: disks, toroids and bicontinuous micelles. *Polym. Chem.* **2011**, *2*, 1018-1028.
12. Steinschulte, A. A.; Gelissen, A. P. H.; Jung, A.; Brugnoni, M.; Caumanns, T.; Lotze, G.; Mayer, J.; Pergushov, D. V.; Plamper, F. A., Facile Screening of Various Micellar Morphologies by Blending Miktoarm Stars and Diblock Copolymers. *ACS Macro Lett.* **2017**, *6*, 711−715.
13. La, Y.; An, T. H.; Shin, T. J.; Park, C.; Kim, K. T. A. Morphological Transition of Inverse

Mesophases of a Branched-Linear Block Copolymer Guided by Using Cosolvents. *Angew. Chem.*, Int. Ed. **2015**, *54*, 10483−10487.

14. Warren, N. J.; Armes, S. P. Polymerization-Induced Self-Assembly of Block Copolymer Nano-objects via RAFT Aqueous Dispersion Polymerization. *J. Am. Chem. Soc.* **2014**, *136*, 10174-10185.

15. La, Y.; Park, C.; Shin, T. J.; Joo, S. H.; Kang, S.; Kim, K. T. Colloidal Inverse Bicontinuous Cubic Membranes of Block Copolymers with Tunable Surface Functional Groups. *Nat. Chem.* **2014**, *6*, 534−541.

16. Matyjaszewski, K., Atom Transfer Radical Polymerization (ATRP): Current Status and Future Perspectives. *Macromolecules* **2012**, *45*, 4015-4039.

17. Theriot, J. C.; Lim, C. H.; Yang, H; Ryan1, M. D.; Musgrave, C. B.; Miyake, G. M., Organocatalyzed atom transfer radical polymerization driven by visible light. *Science* **2016**, *352*, 1082-1086.

18. Zhang, L.; Eisenberg, A., Formation of Crew-cut Aggregates of Various Morphologies from Amphiphilic Block Copolymers in Solution. *Polym. Adv. Technol.* **1998**, *9*, 677-699.

19. Larsson, K.; Tiberg, F. Periodic Minimal Surface Structures in Bicontinuous Lipid−Water Phases and Nanoparticles. *Curr. Opin. Colloid Interface Sci.* **2005**, *9*, 365−369.

20. Almsherqi, Z. A.; Kohlwein, S. D.; Deng, Y. Cubic Membranes: a Legend Beyond the Flatland of Cell Membrane Organization. *J. Cell Biol.* **2006**, *173*, 839−844.

21. Kruijff, B. de, Lipids beyond the bilayer. *Nature* **1997**, *386*, 129–130.

22. Deng, Y.; Mieczkowski, M., Three-dimensional periodic cubic membrane structure in the mitochondria of amoebaeChaos carolinensis. *Protoplasma* **1998**, *203*, 16-25.

23. Larsson, K.; Tiberg, F., Periodic minimal surface structures in bicontinuous lipid–water phases and nanoparticles. *Curr. Opin. Colloid Interface Sci.* **2005**, *9*, 365−369.

24. Benedicto, A. D.; O'Brien , D. F., Bicontinuous Cubic Morphologies in Block Copolymers and Amphiphile/Water Systems: Mathematical Description through the Minimal Surfaces. *Macromolecules* **1997**, *30*, 3395-3402.

25. H. Schwarz, *Monatsber, Berlin Akad*, 1865, 3, 149.

26. H. Schwarz, *Gesammelte Mathematische Abhandlungen*, Springer, Berlin, 1890.

27. Demurtas , D.; Guichard , P.; Martiel, I.; Mezzenga , R. Hébert, C.; Sagalowicz, L., Direct visualization of dispersed lipid bicontinuous cubic phases by cryo-electron tomography. *Nat Commun.* **2015**, *6*, 8915

28. Yu, H.; Qiu, X.; Nunes, S. P.; Peinemann, K. V., Biomimetic block copolymer particles with gated nanopores and ultrahigh protein sorption capacity. *Nat. Commun.* **2014**, *5*, 4110.

29. Williams, R. J.; Pitto-Barry, A.; Kirby, N.; Dove, A. P.; O'Reilly, R. K., Cyclic Graft Copolymer Unimolecular Micelles: Effects of Cyclizationon Particle Morphology and Thermoresponsive Behavior. *Macromolecules* **2016**, *49*, 2802−2813.

30. Song,Y.; Xie, T.; Jiang, R.; Wang, Z.; Yin, Y.; Li, B.; Shi, A. C., Effect of Chain Architecture on Self-Assembled Aggregates from Cyclic AB Diblock and Linear ABA Triblock Copolymers in Solution. *Langmuir* **2018**, 34, 4013−4023.

31. Yamamoto, T.; Tezuka, Y., Cyclic polymers revealing topology effects upon self-assemblies, dynamics and responses. *Soft Matter* **2015**, *11*, 7458-7468.

32. McKenzie, B. E.; Nudelman, F.; Bomans, P. H. H.; Holder, S. J.; Sommerdijk, N. A. J. M. Temperature-Responsive Nanospheres with Bicontinuous Internal Structures from a Semicrystalline Amphiphilic Block Copolymer. *J. Am. Chem. Soc.* **2010**, *132*, 10256−10259.

33. Parry, A. L.; Bomans, P. H. H.; Holder, S. J.; Sommerdijk, N. A. J. M.; Biagini, S. C. G. Cryo Electron Tomography Reveals Confined Complex Morphologies of Tripeptide-Containing Amphiphilic Double-Comb Diblock Copolymers. *Angew. Chem., Int. Ed.* **2008**, *47*, 8859−8862.

34. Percec, V.; Wilson, D. A.; Leowanawat, P.; Wilson, C. J.; Hughes, A. D.; Kaucher, M. S.; Hammer, D. A.; Levine, D. H.; Kim, A. J.; Bates, F. S.; Davis, K. P.; Lodge, T. P.; Klein, M. L.; DeVane, R. H.; Aqad, E.; Rosen, B. M.; Argintaru, A. O.; Sienkowska, M. J.; Rissanen, K.; Nummelin, S.; et al. Self-Assembly of Janus Dendrimers into Uniform Dendrimersomes and Other Complex Architectures. *Science* **2010**, *328*, 1009−1014.

35. Moughton, A.; Hillmyer, M. A.; Lodge, T. P., Multicompartment Block Polymer Micelles. *Macromolecules* **2012**, *45*, 2-19.

36. Wright, D. B.; Patterson, J. P.; Pitto-Barry, A.; Lu, A.; Kirby, N.; Gianneschi, N.C.. ; Chassenieux, C.; Colombani, O.; O'Reilly, R. K., The Copolymer Blending Method: A New Approach for Targeted Assembly of Micellar Nanoparticles. *Macromolecules* **2015**, *48*, 6516−6522.

37. Yan, N.; Yang, X.; Zhu, Y.; Xu, J.; Sheng, Y., Mesh-Like Vesicles Formed From Blends of Poly(4-vinyl pyridine)-b-polystyrene-*b*-poly(4-vinyl pyridine) Block Copolymers via Gradual Blending Method. *Macromol. Chem. Phys.* **2012**, *213*, 2261−2266.

38. Zhu, J.; Zhang, S.: Zhang, K.; Wang, X.; Mays, J. S.; Wooley, K. L.; Pochan, D. J., Disk-cylinder and disk-sphere nanoparticles via a block copolymer blend solution construction. *Nat. Commun.* **2013**, *4*, 2297.

39. Wang, X.; Guerin, G.; Wang, H.; Wang, Y.; Manners, I.; Winnik, M. A., Uniform patchy and hollow rectangular platelet micelles from crystallizable polymer blends. *Science* **2016,** *352,* 697-701.

40. Jain, S.; Bates, F. S., On the origins of Morphological Complexity in Block Copolymer Surfactants. *Science* **2003**, *300*, 460-463.

41. Jain, S.; Bates, F. S., Consequences of Nonergodicity in Aqueous Binary PEO-PB Micellar Dispersions. *Macromolecules* **2004**, *37*, 1511-1523.

42. Dan, N.; Shimoni, K.; Pata, V.; Danino, D., Effect of Mixing on the Morphology of cylindrical Micelles. Langmuir 2006, 22, 9860-9865.

43. Scopes, R. K., *Protein Purification: Principles and Practice*, 3rd ed.; Springer Science & Business Media, 1993.

44. Gaberc-Porekar, V.; Menart, V., Perspectives of immobilized-metal affinity chromatography. *J. Biochem. Biophys. Methods* **2001**, *49*, 335–360.

45. Porath. J., Immobilized Metal Ion Affinity Chromatography. *Protein Expr Purif.* **1992**, *3*, 263-281.

46. Mitchell, D. M.; Gennis, R. B., Rapid purification of wildtype and mutant cytochrome c oxidase from *Rhodobacter sphaeroides* by Ni^{2+}-NTA affinity chromatography. *FEBS Letters* **1995**, *368*, 148-150.

47. Porath, J.; Carlsson, I.; Olsson, I.; Belfrage, G., Metal chelate affinity chromatography, a new approach to protein fractionation. *Nature* **1975**, *258*, 598-599.

48. Xu, C.; Xu, K.; Gu, H.; Zhong, X.; Guo, Z.; Zheng, R.; Zhang, X.; Xu, B., Nitrilotriacetic Acid-Modified Magnetic Nanoparticles as a General Agent to Bind Histidine-Tagged Proteins. *J. Am. Chem. Soc.* **2004**, 12*6*, 3392-3393.

49. Johnsom, D, L.; Martin, L, L., Controlling Protein Orientation at Interfaces Using Histidine Tags: An Alternative to Ni/NTA. *J. Am. Chem. Soc.* **2005**, *127*, 2018-2019.

50. Hudson, Z. M.; Lunn, D. J.; Winnik, M. A.; Manners, I., Colour-tunable fluorescent multiblock micelles. *Nat. Commun.* **2014**, *5*, 3372.

51. Li, Z.; Hillmyer, M. A.; Lodge, T. P., Morphologies of Multicompartment Micelles Formed by ABC Miktoarm Star Terpolymers. *Langmuir* **2006**, *22*, 9409-9417.

52. Vahidi, A. K.; Yang, Y.;Ngo, P. N.; Li, Z., Simple and Efficient Immobilization of Extracellular His-Tagged Enzyme Directly from Cell Culture Supernatant As Active and Recyclable Nanobiocatalyst: High-Performance Production of Biodiesel from Waste Grease. *ACS Catal.* **2015**, *5*, 3157-3161.

53. Lombardo, D.; Kiselev, M. A.; Magazù, S.;Calandra, P., Amphiphiles Self-Assembly: Basic Concepts and Future Perspectives of Supramolecular Approaches. *Advances in Condensed Matter Physics* **2015**, *2015*, 151683.

Chapter 2. Structural Requirements of Block Copolymers for Self-Assembly into Inverse Bicontinuous Cubic Mesophases in Solution

2.1 Abstract

Inverse bicontinuous cubic (IBC) structures consisting of triply periodic minimal surfaces of block copolymers (BCPs) are emerging as materials of interest owing to their structural characteristics, which resemble those of their biological counterparts constructed from lipids. Solution self-assembly of amphiphilic BCPs with nonlinear architectures has recently been shown to form colloidal particles (polymer cubosomes) and macroscopic monoliths having mesoporous networks of water channels embedded in the periodic minimal surfaces of the BCP bilayers. Here we report that BCP architectures play a crucial role in controlling the packing parameter (*P*) of BCPs; a value greater than unity is a prerequisite for preferential self-assembly into IBC mesophases in solution. We show that the branched architecture of the polymer blocks constituting the BCP critically influences the structural parameters, such as the molecular area and, in particular, the critical length of the hydrophobic domain. Adjusting these structural parameters not only increases the *P* value of the BCP without depending on the asymmetry of the volume ratio of two polymer blocks (block ratio) but also dictates the lattice and periodicity of the resulting minimal surfaces of the BCPs. Our results could provide a rationale to design and synthesize amphiphilic block copolymers to directly self-assemble into periodic porous structures in solution, which could be promising materials having highly ordered mesopore networks.

2.2 Introduction

Periodic nanostructures created by self-assembly of block copolymers (BCPs) are important soft materials for applications such as lithography, separation, catalysis, and drug delivery.[1–4] In contrast with self-assembly into two- and three-dimensionally periodic nanostructures achieved by microphase separation in bulk,[5–7] BCPs in dilute solution generally self-assemble into low-dimensional structures such as micelles and vesicles of various morphologies.[8–12] The solution self-assembly of BCPs into periodic nanostructures with structural complexity has been realized for BCPs with unconventional architectures. For example, multiblock copolymers and miktoarm BCPs exhibited microphase separation of incompatible polymer blocks in the hydrophobic domain within the core compartments of micelles and vesicles.[13–19] Recent advances in synthetic polymer chemistry, such as controlled radical polymerization, click chemistry, and modular synthetic approach, have enabled elaborate control over architectures of BCPs, which has resulted in synthesis of multiblock, star, branched, graft, and cyclic BCPs.[21–26] In spite of these results, the direct formation of three-dimensionally well-defined periodic

nanostructures achieved by self-assembly of BCPs in dilute solution has remained a challenge.

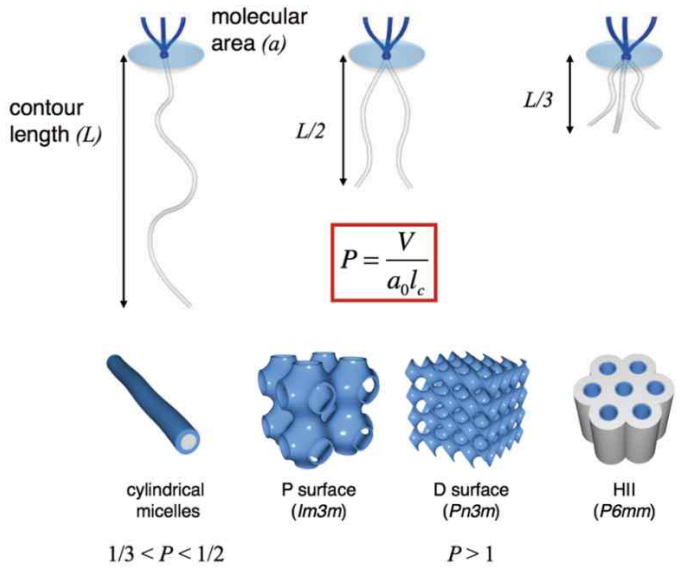

Figure 2-1. Schematic diagram of branched−branched BCPs and their self-assembly in solution. For a fixed molecular weight of the hydrophobic domain, the contour length of the hydrophobic chain (L) is reduced proportionally upon increasing the number of chains comprising the branched hydrophobic block. *P* represents the packing parameter of a BCP, where *V* is the volume of the hydrophobic block, a_0 is the interfacial area of the hydrophilic block, and l_c is the critical length of the hydrophobic block.

Self-assembly of amphiphilic BCPs into inverse bicontinuous cubic (IBC) mesophases in dilute solution is an emerging phenomenon, which allows the direct synthesis of three-dimensionally well-defined periodic porous nanostructures composed of the minimal surfaces of self-assembled bilayers of BCPs.[27–31] We recently reported that diblock copolymers composed of a branched hydrophilic block with peripheral poly(ethylene glycol) (PEG) chains and a linear polystyrene (PS) block preferentially self-assembled into IBC mesophases in dilute solution. This process resulted in the formation of colloidal particles (polymer cubosomes)[27] and large mesoporous films[28] consisting of the triply periodic minimal surfaces (TPMSs)[32,33] of BCP bilayers (Figure 2-1). Analogous to lipid cubic mesophases that occur in vivo[34–36] and in vitro,[37–42] the IBC mesophases of these BCPs exhibited a crystalline order having primitive cubic (P surface, *Im3m* space group), double diamond (D surface, *Pn3m* space group), and gyroid (G surface, *Ia3d* space group) lattices. The surface of the TPMS of the BCP bilayer could be easily functionalized with desired surface functional groups via co-assembly of BCP blends containing the functionalized linear BCPs. Arising from the presence of high molecular weight PS as a hydrophobic block, these IBC structures of the BCPs were structurally robust under ambient conditions,

rendering these mesoporous polymers potentially useful for separation, catalysis, and nanotemplating.[27−31]

Molecular packing parameter theory, which describes the relationship between the chemical structure of an amphiphile and the morphology of its self-assembled structure, has been successfully adopted to rationalize the morphological transition of self-assembled structures of BCPs in solution.[43−47] For the formation of inverse mesophases of lipids, the molecular packing parameter of the lipid (P, defined as $P = V/a_0 l_c$, where V is the volume of the hydrophobic domain, a_0 is the molecular area per amphiphile, and l_c is the critical length of the hydrophobic chain) was presumed to be greater than unity.[38,48] According to the current understanding, amphiphilic BCPs may have a P value greater than unity when the molecular weight of the hydrophobic polymer block is substantially larger than that of the hydrophilic block. Holder and Sommerdijk reported the solution self-assembly of BCPs composed of a PEG block and a comb-like hydrophobic block into bicontinuous polymer nanoparticles (BPNs) that possess internal reticulated water channels.[49−54] The low weight fraction of the water-soluble PEG block was suggested to be a crucial factor for the formation of inverse phase structures.[51,52] Peinemann and coworkers recently reported the formation of polymer cubosomes having an internal P minimal surface from the self-assembly of asymmetric poly(acrylic acid)-*b*-PS (PAA_{22}-*b*-PS_{144}, the subscript indicates the degree of polymerization of each polymer block) in a toluene/methanol mixture.[31] In spite of the self-assembly of highly asymmetric BCPs into inverse phase structures, such as inverse micelles, large compound micelles and vesicles, and inverse hexagonal structures,[55−62] the formation of IBC structures of such BCPs in dilute solution has rarely been observed. The instability of a highly asymmetric BCP in a given solvent might prevent the self-assembly process from reaching the thermodynamically stable state such as IBC mesophases. Therefore, for achieving self-assembly of BCPs into IBC mesophases in solution, it is important to develop the synthetic strategy to dictate the P value of a BCP to be greater than unity without only relying on high asymmetry of the block ratio.

We previously suggested that the branched hydrophilic block increased the molecular area of the branched−linear BCP at the air−water interface, which consequently influenced the chain conformation of the hydrophobic polymer chain upon self-assembly. [29] We inferred that the increased molecular area might force the hydrophobic chain to be less stretched to have a reduced dimension upon the formation of bilayers.[29,30] To support this assumption, we previously synthesized BCPs having branched architectures in both polymer blocks.[29] The BCPs having a branched PS block showed a strong tendency to form inverse mesophases in dilute solution, suggesting that the dimension of the hydrophobic block at the given molecular weight could critically influence the self-assembly behavior of the BCP in solution.

On the basis of our preliminary results, we report here that the packing parameter of a BCP is strongly

influenced not only by the block ratio but also by the architecture of each polymer block of the BCP. We show that the critical length of the hydrophobic block of the BCP is an important structural variable to control the packing parameter of the BCP at the given block ratio and molecular weight, which would guide the self-assembly of the BCP to preferentially form IBC mesophases in solution. By introducing a branched architecture into the hydrophobic block, the contour length of the PS chain was controlled to be substantially smaller than that of a linear polymer with the same molecular weight. We demonstrate that these BCPs composed of branched hydrophilic and hydrophobic blocks (bb-BCPs) strongly favor self-assembly into inverse mesophases due to the reduced critical chain length of the hydrophobic domain. In contrast to conventional linear BCPs, bb-BCPs can self-assemble into IBC structures without relying on high asymmetry of the block ratio. In particular, we synthesized a series of bb-BCPs having the PS blocks of the same molecular weight but only differing in their architectures to find the relationships between the architectures of the BCP and its self-assembly to IBC mesophases. This study revealed that the architecture and length of the hydrophobic block of the bb-BCP critically influence the lattice and periodicity of the minimal surface of the resulting polymer cubosomes. Our results shown in this work could help establish a rationale for the self-assembly of BCPs into inverse mesophases in solution and broaden the scope and diversity of solution self-assembly of BCPs for creating elaborate periodic nanostructures.

2.3 Results and discussion

Design and Synthesis of BCPs with Branched Polymer Blocks.

We adopted a modular synthetic approach based on Cu(I)-catalyzed azide−alkyne cycloaddition (click chemistry) to synthesize BCPs having branched architectures in both polymer blocks (Scheme 2-1).[29,63] For the branched hydrophilic modules, we used peripheral PEG chains (number-average molecular weight (Mn) of 750 and 1000 g mol^{-1}) linked to the focal benzoyl group with propargyloxy groups. These hydrophilic modules were fully characterized by ^{1}H and ^{13}C NMR, MALDI-TOF mass spectrometry, and GPC. As hydrophobic polymer modules, azido-PS (PS-N_3) chains were prepared by atom-transfer radical polymerization (ATRP) of styrene using 1-bromoethylbenzene as an initiator, followed by the end-group conversion with NaN_3 in DMF. The hydrophilic modules were then reacted with PS-N_3 using click chemistry in THF. The progress of the click reaction was monitored by GPC, which showed a gradual increase of the peak corresponding to the desired branched-branched BCP (bb-BCP) over a period of 24 h (Figure 2-2). After completion of the click reaction, the reaction mixture was purified by SiO_2 flash column chromatography using CH_2Cl_2 as an eluent to remove excess PS-N_3, followed, if necessary, by preparative GPC to remove the BCPs having incomplete structures. All bb

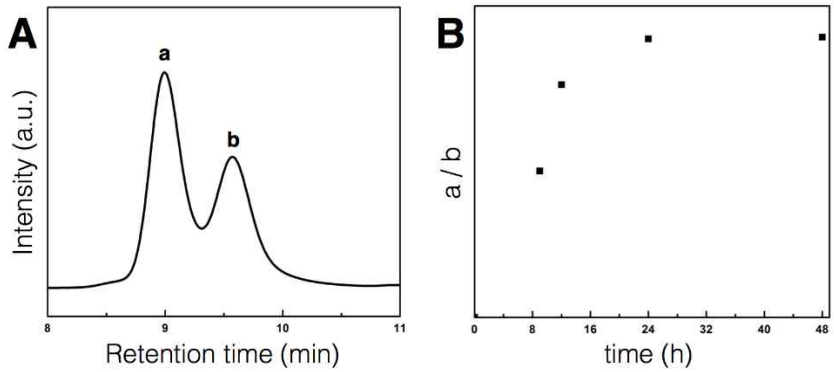

Figure 2-2. (A) GPC trace of the reaction mixture showing the peaks corresponding the coupled block copolymer (a) and the unreacted PS-N_3 (b). (B) A plot of the intensity ratio of the peaks corresponding the block copolymer and the unreacted PS-N_3 over time. The constant ratio (after 24h) indicated the completion of the click reaction.

BCPs were characterized by 1H NMR and GPC, which confirmed that the modular synthesis of BCPs was successful. The resulting bb-BCPs possessed well-defined molecular weights and molecular weight distributions (Table 2-1). By using this modular approach, we were able to synthesize bb-BCPs with the identical molecular weight and block ratio (f_{PEG}, defined as the ratio of the molecular weight of the hydrophilic PEG domain to that of the hydrophobic PS chain), but with different architectures of the hydrophobic block (Scheme 2-1).[29,64] To examine the effect of the changed architecture of the BCPs on self-assembly, we also synthesized linear diblock copolymers, PEG-b-PSn (the subscript n refers to the degree of polymerization (DP_n) of the PS block), and branched−linear BCPs, $PEG750_3$-PS_n, having similar block ratios as references. These BCPs were synthesized by ATRP using corresponding PEG macroinitiators.[29]

Self-Assembly of bb-BCPs into Inverse Mesophases.

We investigated the solution self-assembly of the series of bb- BCPs, $PEG750_3$-(*3,4*)-$(PS_n)_2$, $PEG750_3$-(*3,5*)-$(PS_n)_2$, and $PEG750_3$-(*3,4,5*)-$(PS_n)_3$ (Scheme 2-1). These bb-BCPs were allowed to self-assemble from a dioxane solution (2 mL, 1 wt %) by adding an equal volume of water at a controlled rate (1 mL h^{-1}) with stirring, followed by dialysis against water. All BCPs were self-assembled under identical conditions for comparison.

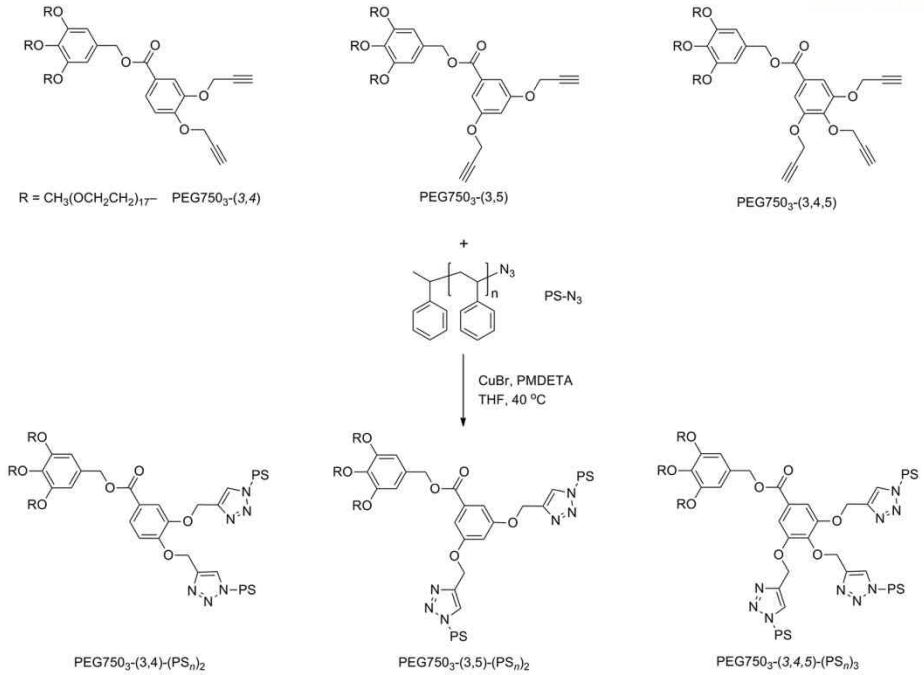

Scheme 2-1. Modular synthesis of branched-branched block copolymers by click chemistry

We first examined the morphologies of the self-assembled structures of PEG750$_3$-(*3,5*)-(PS$_n$)$_2$, which has PS chains of different DP_n in the branched hydrophobic block, using scanning electron microscopy (SEM) and transmission electron microscopy (TEM). In the SEM images of the dried aqueous suspension, we observed polymer cubosomes consisting of the IBC structures of the bilayer of PEG750$_3$-(*3,5*)-(PS$_{60}$)$_2$ (f_{PEG} = 18.0%) (Figure 2-3). The polymer cubosomes of PEG750$_3$- (*3,5*)-(PS$_n$)$_2$ were predominantly obtained from the self-assembly of PEG750$_3$-(*3,5*)-(PS$_n$)$_2$ with n ranging from 60 to 65 (f_{PEG} = 16.6−18.0%) (Figure 2-4c,d). PEG750$_3$-(*3,5*)-(PS$_{54}$)$_2$ (f_{PEG} = 20.0%) preferentially self-assembled into flat lamella and polymer vesicles under the same condition of self-assembly (Figure 2-4b). Moreover, the bb-BCPs with the f_{PEG} values smaller than 15.9% (DP_n of PS >68) formed large irregular aggregates consisting of the inverse hexagonal phases (H_{II}) (polymer hexasomes). The internal hexagonally packed pores of these structures were visualized by TEM (Figure 2-4e). Such block-ratio-dependent phase behavior was also observed for the self-assembly of PEG750$_3$-(*3,4*)-(PS$_n$)$_2$ (Figure 2-5), which is an isomer of PEG750$_3$-(*3,5*)-(PS$_n$)$_2$ (Scheme 2-1). Interestingly, PEG750$_3$-(*3,4*)-(PS$_n$)$_2$ self-assembled into polymer cubosomes having IBC structures for a broader range of f_{PEG} values (13.5−20.0%) than the range of f PEG values that yielded polymer cubosomes for PEG750$_3$-(*3,5*)-(PS$_n$)$_2$ (Figure 2-4a).

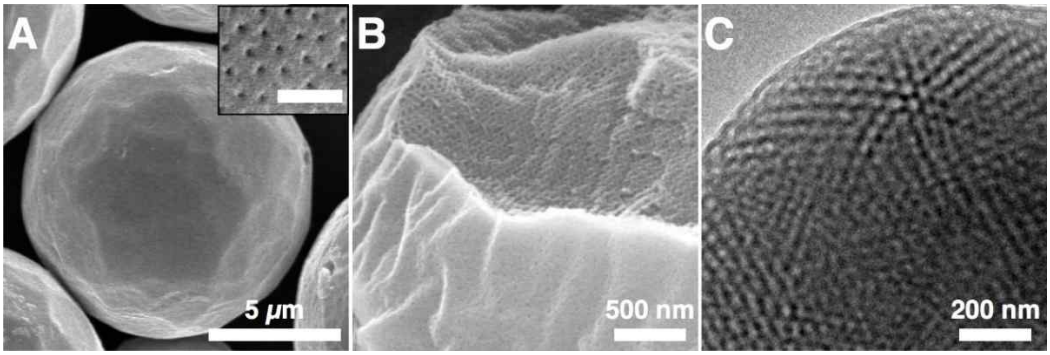

Figure 2-3. Representative SEM and TEM images of polymer cubosomes of bb-BCP, $PEG750_3$-(*3,5*)-$(PS_{60})_2$. (a) SEM images of the polymer cubosomes. The inset shows the perforated morphology of the surface (scale bar = 100 nm). (b) A SEM image of fractured polymer cubosomes showing the internal bicontinuous cubic structure. (c) A TEM image of the polymer cubosomes consisting of a minimal surface of the bilayers of bb-BCP.

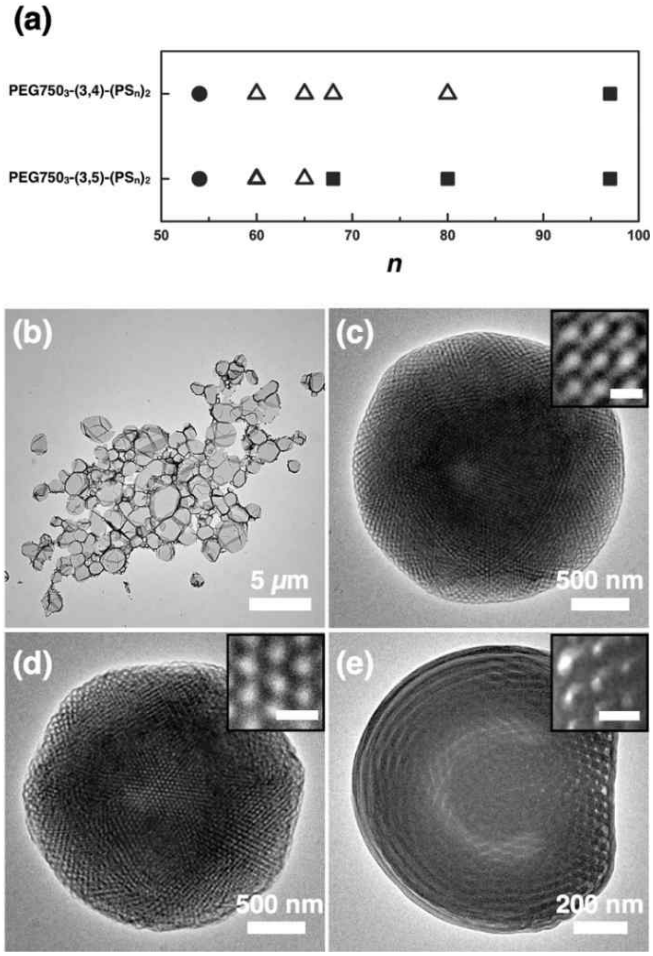

Figure 2-4. (a) Simple phase diagrams for solution self-assembly of bb-BCPs (1 wt% in dioxane) with respect to the molecular weight of the PS chains. *n* indicates the number average degree of polymerization of the PS chains. (filled circle: vesicle, open triangle: cubosome, filled square: hexasome). (b–e) TEM images showing representative morphologies of self-assembled structures of PEG750$_3$-(*3,5*)-(PS$_n$)$_2$ at varying DP_n values of the PS chains. (b) flat lamella and polymer vesicles (n = 54, f_{PEG} = 20.0%); (c and d) polymer cubosomes (n = 60, f_{PEG} = 18.0% for c and n = 65, f_{PEG} = 16.6% for d). (e) polymer hexasomes (n = 80, f_{PEG} = 13.5%). The insets are magnified views of the internal lattices (scale bars = 50 nm).

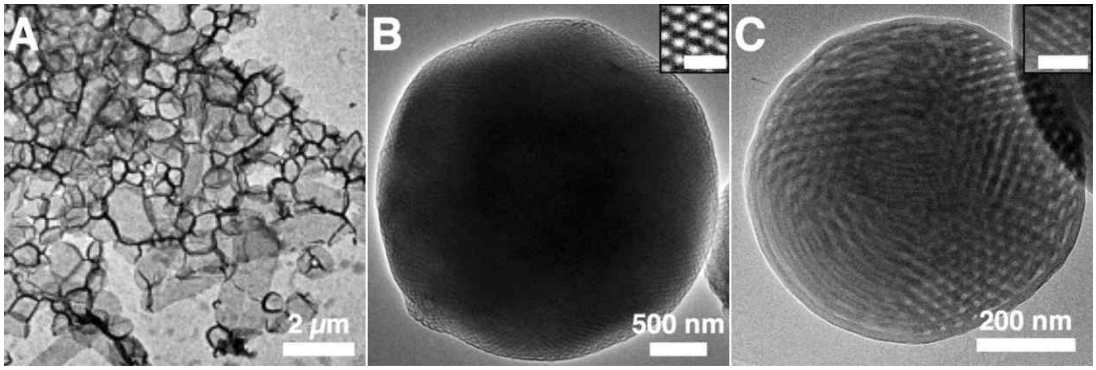

Figure 2-5. Representative TEM images of self-assembled structures of PEG750$_3$-(*3,4*)-(PS$_n$)$_2$ at varying DP_n values of the PS chains. (a) flat lamella and polymer vesicles (n = 54, f_{PEG} = 20.0%); (b) polymer cubosomes (n = 68, f_{PEG} = 15.9%); (c) polymer hexasomes (n = 97, f_{PEG} = 11.2%). The insets are magnified views of the internal lattices (scale bars = 100 nm).

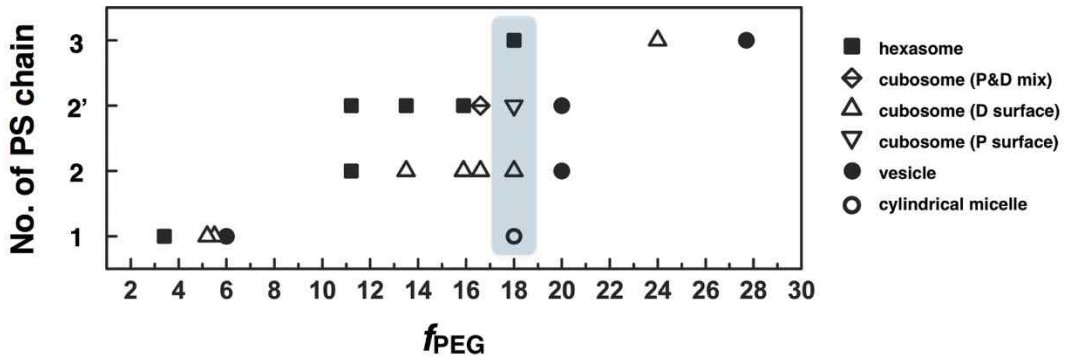

Figure 2-6. Simple phase diagram for solution self-assembly of bb-BCPs (1 wt% in dioxane) with an identical branched hydrophilic block (PEG750$_3$) and different numbers of PS chains of varying molecular weights in the hydrophobic block. (1: PEG750$_3$-PS$_n$, 2: PEG750$_3$-(*3,4*)-(PS$_n$)$_2$, 2': PEG750$_3$-(*3,5*)-(PS$_n$)$_2$, and 3: PEG750$_3$-(*3,4,5*)-(PS$_n$)$_3$). f_{PEG} is the ratio of the molecular weight of the PEG domain to that of the PS chain.

As the change in phase behavior for the solution self-assembly of the dendritic-linear and branched-linear BCPs coincided with the increasing molecular weight of the linear PS chain at a fixed molecular weight of the PEG domain,[27–30] the phase transition for the self-assembly of PEG750$_3$-(*3,4*)-(PS$_n$)$_2$ and PEG750$_3$-(*3,5*)-(PS$_n$)$_2$ could be rationalized qualitatively using packing parameter theory. For a branched hydrophilic block at a fixed molecular weight of the PEG domain, the increased volume of the hydrophobic block (V), arising from the increase in the molecular weight of the PS chains, was

translated into an increased packing parameter (*P*) of the BCP. When this value was greater than 1, the formation of IBC and inverse hexagonal phases in solution was preferential.[29,30]

In contrast to the formation of identical inverse mesophases from the self-assembly of branched-linear BCPs with the same $PEG750_3$ hydrophilic block, bb-BCPs having the branched hydrophobic blocks exhibited the formation of IBC mesophases at significantly higher f_{PEG} values (Figure 2-6). For example, the f_{PEG} values of $PEG750_3$-PS_n that showed preferential self-assembly into IBC mesophases ranged from 5.4 to 5.7%.[29] To clearly demonstrate the effect of the architecture of the hydrophobic block on the self-assembly of bb-BCPs, we compared the morphology of the self-assembled structure of a branched−linear BCP, $PEG750_3$-PS_{120}, with an identical branched hydrophilic block and block ratio (f_{PEG} = 18.0%) to those of bb-BCPs that self-assembled into polymer cubosomes. Under the same condition for self-assembly of $PEG750_3$-(*3,4*)-$(PS_n)_2$ and $PEG750_3$-(*3,5*)-$(PS_n)_2$ into polymer cubosomes, the branched-linear BCP, $PEG750_3$-PS_{120}, self-assembled into cylindrical micelles (Figure 2-7b). In addition, the linear diblock copolymer PEG2000-PS_{121}, which has a similar f_{PEG} value (15.9%) and overall molecular weight to the BCPs with branched architectures, only self-assembled into polymer vesicles (average diameter = 380 nm as determined by DLS, Figure 2-7a). Moreover, $PEG750_3$-(*3,4,5*)-$(PS_{40})_3$ with three PS chains in the hydrophobic block (f_{PEG} = 18.0%) self-assembled into polymer hexasomes (H_{II} phase) under identical selfassembly conditions (Figure 2-7d).

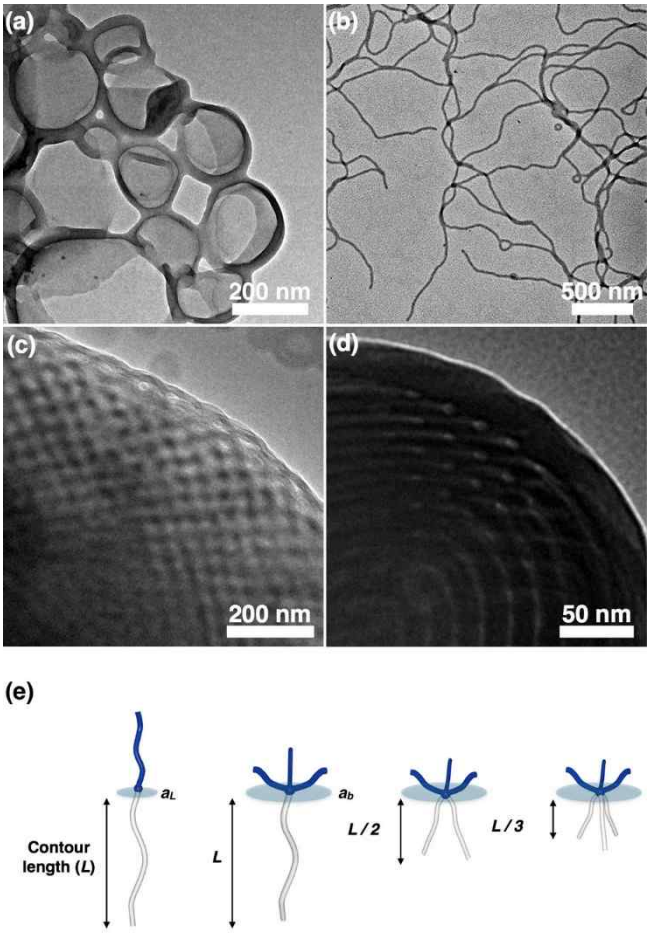

Figure 2-7. (a–d) TEM images of self-assembled structures of (a) PEG2000-PS_{121} (f_{PEG} = 15.9 %), (b) $PEG750_3$-PS_{120} (f_{PEG} = 18.0 %), (c) $PEG750_3$-(*3,4*)-$(PS_{60})_2$ (f_{PEG} = 18.0 %), and (d) $PEG750_3$-(*3,4,5*)-$(PS_{40})_3$ (f_{PEG} = 18.0 %). (e) A schematic representation of BCPs of different architectures at the fixed molecular weight and block ratio.

These results strongly supported our assumption that the reduced critical chain length (l_c) of the hydrophobic block, resulting from the dissection of a linear PS chain into multiple PS chains without altering the overall molecular weight of the PS domain, would contribute to an increase of the *P* value of the BCP, resulting in a value that exceeds unity. The self-assembly of bb-BCPs in dilute solution was consequently steered toward the formation of inverse mesophases, even at block ratios that lead to the formation of cylindrical micelles and polymer vesicles for the BCPs having the linear hydrophobic block of the same overall molecular weight (Figure 2-7e).

Structural Characterization of IBC Structures of bb-BCPs.

After confirming that the branched architecture of the hydrophobic block critically influenced the self-assembly of the bb-BCPs, we investigated the effect of the architecture of the hydrophobic block of the bb-BCPs on the crystalline lattice of the inverse mesophases. For comparison, we fixed the molecular weight of the hydrophobic PS domain at ~12 kg mol_{-1} and tethered the constituent PS chains to the hydrophilic module, $PEG750_3$ (f_{PEG} ~ 18%).

By adding water to the dioxane solution of $PEG750_3$-(*3,5*)-$(PS_{60})_2$ (1 wt %), we observed preferential self-assembly into polymer cubosomes (Figure 2-8a,b), of which the average diameter was 10.3 μm, as determined by analysis of SEM images (Figure 2-9). The synchrotron SAXS results for the dried polymer cubosomes of $PEG750_3$-(*3,5*)-$(PS_{60})_2$ showed a set of peaks corresponding to the Schwarz P minimal surface (*Im3m* symmetry, lattice constant (a) = 81.1 nm) (Figure 2-8c). The structural details of the P surface of $PEG750_3$-(*3,5*)-$(PS_{60})_2$ were clearly revealed in SEM images (Figure 2-8d−g), corroborating the internal P minimal surface structures of the polymer cubosomes suggested by the SAXS results. The BCPs having PS chains of slightly increased molecular weight ($PEG750_3$-(*3,5*)-$(PS_{65})_2$, f_{PEG} = 16.6%) formed polymer cubosomes that demonstrated mixed structures of Schwartz P and D surfaces (*Im3m* symmetry, a = 42.5 nm; *Pn3m* symmetry, a = 33.2 nm) (Figure 2-10).

In comparison, $PEG750_3$-(*3,4*)-$(PS_{60})_2$, which has two PS chains at the 3- and 4-positions of the focal benzoyl unit of the hydrophilic module, self-assembled into polymer cubosomes (average diameter of 9.6 μm). The dried polymer cubosomes showed the peaks corresponding to the Schwartz D surface (*Pn3m* symmetry, a = 50.0 nm) in the SAXS experiments. The D surface structure of the TPMS of the bilayer of $PEG750_3$- (*3,4*)-$(PS_{60})_2$ was confirmed by the SEM images shown in Figure 2-11. However, upon increasing the DP_n of the PS chains from 60 to 80, we observed that the average diameter of the polymer cubosomes increased, but the periodic minimal surface of the polymer cubosomes maintained Pn3m symmetry. $PEG750_3$-(*3,4,5*)-$(PS_{40})_3$ (f_{PEG} = 18.0%), which has the same f_{PEG} value as $PEG750_3$-(*3,4*)-$(PS_{60})_2$ and $PEG750_3$-(*3,5*)-$(PS_{60})_2$, but three PS chains tethered to the benzoyl core of the hydrophilic module, self-assembled into large hexasomes consisting of inverse hexagonal phases (*P6mm* symmetry, a = 18.0 nm) (Figure 2-12). An increase of the f_{PEG} value to 24.0% was required for the formation of polymer cubosomes, with only illordered bicontinuous inverse phases observed for self-assembly of $PEG750_3$-(*3,4,5*)-$(PS_{30})_3$ (Figure 2-13). Analogous to the phase transition from flat bilayers to bicontinuous cubic and inverse hexagonal phases of lipids with increasing the *P* values,[38,48] we concluded that the phase transition observed from polymer inverse mesophases from lamella (*P* = 1) to Pminimal surface (*Im3m*), D-minimal surface (*Pn3m*), and inverse hexagonal structure (*P6mm*) with an increasing the *P* value of the BCP.

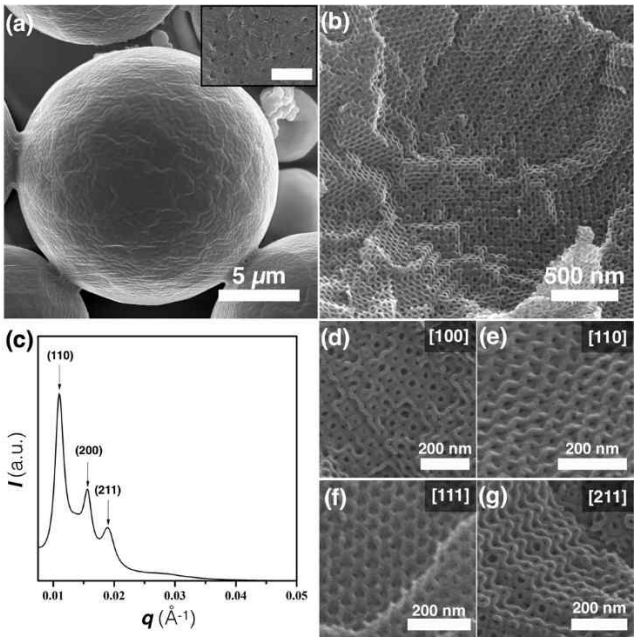

Figure 2-8. (a) SEM images showing the polymer cubosomes of $PEG750_3$-(*3,5*)-$(PS_{60})_2$. The inset shows the surface morphology (scale bar = 100 nm). (b) SEM image of the internal IBC structures. (c) SAXS result obtained from dried polymer cubosomes indicating *Im3m* symmetry (a = 81.1 nm). (d−g) SEM images showing the P minimal surface (*Im3m*) viewed at the indicated directions.

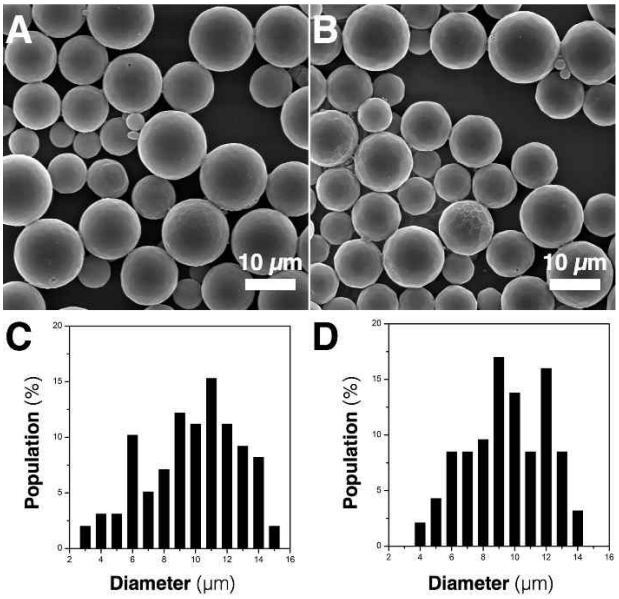

Figure 2-9. (A and B) SEM image of the polymer cubosomes of (A) PEG750$_3$-(3,5)-(PS$_{60}$)$_2$ and (B) PEG750$_3$-(3,4)-(PS$_{60}$)$_2$. (C and D) Size distribution of polymer cubosomes of (C) PEG750$_3$-(3,5)-(PS$_{60}$)$_2$ (average = 10.3 μm) and (D) PEG750$_3$-(3,4)-(PS$_{60}$)$_2$ (average = 9.6 μm) obtained by SEM image analysis.

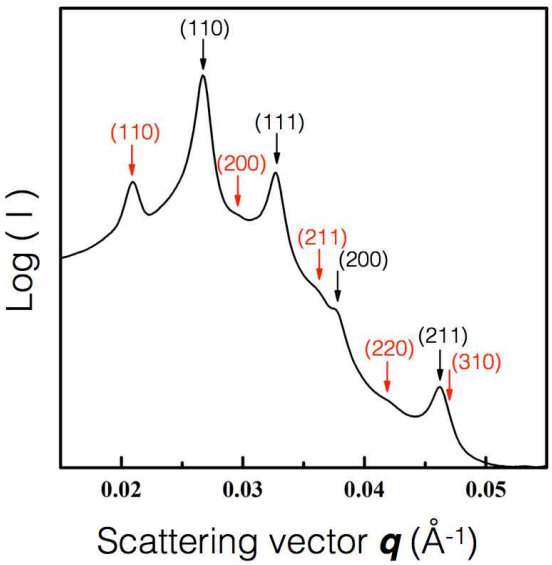

Figure 2-10. SAXS result of the polymer cubosomes of PEG750$_3$-(3,5)-(PS$_{65}$)$_2$ having mixed structures of Schwartz P and D surfaces (*Im3m* space group, lattice constant a = 42.5 nm, for *Pn3m* space group, a = 33.2 nm).

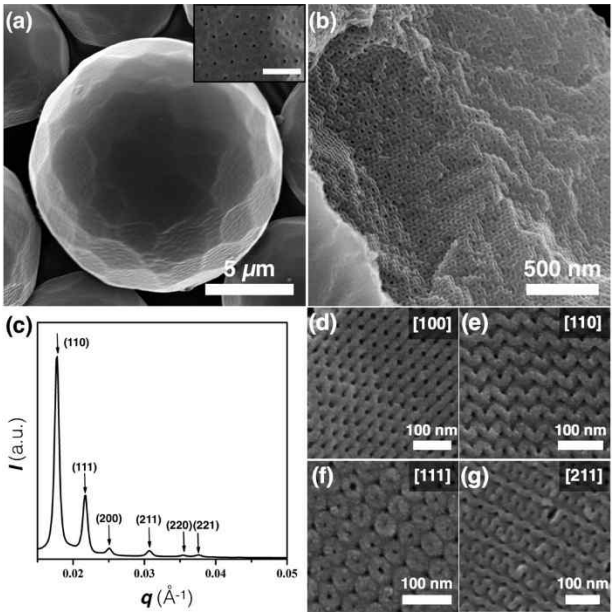

Figure 2-11. (a) SEM images showing the polymer cubosomes of $PEG750_3$-(*3,4*)-$(PS_{60})_2$. The inset shows the surface morphology (scale bar = 100 nm). (b) A SEM image of the internal IBC structures. (c) SAXS result obtained from dried polymer cubosomes indicating *Pn3m* symmetry (a = 50.0 nm). (d–g) SEM images showing the D minimal surface (*Pn3m*) viewed at the indicated directions.

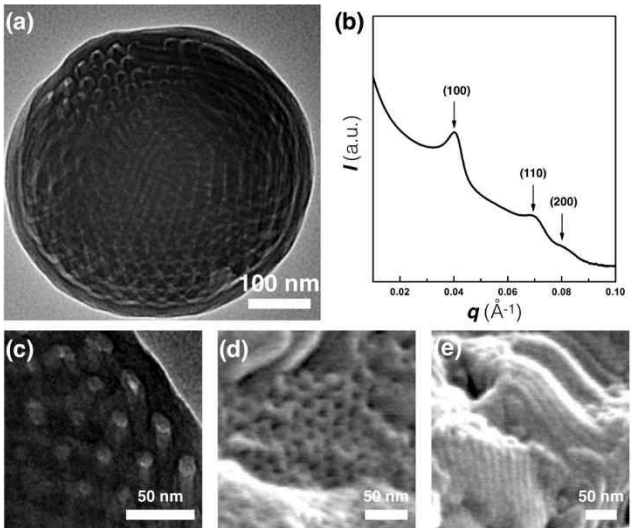

Figure 2-12. (a) TEM image showing the polymer hexasomes of PEG750$_3$-(*3,4,5*)-(PS$_{40}$)$_3$. (b) SAXS result obtained from dried polymer hexasomes indicating *P6mm* symmetry (a = 18.0 nm). (c) TEM and (d and e) SEM images showing the internal inverse hexagonal structures of the polymer hexasomes.

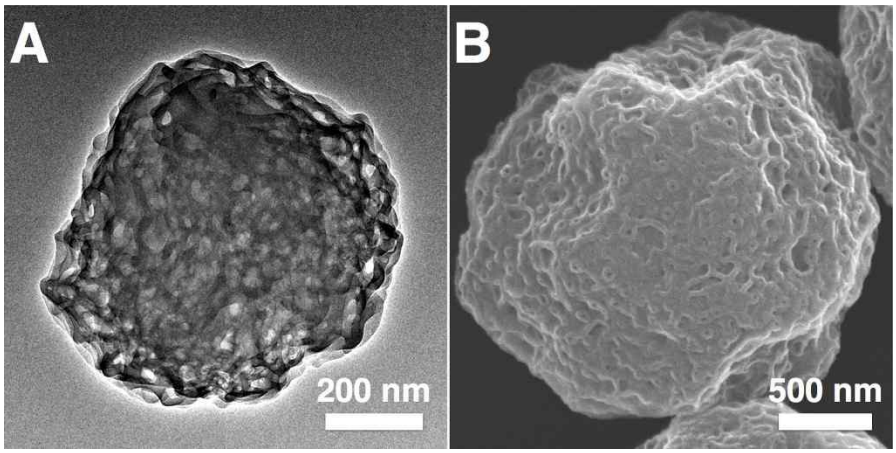

Figure 2-13. (A) TEM and (B) SEM image of ill-ordered bicontinuous inverse phases of PEG750$_3$-(*3,4,5*)-(PS$_{30}$)$_3$.

Effect of the Length of the Hydrophobic Block on the Lattice Constant of the IBC Structure.

Inverse bicontinuous cubic mesophases of lipids in nature such as smooth endoplasmic reticulum serve as templates for chitin gyroid networks, resulting in the formation of 3-D photonic crystals found in the scales of butterfly wings.[65] These bicontinuous cubic membranes found in nature are highly swollen and exhibit lattice constants exceeding a few hundred nanometers. [66,67] In contrast, lipid cubic phases formed in vitro only exhibited periodicities and pore sizes that are an order of magnitude smaller than those found from natural counterparts. [68−70] The control over the periodicity and pore size of water channels in lipid cubic mesophases therefore remains an important challenge for utilizing these self-assembled periodic porous structures for delivery, storage, and separation of biomacromolecules.

For IBC structures of BCPs, it is evident that the lattice constant (*a*) and, thus, periodicity of the IBC structure of BCPs are proportional to the increased dimension of the building blocks forming the minimal surface. For example, the a value of the D surface of the polymer cubosomes of $PEG750_3$-PS_{390} was determined to 64.2 nm, while the same bicontinuous cubic structures of $PEG550_3$-PS_{231} showed the a value of 45.3 nm from the SAXS experiments.[29] From the SAXS experiments, the dried polymer cubosomes of $PEG1000_3$-PS_{450}, which possessed a branched hydrophilic block with longer PEG chains and a linear high molecular weight PS chain as the hydrophobic block (f_{PEG} = 6.4%), showed a *Pn3m* lattice (D surface) with an a value of 70.2 nm (Figure 2-14a,b).

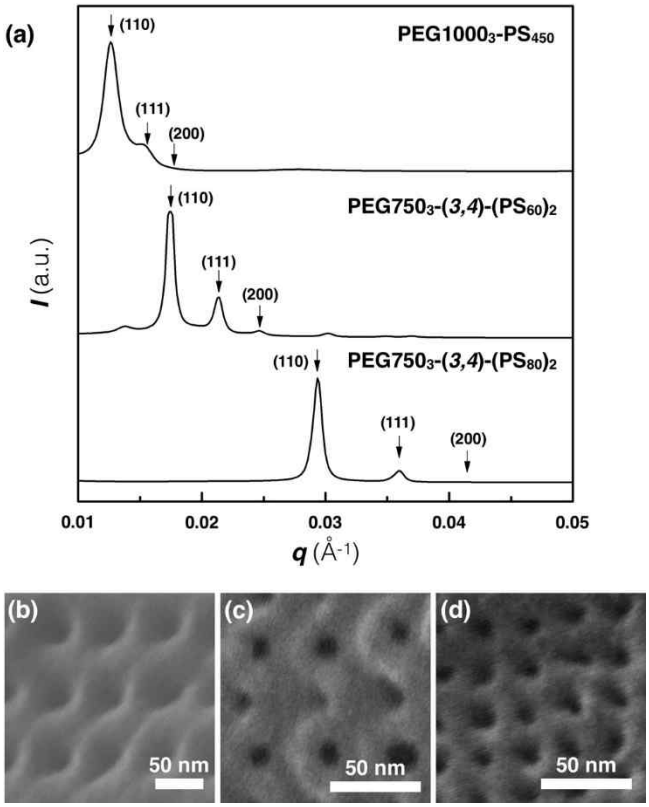

Figure 2-14. (a) SAXS results of the polymer cubosomes of PEG1000$_3$-PS$_{450}$ (*Pn3m*, a = 70.2 nm), PEG750$_3$-(*3,4*)-(PS$_{60}$)$_2$ (*Pn3m*, a = 50.0 nm), and PEG750$_3$-(*3,4*)-(PS$_{80}$)$_2$ (*Pn3m*, a = 30.2 nm). (b–d) SEM images showing (100) plane of the P surface of (b) PEG1000$_3$-PS$_{450}$, (c) PEG750$_3$-(*3,4*)-(PS$_{60}$)$_2$ and (d) PEG750$_3$-(*3,4*)-(PS$_{80}$)$_2$.

We studied the effect of the molecular weight of the PS chains constituting the hydrophobic block of PEG750$_3$-(*3,4*)- (PS$_n$)$_2$ as these BCPs self-assembled into polymer cubosomes having D surfaces in a wide range of f PEG values (Figure 2-6). Unexpectedly, from the SAXS results for the polymer cubosomes of PEG750$_3$-(*3,4*)-(PS$_n$)$_2$, we observed that an increase of the DP_n of the PS chains constituting the hydrophobic block reduced the lattice parameter of the self-assembled D minimal surface. As shown in Figure 2-14, the D minimal surface of PEG750$_3$-(*3,4*)-(PS$_{60}$)$_2$ had an a value of of 50.0 nm, whereas the D surface of PEG750$_3$-(*3,4*)-(PS$_{80}$)$_2$ possessed a reduced a value of 30.2 nm. The reduced lattice parameter of the D surfaces of the PEG750$_3$-(*3,4*)-(PS$_{80}$)$_2$ compared to the a value of the minimal surface of PEG750$_3$-(*3,4*)-(PS$_{60}$)$_2$ was also observed by SEM, which supported the SAXS results (Figure 2-14c,d).

For lipid bicontinuous cubic phases, the length of the lipid (l) and the volume fraction of lipids within a lattice of minimal surface (ϕ) are proportional, as shown by the equation[68,69]

$$\phi = 2A_0\left(\frac{l}{a}\right) + \frac{4}{3}\pi\chi\left(\frac{l}{a}\right)^3 \qquad (1)$$

where a is the lattice parameter measured by SAXS, ϕ is the BCP volume fraction, A_0 is the ratio of the area of the minimal surface in a unit cell to (unit cell volume)$^{2/3}$, and χ is the Euler−Poincaire characteristic (for *Pn3m*, A_0 = 1.191 and $\chi = -2$). For a given dimension of the lipid, the radius of the water channels (r) embedded within the minimal surface can be expressed by

$$r = 0.391a - l \qquad (2)$$

As suggested from these relationships, increasing only the length of the hydrophobic block of the bb-BCP without changing the hydrophilic block could reduce the radius of the water channels embedded in the minimal surface. As a result, the periodicity of the minimal surface could be reduced. This result suggested that the periodicity of the TPMS of bb-BCPs and the radius of water channel networks embedded in the polymer cubosomes could be rationally controlled by adjusting the dimensions of the constituting polymer blocks of the BCPs.[51]

Effect of Architectures of BCPs on Their Packing Parameters.

We suggested that the packing parameter (P) of a BCP exceeding unity could be a structural prerequisite of a BCP for self-assembly into inverse mesophases in solution.[26–29] A conventional strategy to increase the P value of a BCP is to increase a volume fraction of a solvophobic block.[11] When this asymmetry of the block ratio becomes high enough to increase the P value of the BCP greater than 1, self-assembly would favor the formation of inverse mesophase in solution. Sommerdijk and co-workers proposed that high asymmetry of the block ratio of BCP was critical for their linear-brush block copolymers to form BPNs in solution.[51] In spite of these results, however, BCPs having a high molecular weight hydrophobic block rarely self-assembled into IBC mesophases in solution, partly, because the high molecular weight of the hydrophobic polymer block relative to that of solvent-soluble block might render the aggregates to be unstable during self-assembly in solution. In this case, self-assembled structures of the resulting BCP could be kinetically trapped to yield only intermediate morphology rather than thermodynamically stable morphology such as IBC structures. Our design for bb-BCPs allowed us to maintain the P value above 1 by limiting the critical length of the hydrophobic block without relying on high asymmetry in a block ratio. We further investigated that the effect of the critical length of the hydrophobic block on the P value of the BCP by using a model BCP having a linear PEG hydrophilic block and a branched PS hydrophobic block.

We synthesized a block copolymer with a linear PEG chain in the hydrophilic block, which was

coupled to the branched hydrophobic block having two PS chains, PEG2000-(*3,5*)- $(PS_{60})_2$ (f_{PEG} = 16.0%). From the Langmuir isotherms, the molecular area for PEG2000-(*3,5*)-$(PS_{60})_2$ at the air-water interface was determined to be 1286 $Å^2$. In contrast, the molecular area of $PEG750_3$-(*3,5*)-$(PS_{60})_2$ having the branched hydrophilic block of comparable molecular weight of the PEG domain and the identical hydrophobic block was 1860 $Å^2$ (Figure 2-15A). The reduced molecular area of PEG2000-(*3,5*)-$(PS_{60})_2$ should be translated to a smaller a_0 than that of $PEG750_3$-(*3,5*)-$(PS_{60})_2$ having a branched PEG block. On the basis of this rationale, we expected that the *P* value of PEG2000-(*3,5*)-$(PS_{60})_2$ might be greater than that of $PEG750_3$-(*3,5*)-$(PS_{60})_2$, which would result in the greater tendency to form inverse mesophases by self-assembly of linear-branched BCP. Compared to the self-assembly of $PEG750_3$-(*3,5*)-$(PS_{60})_2$ into the polymer cubosomes consisting of D minimal surfaces, PEG2000-(*3,5*)-$(PS_{60})_2$ only self-assembled into large irregular particles having no internal periodic structures. We only observed ill-defined inverse mesophases possessing inverse hexagonal (H_{II}) structures from the self-assembly of PEG2000-(*3,5*)-$(PS_{45})_2$, of which the f_{PEG} value was 21.4% (Figure 2-15B). These results clearly showed that the adjustment of the structural parameters such as a molecular area and a critical length of a hydrophobic block directly influenced the packing parameter of a BCP without relying only on asymmetry in a block ratio, which results in the control over the morphology of the self-assembled inverse phase structures in solution.

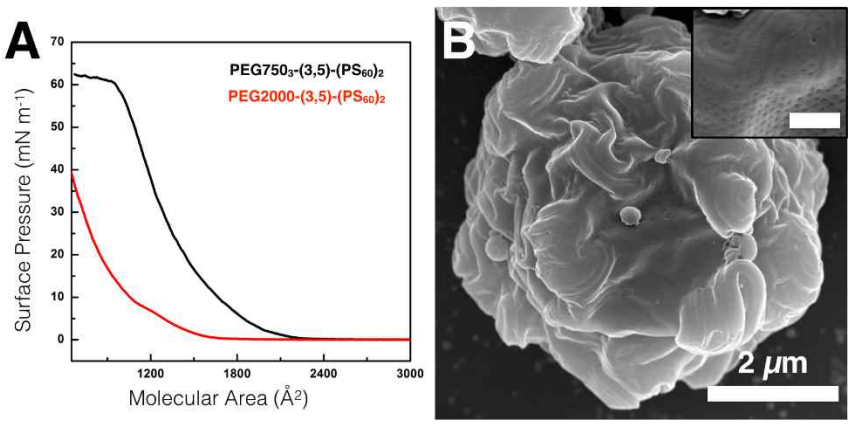

Figure 2-15. (A) Surface pressure to molecular area isotherms of $PEG750_3$-(3,5)-$(PS_{60})_2$ and PEG2000-(3,5)-$(PS_{60})_2$ at 293K. The molecular area was determined by extrapolating the region of increasing surface pressure to the x-axis (1860 $Å^2$ for $PEG750_3$-(3,5)-$(PS_{60})_2$, 1286 $Å^2$ for PEG2000-(3,5)-$(PS_{60})_2$). (B) SEM image of inverse hexagonal phase from the self-assembly of PEG2000-(3,5)-$(PS_{45})_2$ (The inset shows magnified view of surface structure. scale bar : 200 nm).

2.4 Summary

In this work, we show the effect of the architecture of a BCP on its self-assembly in solution with an emphasis on the formation of inverse bicontinuous mesophases. The incorporation of the branched architecture in both the hydrophilic and hydrophobic block of a BCP allowed us to change the variables affecting the critical packing parameter of a BCP in a systematic manner. By using the synthetic strategy discussed in our work, the apparent critical packing parameter of a BCP could be significantly increased without altering the block ratio. As a result, a bb-BCP preferentially self-assembled into polymer cubosomes consisting of periodic minimal surfaces of BCP bilayers at a block ratio generally guiding the self-assembly in solution into conventional morphologies such as cylindrical micelles and polymer vesicles if the architecture of a BCP is linear.

For conventional linear BCPs, the block ratio (the weight fraction of a polymer block) has been a deciding structural factor for the determination of the morphology of self-assembled structures in solution. Therefore, a highly asymmetric block ratio is required for self-assembly of BCPs into inverse phases in solution, for which the large packing parameter (> 1) of a BCP is believed to be a prerequisite. The formation of inverse mesophases of BCPs in dilute solution such as inverse hexagonal structures, bicontinuous polymer nanoparticles, and polymer cubosomes consisting of minimal surfaces has been reported previously. However, IBC mesophases of BCPs have been rarely observed from solution self-assembly of highly asymmetric BCPs, which suggested that a fine control of the molecular structure of a BCP should be required to realize the preferential self-assembly into IBC mesophases in solution. Our report might contribute to this means as the branched architecture introduced to construct BCPs allowed us to change the structural variables such as a molecular area and a critical length of a hydrophobic domain for optimizing the critical packing parameter of a BCP to form IBC mesophases, which could be valuable periodic polymers for future applications.

In summary, we synthesized amphiphilic block copolymers comprised of branched polymer blocks with an aim to directly control the molecular parameters such as the interfacial area of the molecules and the critical length of the hydrophobic block. The resulting branched-branched block copolymers (bb-BCPs) preferentially self-assembled into inverse bicontinuous cubic mesophases of the BCP bilayers in dilute solution, resulting in the formation of colloidal polymer cubosomes. In particular, reducing the contour length of the hydrophobic block without reducing the overall molecular weight strongly influenced the self-assembly behavior of bb-BCPs by increasing the molecular packing parameter (P) of the BCP even at the block ratio guiding the self-assembly of linear diblock copolymers and BCPs with a linear hydrophobic polymer block to form micelles and vesicles. The internal crystalline lattice and lattice parameter of the polymer cubosomes of bb-BCPs were also strongly affected by the architecture of the bb-BCP. These findings allowed us to design BCPs to preferentially

self-assemble in dilute solution into IBC structures with the desired lattice and periodicity. Our results could contribute to expanding the availability of highly defined periodic nanostructures created by simple solution self-assembly of BCPs, which might be valuable for applications such as separation and nanotemplating.

2.5 Experimental

General. Unless otherwise noted, all reagents and chemicals were purchased from Sigma Aldrich and TCI and used as received. Styrene monomer was purified by using basic alumina column before use. Dichloromethane (MC) was dried over CaH_2 under N_2 and Tetrahydrofuran (THF) was refluxed over a mixture of Na and benzophenone under N_2 and distilled before use. All reactions were performed under N_2 unless otherwise noted.

Methods. ^{1}H and ^{13}C NMR spectra were recorded on a Agilent 400-MR DD2 spectrometer, using CD_2Cl_2, $CDCl_3$ and DMSO-*d6* as solvents. Molecular weights of block copolymers were measured by Agilent 1260 Infinity GPC system equipped with a PL gel 5 μm mixed D column (Agilent Technologies) and differential refractive index detectors. THF was used as an eluent with a flow rate of 1 mL min^{-1} at 35 °C and the analytical sample was filtered by using PTFE filter before injection. A PS standard (Agilent Technologies) was used for calibration.

Matrix-assisted laser desorption ionization time-of-flight mass spectroscopy (MALDI-TOF-MS) was performed on a Bruker Ultraflex III TOF-TOF mass spectrometer equipped with a nitrogen laser (335 nm). The experimental sample was obtained by mixing a THF solution of block copolymers (5 mg mL^{-1}) and THF solution of matrix (sinapinic acid or dithranol, 10mg ml^{-1}). The prepared mixture was loaded on the MALDI plate and dried before measurement.

The Langmuir isotherms were obtained using a film balance (KSV NIMA) with a platinum Wilhelmy plate. The subphase was maintained at 20 (± 0.5) °C. Typically, the polymer solution (40 μl, 1 mg mL^{-1}) was spread evenly over the water surface in small drops. After 5 min delay to allow for the solvent evaporation, compression was applied at a constant rate of 10 mm min^{-1} (12.5 mm^2 s^{-1}).

The particle size distribution of polymer cubosomes was measured by analyzing SEM images of polymer cubosomes with ImageJ software. 300 particles were selected for the image analysis from SEM images taken from 5~10 different positions.

Synthesis of 750$_3$-OH

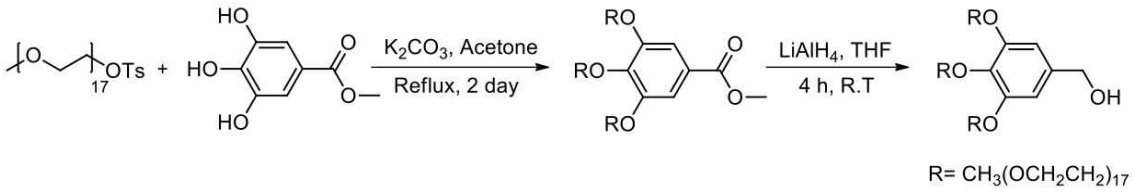

Scheme 2-2. Synthesis of PEG750$_3$-OH

PEG750$_3$-OH. PEG750$_3$-OH is synthesized in multi-gram quantity by following the literature methods.[1,2]

^{1}H NMR (400 MHz, $CDCl_3$) 6.64(s, 2H), 4.58(d, *J*=5.6 Hz, 2H), 4.18(t, *J*=5.2 Hz, 4H), 4.14(t, *J*=5.2 Hz, 2H), 3.93-3.45 (m, -CH_2CH_2O-), 3.39(s, 9H), 2.52(t, *J*=5.6 Hz, 1H); **^{13}C NMR** (400 MHz, $CDCl_3$) 152.60, 137.49,137.22, 106.50, 72.29, 71.95, 70.77-70.57, 69.83, 68.79, 64.86, 59.07; **GPC** M_n = 3190 g mol^{-1}, $Đ$ =1.03; **MALDI-TOF** M_n = 2411.34 g mol^{-1}.

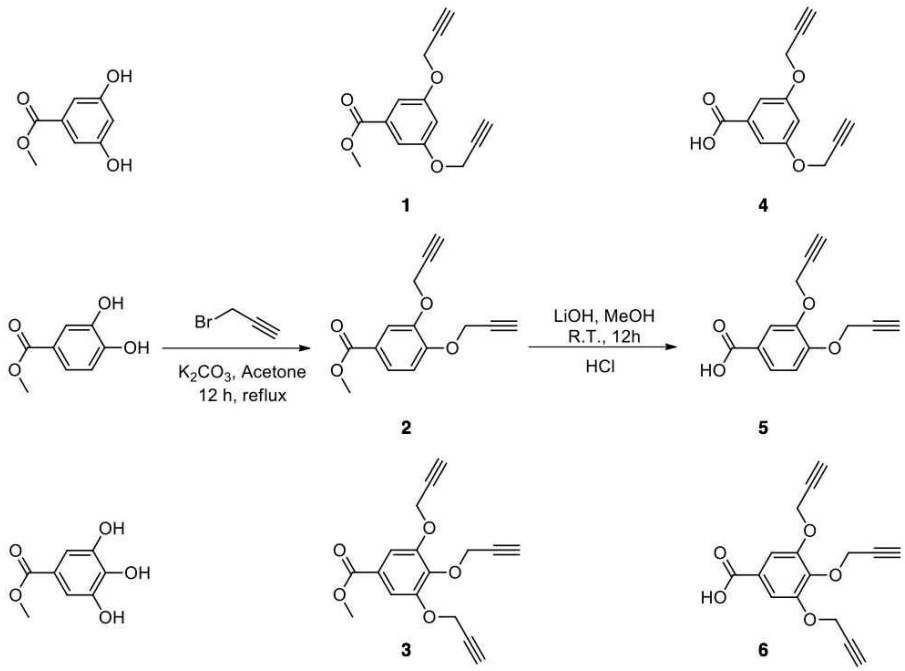

Scheme 2-3. Synthesis of 3,5-bisproparyloxybenzoic acid, 3, 4-bisproparyloxybenzoic acid, 3,4,5-trisproparyloxybenzoic acid.

Synthesis of propargyloxybenzoates (1–3).

Methyl-3,5-dipropargyloxybenzoate (1). A mixture of methyl-3,5-dihydroxybenzoate (10 g, 59 mmol) and propargyl bromide (15.2 mL, 140 mmol, 2.3 eq., 80 wt% in toluene) was stirred for 10 min in acetone (200 mL). K_2CO_3 (35 g) was then added, and the reaction was stirred for 18 h under reflux. Thereafter, the solid was removed by filtration and acetone was evaporated. Water was added and the mixture was extracted with dichloromethane. The organic phase was dried over $MgSO_4$ and filtered. The solvent was removed by rotary evaporation and then crystallized in methanol. Compound **1** was obtained as yellow solid. The compounds **2** and **3** were synthesized by following the same procedure.

Methyl-3,5-dipropargyloxybenzoate (1). Yield: 12.5 g, 86 %. **^{1}H NMR** (400 MHz, $CDCl_3$) 7.29 (d, *J*=2.4 Hz, 2H), 6.80 (t, *J*= 2.4 Hz, 1H), 4.71 (d, *J*=2.4 Hz, 4H), 3.90 (s, 3H), 2.54 (t, *J*=2.4 Hz, 2H); **^{13}C NMR** (400 MHz, $CDCl_3$) 166.61, 158.66, 132.32, 109.04, 107.68, 78.12, 76.15, 56.28, 52.58.
Methyl-3,4-dipropargyloxybenzoate (2). Compound **2** was obtained as yellow solid. Yield: 11 g, 76 %. **^{1}H NMR** (400 MHz, $CDCl_3$) 7.74 (d, *J*=2, 1H), 7.72 (t, *J*=1 Hz, 1H), 7.07 (tt, , *J*=8.6, 1, 1H), 4.80 (dd, *J*=7.0, 2.4 Hz, 4H), 3.90 (s, 3H), 2.54 (tt, , *J*=2.4, 1.6, 2H); **^{13}C NMR** (400 MHz, $CDCl_3$) 166.58, 151.38, 146.92, 124.43, 123.73, 115.37, 113.19, 78.04, 77.81, 76.55, 76.36, 56.91, 56.67, 52.17.

Methyl-3,4,5-tripropargyloxybenzoate (3). Compound **3** was obtained as pale-yellow solid. Yield: 9.3 g, 57 %. **^{1}H NMR** (400 MHz, $CDCl_3$) 7.47 (s, 2H), 4.81 (dd, *J*=8.0, 2.4 Hz, 6H), 3.91 (s, 3H), 2.53 (t, *J*=2.4 Hz, 2H), 2.46 (t, *J*=2.4 Hz, 1H); **^{13}C NMR** (400 MHz, $CDCl_3$) 166.44, 151.47, 141.24, 125.95, 110.02, 78.96, 78.12, 76.37, 75.75, 60.51, 57.24, 52.56.

Synthesis of propargyloxybenzoic acids (4–6)

3,5-dipropargyloxybenzoic acid (4). Methyl-3,5-dipropargyloxybenzoate (**1**) (1.5 g, 6.1 mmol) was dissolved in methanol (100 mL) and a solution of 2M LiOH in water (15.3 mL) was added. The reaction mixture was stirred at room temperature for 12 h and monitored by TLC. The solvent was removed by rotary evaporation. 2 M HCl was added to the mixture. When pH was dropped to pH 5~6, pale-yellow solid was precipitated. The resulting solid was collected by vacuum filtration and dried in vacuo. Compounds **5** and **6** were prepared by following the same procedure with the corresponding methylbenzoate.

3,5-dipropargyloxybenzoic acid (4). Yield: 1.27 g, 91 %. **^{1}H NMR** (400 MHz, DMSO-d_6) 7.14 (d, *J*=2.4 Hz, 2H), 6.84 (t, *J*=2.4 Hz, 1H), 4.83(d, *J*=2.4 Hz, 4H), 3.58 (t, *J*=2.4 Hz, 2H); **^{13}C NMR** (400 MHz, $CDCl_3$) 166.75, 158.18, 132.90, 108.35, 106.98, 78.89, 78.63, 55.78.

3,4-dipropargyloxybenzoic acid (5). Yield: 1.2 g, 86 %.**^{1}H NMR** (400 MHz, DMSO-d_6) 7.59 (d, *J*=2.0 Hz, 1H), 7.57 (d, *J*=1.5 Hz, 1H), 7.13 (d, *J*=9 Hz, 1H), 4.86 (dd, *J*=14.8, 2.4 Hz, 4H), 3.59 (tt, *J*=8, 2.4 Hz, 2H); **^{13}C NMR** (400 MHz, $CDCl_3$) 166.91, 150.66, 146.32, 123.71, 123.65, 114.50, 113.05, 78.99, 78.85, 78.77, 78.74, 56.08.

3,4,5-tripropargyloxybenzoic acid (6). Yield: 1.23 g, 88 %. **^{1}H NMR** (400 MHz, DMSO-d_6) 7.38(s, 2H), 4.89 (d, *J*=2.4 Hz, 2H), 4.72 (d, *J*=2.4 Hz, 1H), 3.84 (s, 2H), 3.60 (t, *J*=2.4 Hz, 2H), 3.45 (t, *J*=2.4 Hz, 2H); **^{13}C NMR** (400 MHz, $CDCl_3$) 166.66, 150.94, 139.68, 126.31, 108.88, 79.11, 78.89, 78.82, 78.36, 59.50, 56.48.

Synthesis of of hydrophilic modules (7-10)

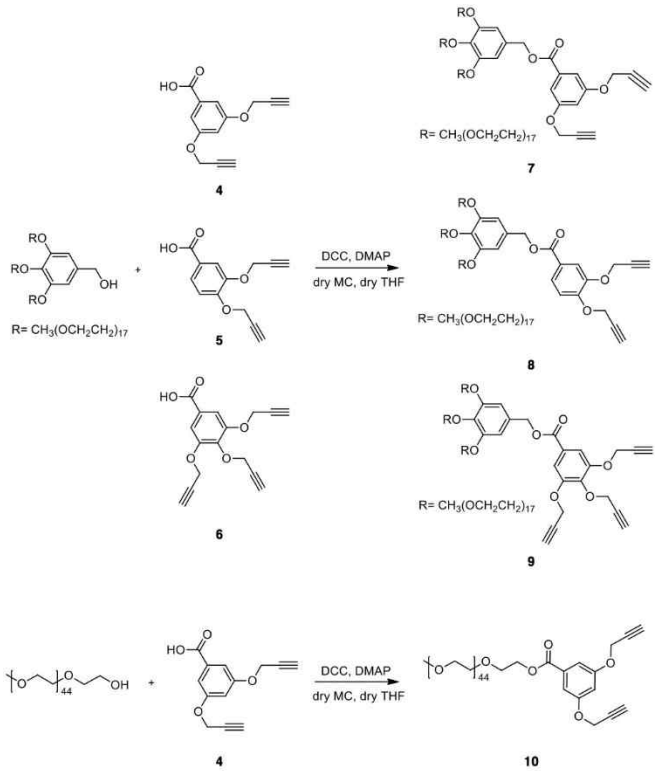

Scheme 2-4. Synthesis of branched and linear hydrophilic modules.

PEG750$_3$-3,5-bispropargyl ether (7). The same procedure was used for all hydrophilic modules: 3, 5-Bisproparyloxybenzoic acid (**4**) (1.25 g, 5 mmol, 5.2 eq.), DCC (1.29 g, 6 mmol, 6 eq.), and DMAP (0.025 g, 0.2 mmol, 0.2 eq.) were dissolved in dry THF (100 mL) at 0℃. The mixture was slowly added to the CH_2Cl_2 solution (50 mL) of PEGylated benzyl alcohol (PEG750$_3$-OH) (2.5g, 1 mmol, 1 eq.) at 0℃. The resulting mixture was gradually warmed to room temperature. After 24 h, the crude mixture was cooled, and urea was removed. Then mixture was purified by flash column chromatography using silica gel (dichloromethane : methanol = 95:5 v/v).

PEG750$_3$-3,5-bispropargyl ether (7). Yield: 1.8 g, 66 %. **^{1}H NMR** (400 MHz, $CDCl_3$) 7.32(d, *J*=2.4 Hz, 2H), 6.81 (t, *J*=2.4 Hz, 1H), 6.66(s, 2H), 5.23(s, 2H), 4.71(d, *J*=2.4 Hz, 4H), 4.18-4.1(m, 6H), 3.85-3.52(m, -CH_2CH_2O-), 3.37(s, 9H), 2.60(t, *J*=2.4 Hz, 2H); **^{13}C NMR** (400 MHz, $CDCl_3$) 165.61, 158.48, 152.63, 138.40, 132.01, 131.21, 109.94, 107.96, 107.47, 77.90, 76.32, 72.24, 71.85, 70.71-70.49, 69.63, 68.84, 66.88, 58.96, 56.008; **GPC** M_n = 3190 g mol^{-1}, $Đ$ = 1.04; **MALDI-TOF** M_n = 2667 g mol^{-1}.

PEG750$_3$-3,4-bispropargyl ether (8). Yield: 2 g, 73 %. **^{1}H NMR** (400 MHz, $CDCl_3$) 7.73(dd, *J*=5.2, 1.8 Hz, 2H), 7.07(d, *J*=9.0 Hz, 1H), 6.66 (s, 2H), 5.21(s, 2H), 4.8(d, *J*=8.3 Hz, 4H), 4.19-4.08(m, 6H), 3.9-3.49(m, -CH_2CH_2O-), 3.36(s, 9H), 2.62(t, *J*=2.2 Hz, 1H), 2.56(t, *J*=2.2 Hz, 1H); **^{13}C NMR** (400 MHz, $CDCl_3$) 165.45, 152.40, 151.21, 146.62, 124.20, 123.19, 115.13, 112.94, 108.64, 107.66, 72.03, 71.64, 70.49-70.28, 69.44, 68.65, 66.31, 58.73, 56.61, 56.36; **GPC** M_n = 3290 g mol^{-1}, $Đ$ = 1.03; **MALDI-TOF** M_n = 2606 g mol^{-1}.

PEG750$_3$-3,4,5-trispropargyl ether (9). Yield: 2.1 g, 75 %. **^{1}H NMR** (400 MHz, $CDCl_3$) 7.49(s, 2H), 6.67(s, 2H), 5.23(s, 2H), 4.83-4.78(m, 6H), 3.84-3.51(m, -CH_2CH_2O-), 3.37(s, 9H), 2.62(t, *J*=2.4 Hz, 2H), 2.56(t, *J*=2.4 Hz, 1H); **^{13}C NMR** (400 MHz, $CDCl_3$) 165.15, 152.45, 151.10, 140.89, 138.16, 131.15, 125.36, 109.63, 107.62, 78.43, 77.75, 76.60, 75.70, 72.07, 71.66, 70.51-70.30, 69.45, 68.68, 66.55, 60.02, 58.74, 56.36; **GPC** M_n = 3340 g mol^{-1}, $Đ$ = 1.03; **MALDI-TOF** M_n = 2661 g mol^{-1}.

PEG2000-3,5-bispropargyl ether (10). Yield: 10.2 g, 88 %. **^{1}H NMR** (400 MHz, $CDCl_3$) 7.29(d, *J*=2.4 Hz, 2H), 6.79(t, *J*=2.4 Hz, 1H), 4.69 (d, *J*=2.4 Hz, 2H), 4.46-4.41(m, 2H), 3.82-3.41(m, -CH_2CH_2O-), 3.35(s, 3H), 2.56(t, *J*=2.4 Hz, 2H); **^{13}C NMR** (400 MHz, $CDCl_3$) 165.23, 158.07, 131.65, 108.55, 106.34, 77.61, 76.20, 71.46, 70.29-70.03, 68.65, 64.03, 58.68, 55.68; **GPC** M_n (GPC) = 2750 g mol^{-1}, $Đ$ = 1.05; **MALDI-TOF** M_n = 1990 g mol^{-1}.

NMR and MALDI-TOF spectra of hydrophilic modules

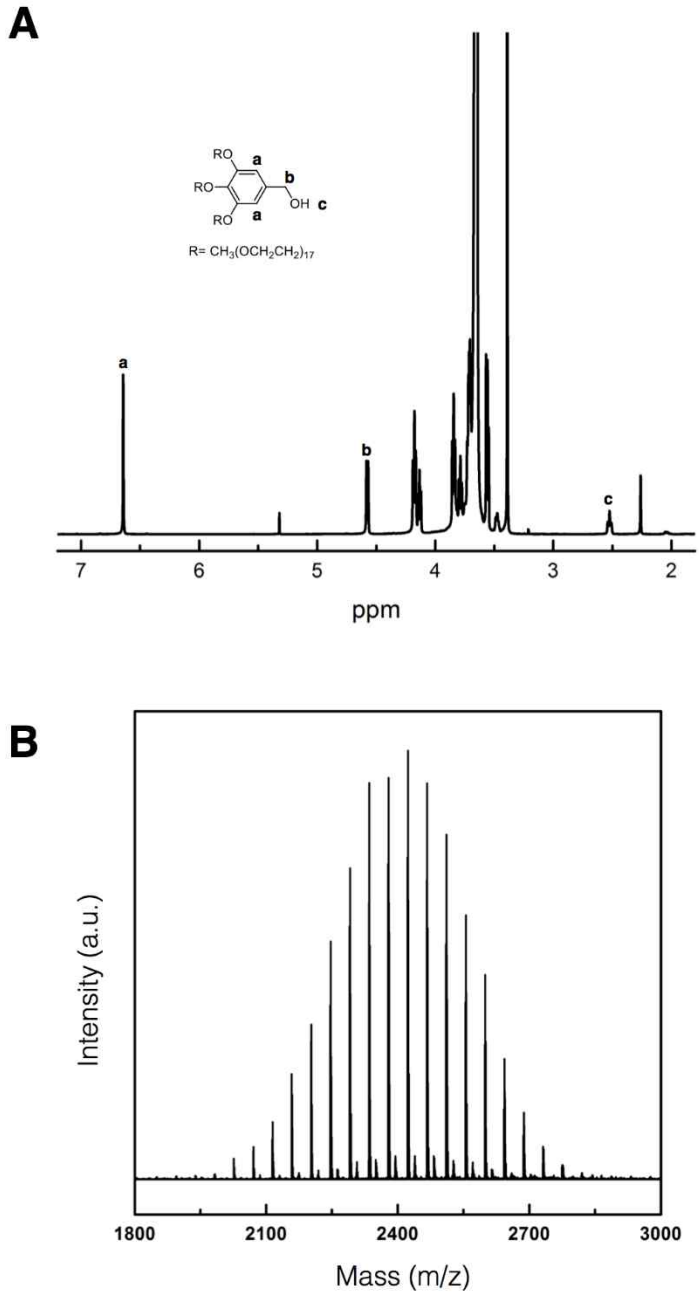

Figure 2-16. ^{1}H NMR (400 MHz, $CDCl_3$) and MALDI-TOF spectra of PEG750$_3$-OH dendron.

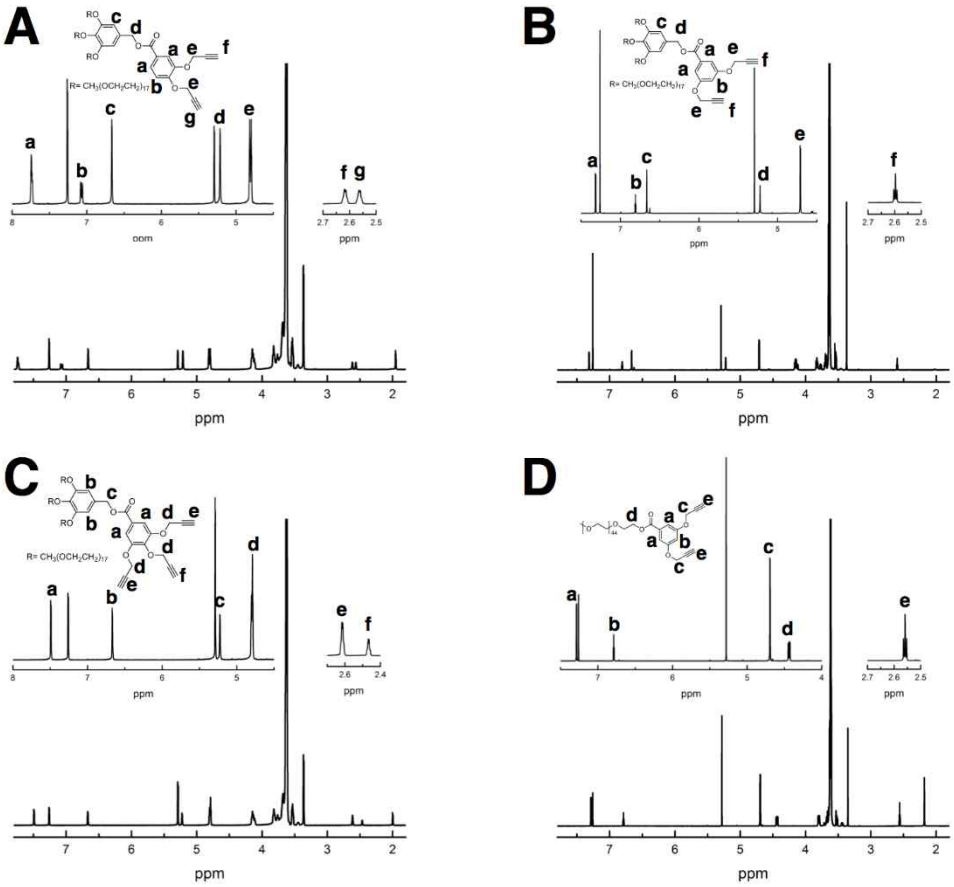

Figure 2-17. ^{1}H NMR (400 MHz, $CDCl_3$) spectra of (A) PEG750$_3$-3,4-bispropargyl ether (**7**), (B) PEG750$_3$-3,5-bispropargyl ether (**8**), (C) PEG750$_3$-3,4,5-trispropargyl ether (**9**), and (D) PEG2000-3,5-bispropargyl ether (**10**).

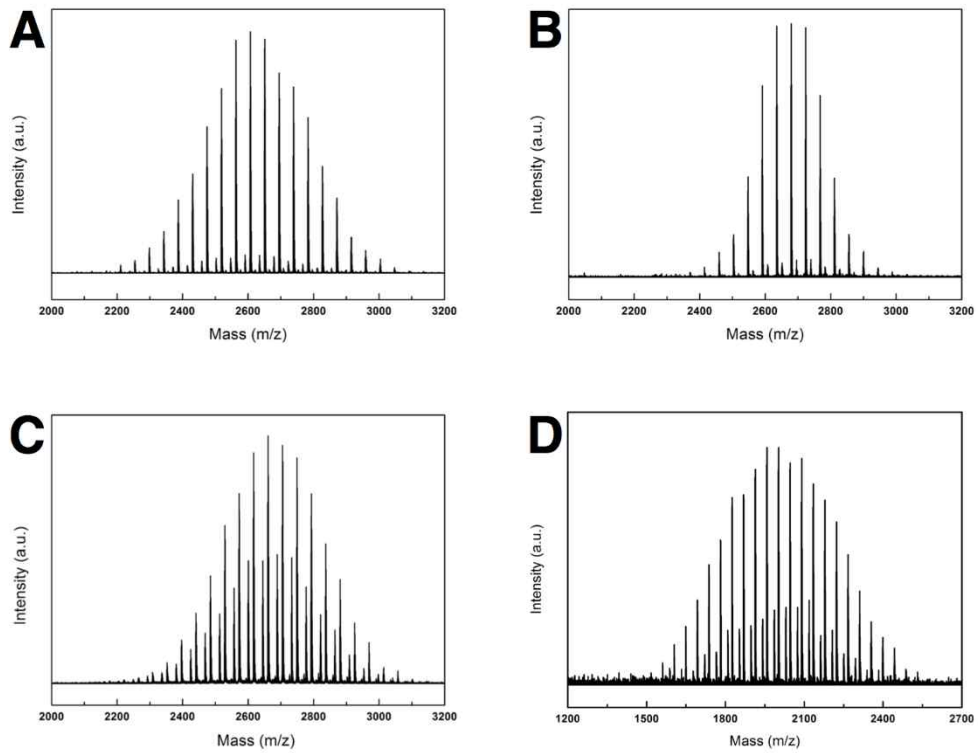

Figure 2-18. MALDI-TOF spectra of (A) PEG750$_3$-3,4-bispropargyl ether (**7**), (B) PEG750$_3$-3,5-bispropargyl ether (**8**), and (C) PEG750$_3$-3,4,5-trispropargyl ether (**9**), and (D) PEG2000-3,5-bispropargyl ether (**10**).

Modular synthesis of block copolymers

Synthesis of of N_3-PS

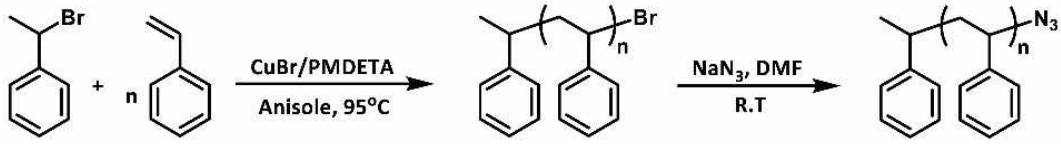

Scheme 2-5. Synthesis of azido polystyrene.

A representative procedure is described: CuBr (40 mg) was charged in Schlenk flask and dried in vacuum for 15 min. *N,N,N′,N″,N″*-pentamethyldiethylenetriamine (PMDETA) (80 mg) dissolved in anisole (1.5 mL) was introduced, and the mixture was stirred under N_2 for 15 min. To this mixture, 1-

bromoethyl benzene (100 mg, 0.188 mol) and styrene (7 g, 0.0037 mol) dissolved in anisole (1.5 mL) were added. After the resulting mixture was bubbled with N_2 for 15 min, the reaction was proceeded at 95 ℃. The reaction was quenched by exposing the solution to air in water bath and diluted with chloroform. The cooled solution was filtered through a column of aluminum oxide (basic) using chloroform as an eluent to remove the Cu catalyst. The filtered solution was concentrated on rotary evaporation, and then crude products were dissolved in a small amount of dichloromethane and precipitated into methanol. White powder was collected by vacuum filtration and dried in vacuo.
Subsequently, the brominated PS (PS-Br) (1.5 g, 0.25 mmol, 1 eq.) and sodium azide (0.24 g, 0.38 mmol, 1.5 eq.) were dissolved in DMF (50 mL) and stirred at room temperature. After 10 h, DMF was removed by a rotary evaporator and precipitated into methanol. The azido terminated PS (N_3-PS) is dried under vacuum. **GPC** M_n = 6400 g mol^{-1}, $Đ$ = 1.06; **MALDI-TOF** M_n = 6432.0 g mol^{-1}.

Synthesis of bb-BCPs by click reaction

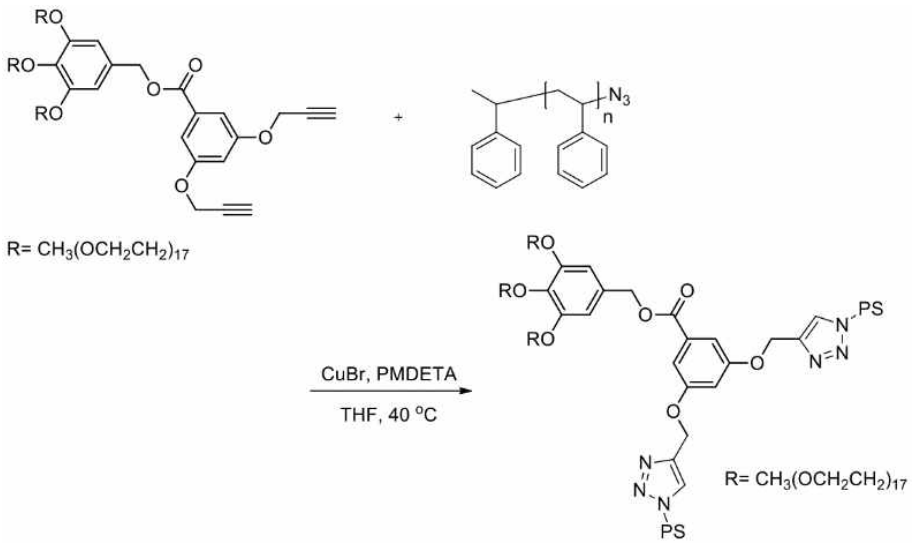

Scheme 2-6. Synthesis of block copolymers by click reation.

CuBr (40 mg) was dried in vacuum for 15 min. *N,N,N′,N″,N″*-pentamethyldiethylenetriamine (PMDETA) (80 mg) mixed with THF (1.5 mL) was added and the mixture was stirred in N_2 for 15 min. To this solution, a solution of PEG750$_3$-bispropargyl ether (0.2 g, 0.08 mmol eq.) and N_3-PS (0.31 mmol, 4 eq.) in THF(3 mL) was added. The mixture was degassed by bubbling N_2 for 15 min. After degassing, the click reaction was proceeded at 40 °C until completion. The extent of the reaction was monitored by GPC. The reaction was quenched by exposing the solution to air, followed by dilution with chloroform. The cooled solution was filtered through a pack of aluminum oxide (basic) with $CHCl_3$ to

remove the Cu catalyst. The filtered solution was concentrated on a rotary evaporator, and then crude products were dissolved in a small amount of dichloromethane and precipitated into methanol. White powder was collected by vacuum filtration and dried in vacuo. The crude mixture was further purified by flash column chromatography (SiO_2, CH_2Cl_2) to remove excess PS-N_3, and, if necessary, by preparatory size exclusion chromatography.

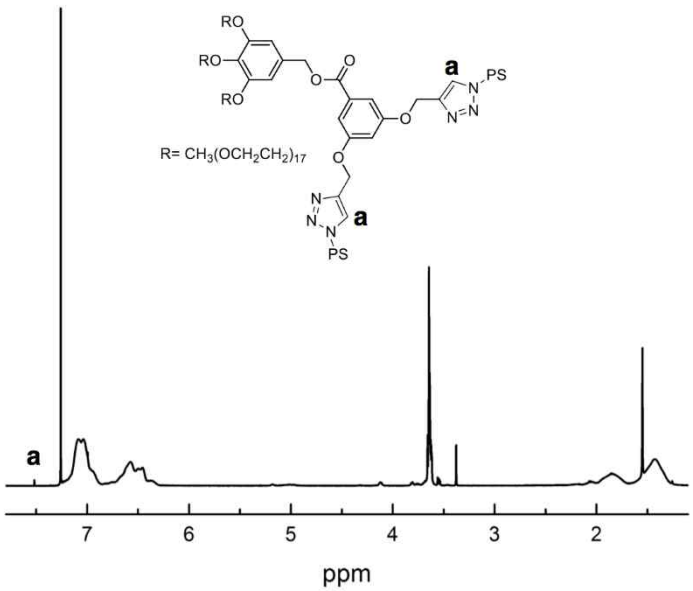

Figure 2-19. ^{1}H NMR (400 MHz, $CDCl_3$) spectrum of PEG750$_3$-(3,5)-(PS$_{60}$)$_2$.

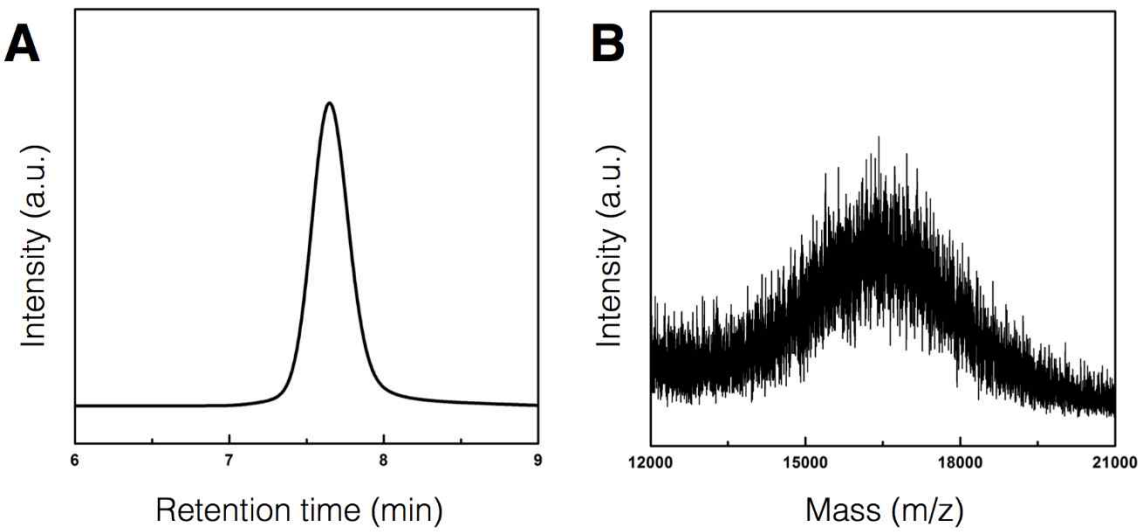

Figure 2-20. (A) GPC and (B) MALDI-TOF spectra of PEG750$_3$-(3,5)-(PS$_{60}$)$_2$.

Characterization of block copolymers

Table 2-1. Characterization of block copolymers.

Sample	M_n (g mol^{-1}) [a]	$Đ$ [a]	DP_n (PS)	f_{PEG} (%) [c]
PEG750$_3$-(3,4)-(PS$_{54}$)$_2$	13100	1.08	54 [b]	20.0
PEG750$_3$-(3,4)-(PS$_{60}$)$_2$	16110	1.04	60 [b]	18.0
PEG750$_3$-(3,4)-(PS$_{65}$)$_2$	16330	1.03	65 [b]	16.6
PEG750$_3$-(3,4)-(PS$_{68}$)$_2$	17400	1.06	68 [b]	15.9
PEG750$_3$-(3,4)-(PS$_{80}$)$_2$	20290	1.03	80 [b]	13.5
PEG750$_3$-(3,4)-(PS$_{97}$)$_2$	21950	1.05	97 [b]	11.2
PEG750$_3$-(3,5)-(PS$_{54}$)$_2$	13640	1.10	54 [b]	20.0
PEG750$_3$-(3,5)-(PS$_{60}$)$_2$	16350	1.04	60 [b]	18.0
PEG750$_3$-(3,5)-(PS$_{65}$)$_2$	16890	1.03	65 [b]	16.6
PEG750$_3$-(3,5)-(PS$_{68}$)$_2$	17820	1.06	68 [b]	15.9
PEG750$_3$-(3,5)-(PS$_{80}$)$_2$	20550	1.03	80 [b]	13.5
PEG750$_3$-(3,5)-(PS$_{97}$)$_2$	23580	1.08	97 [b]	11.2
PEG750$_3$-(3,4,5)-(PS$_{26}$)$_3$	10280	1.05	26 [b]	27.7
PEG750$_3$-(3,4,5)-(PS$_{30}$)$_3$	10600	1.05	30 [b]	24.0
PEG750$_3$-(3,4,5)-(PS$_{40}$)$_3$	12830	1.05	40 [b]	18.0
PEG750$_3$-PS$_{120}$	13500	1.05	120 [d]	18.0
PEG750$_3$-PS$_{363}$	39480	1.04	363 [d]	6.0
PEG750$_3$-PS$_{390}$	42500	1.09	390 [d]	5.5
PEG750$_3$-PS$_{413}$	44500	1.16	413 [d]	5.2
PEG750$_3$-PS$_{632}$	66300	1.11	632 [d]	3.4
PEG1000$_3$-PS$_{450}$	47590	1.12	450 [d]	6.4
PEG2000-(3,5)-(PS$_{45}$)$_2$	11900	1.05	45 [b]	21.4
PEG2000-(3,5)-(PS$_{60}$)$_2$	14300	1.08	60 [b]	16.0
PEG2000-PS$_{121}$	14000	1.05	121 [d]	15.9

[a] The number average molecular weight and molecular weight distribution determined by GPC (THF, 35 °C, 1 mL min^{-1} flow rate) using PS standards. [b] The number average degree of polymerization of homo PS chains determined by GPC measurements. [c] The molecular weight ratio of the PEG domain to that of the PS block. (2000 g mol^{-1} for PEG$_{45}$-PS$_n$, and 2250 g mol^{-1} for 750$_3$-PS$_n$). [d] DP_n determined by ^{1}H NMR integration.

General procedure for self-assembly of block copolymers. 20 mg of the block copolymers and 2 mL of 1,4-dioxane was added in a capped vial (1 wt %), and the polymer solution was stirred for 3 h at room temperature. Water was added at a controlled rate (1 mL h^{-1}, total 2 mL) to the solution with vigorous stirring (850 rpm). The resulting milky suspension was dialyzed by using dialysis bag (molecular weight cutoff (MWCO) = ~12-14 kDa, SpectraPor) against water for 24 h to remove the organic solvent. For self-assembly of BCP blends, a block copolymer mixture was prepared by mixing stock solutions of the bb-BCPs and linear BCPs in a suitable ratio (2 mL). Before addition of water, the resulting solution of mixture was allowed to equilibrate for 12 h at room temperature in a sealed vial.

Observation of structure of polymer cubosomes using electron microscope images. Scanning electron microscopy (SEM) was performed on Hitachi S-4800 FE SEM at an acceleration voltage of 10 kV. Dried polymer cubosomes were placed on a conductive carbon tape and then coated with Pt by using a K575X Sputter Coater. Transmission electron microscopy (TEM) was recorded on a JEOL JEM-2100 microscope at 200 kV and JEOL JEM-1400 microscope at 120 kV. Specimens were prepared by placing a drop of the suspension of the polymer cubosomes on a carbon-coated Cu grid (200 mesh, EM science). After 30 min, remaining solution on a grid was removed with a filter paper, and the grid was air-dried overnight.

Structural analysis of the polymer cubosomes with SAXS. Synchrotron small angle X-ray scattering data were obtained on the SAXS beam line (PLS-II 6D, 11.18 keV, 6.5m) at Pohang acceleration laboratory (Pohang, Korea). The concentrated suspension of the polymer cubosomes was dried for 2 days in freeze dryer. The resulting powder was placed on a customized holder. Ti-SBA standard was used and X-ray irradiation time was 2~10 seconds dependent on the saturation level of the detector.

2.6 Reference

1. Blanazs, A.; Armes, S. P.; Ryan, A. J. Self-Assembled Block Copolymer Aggregates: From Micelles to Vesicles and their Biological Applications. *Macromol. Rapid Commun.* **2009**, *30*, 267–277.
2. Schacher, F. H.; Rupar, P. A.; Manners, I. Functional Block Copolymers: Nanostructured Materials with Emerging Applications. *Angew. Chem. Int. Ed*. **2012**, *51*, 7898–7921.
3. Förster, S.; Antonietti, M. Amphiphilic Block Copolymers in Structure-Controlled Nanomaterial Hybrids. *Adv. Mater*. **1998**, *10*, 195.
4. Elsabahy, M.; Wooley, K. L. Design of Polymeric Nanoparticles for Biomedical Delivery Applications. *Chem. Soc. Rev*. **2012**, *41*, 2545–2561.
5. Bates, F. S.; Fredrickson, G. H. Block Copolymers—Designer Soft Materials. *Phys. Today* **1999**, *52*, 32–38.
6. Bates, F. S.; Hillmyer, M. A.; Lodge, T. P.; Bates, C. M.; Delaney, K. T.; Fredrickson, G. H. Multiblock Polymers: Panacea or Pandora's Box? *Science* **2012**, *336*, 434–440.
7. Kim, H.-C.; Park, S.-M.; Hinsberg, W. D. Block Copolymer Based Nanostructures: Materials, Processes, and Applications to Electronics. *Chem. Rev*. **2010**, *110*, 146–177.
8. Hamley, I. W. *Block Copolymers in Solution: Fundamentals and Applications*; Wiley: Chichester, 2005.
9. Riess, G. Micellization of Block Copolymers. *Prog. Polym. Sci*. **2003**, *28*, 1107–1170.
10. Raffa, P.; Wever, D. A. Z.; Picchioni, F.; Broekhuis, A. Polymeric Surfactants: Synthesis, Properties, and Links to Applications. *Chem. Rev.* **2015**, *115*, 8504–8563.
11. Mai, Y.; Eisenberg, A. Self-assembly of Block Copolymers. *Chem. Soc. Rev*. **2012**, *41*, 5969–5985.
12. Holder, S. J.; Sommerdijk, N. A. J. M. New Micellar Morphologies from Amphiphilic Block Copolymers: Disks, Toroids and Bicontinuous micelles. *Polym. Chem*. **2011**, *2*, 1018–1028.
13. Zhu, J.; Zhang, S.;; Zhang, K.; Wang, X.; Mays, J. W.; Wooley, K. L.; Pochan, D. J. Disk-cylinder and Disk-sphere Nanoparticles via a Block Copolymer Blend Solution Construction. *Nat. Commun*. **2013**, *4*, 2297.
14. Gröschel, A. H.; Walther, A.; Löbling, T. I.; Schacher, F. H.; Schmalz, H.; Müller, A. H. E. Guided Hierarchical Co-Assembly of Soft Patchy Nanoparticles. *Nature* **2013**, *503*, 247–251.
15. Gröschel, A. H.; Schacher, F. H.; Schmalz, H.; Borisov, O. V.; Zhulina, E. B.; Walther, A.; Müller, A. H. E. Precise Hierarchical Self-assembly of Multicompartment Micelles. *Nat. Commun*. **2012**, *3*, 710.

16. Gröschel, A. H.; Müller, A. H. E. Self-Assembly Concepts for Multicompartment Nanostructures. *Nanoscale* **2015**, *7*, 11841–11876.
17. Cui, H.; Chen, Z.; Wooley, K. L.; Pochan, D. J. Block Copolymer Assembly via Kinetic Control. *Science* **2007**, *317*, 647–650.
18. Li, Z.; Kesselman, E.; Talmon, Y.; Hillmyer, M. A.; Lodge, T. P. Multicompartment Micelles from ABC Miktoarm Stars in Water. *Science* **2004**, *306*, 98–101.
19. Moughton, A. O.; Hillmyer, M. A.; Lodge, T. P. Multicompartment Block Copolymer Micelles. *Macromolecules* **2012**, *45*, 2–19.
20. Christian, D. A.; Tian, A.; Ellenbroek, W. G.; Levental, I.; Rajagopal, K.; Janmey, P. A.; Liu, A. J.; Baumgart, T.; Discher, D. E. Spotted Vesicles, Striped Micelles and Janus Assemblies Induced by Ligand Binding. *Nature Mater.* **2009**, *8*, 843–849.
21. Golas, P. L.; Matyjaszewski, K. Marrying Click Chemistry with Polymerization: Expanding the Scope of Polymeric Materials. *Chem. Soc. Rev*. **2010**, *39*, 1338–1354.
22. Matyjaszewski, K.; Xia, J. Atom Transfer Radical Polymerization. *Chem. Rev.* **2001**, *101*, 2921–2990.
23. Kamigaito, M.; Ando, T.; Sawamoto, M. Metal-Catalyzed Living Radical Polymerization: Discovery and Developments. *Chem. Rev.* **2001**, *101*, 3689-3745.
24. Hawker, C. J.; Wooley, K. L. The Convergence of Synthetic Organic and Polymer Chemistries. *Science* **2005**, *309*, 1200–1205.
25. Laurent, B. A.; Grayson, S. M. Synthetic Approaches for the Preparation of Cyclic Polymers. *Chem. Soc. Rev*. **2009**, *38*, 2202–2213.
26. Williams, R. J.; Dove, A. P.; O'Reilly, R. K. Self-Assembly of Cyclic Polymers. *Polym. Chem.* **2015**, *6*, 2998–3008.
27. La, Y.; Park, C.; Shin, T. J.; Joo, S. H.; Kang, S.; Kim, K. T. Colloidal Inverse Bicontinuous Cubic Membranes of Block Copolymers with Tunable Surface Functional Groups. *Nat. Chem.* **2014**, *6*, 534–541.
28. Park, C.; La, Y.; An, T. H.; Jeong, H. Y.; Kang, S.; Joo, S. H.; Ahn, H.; Shin, T. J.; Kim, K. T. Mesoporous Monoliths of Inverse Bicontinuous Cubic Phases of Block Copolymer Bilayers. *Nat. Commun.* **2015**, 6, 6392.
29. An, T. H.; La, Y.; Cho, A.; Jeong, M. G.; Shin, T. J.; Park, C.; Kim, K. T. Solution Self-Assembly of Block Copolymers Containing a Branched Hydrophilic Block into Inverse Bicontinuous Cubic Mesophases. *ACS Nano* **2015**, *9*, 3084–3096.

30. La, Y.; An, T. H.; Shin, T. J.; Park, C.; Kim, K. T. A Morphological Transition of Inverse Mesophases of a Branched-Linear Block Copolymer Guided by Using Cosolvents. *Angew. Chem., Int. Ed.* **2015**, *54*, 10483–10487.
31. Yu, H.; Qiu, X.; Nunes, S. P.; Peinemann, K.-V. Biomimetic Block Copolymer Particles with Gated Nanopores and Ultrahigh Protein Sorption Capacity. *Nat. Commun.* **2014**, *5*, 4110.
32. Scriven, L. E. Equilibrium Bicontinuous Structure. *Nature* **1976**, *263*, 123–125.
33. Larsson, K.; Tiberg, F. Periodic Minimal Surface Structures in Bicontinuous Lipid–Water Phases and Nanoparticles. *Curr. Opin. Colloid Interface Sci.* **2005**, *9*, 365–369.
34. Almsherqi, Z. A.; Kohlwein, S. D.; Deng, Y. Cubic Membranes: a Legend Beyond the Flatland of Cell Membrane Organization. *J. Cell Biol.* **2006**, *173*, 839–844.
35. Salentinig, S.; Phan, S.; Hawley, A.; Boyd, B. J. Self-Assembly Structure Formation during the Digestion of Human Breast Milk. *Angew. Chem., Int. Ed.* **2015**, *54*, 1600–1603.
36. Salentinig, S.; Phan, S.; Khan, J.; Hawley, A.; Boyd, B. J. Formation of Highly Organized Nanostructures during the Digestion of Milk. *ACS Nano* **2013**, *7*, 10904–10911.
37. Larsson, K. Cubic Lipid-Water Phases: Structures and Biomembrane Aspects. *J. Phys. Chem.* **1989**, *93*, 7304–7314.
38. Kulkarni, C. V.; Wachter, W.; Iglesias-Salto, G.; Engelskirchen, S.; Ahualli, S. Monoolein: a Magic Lipid? *Phys. Chem. Chem. Phys.* **2011**, *13*, 3004–3021.
39. Gustavsson, J.; Ljusberg-Wahren, H.; Almgren, M.; Larsson, K. Cubic Lipid−Water Phase Dispersed into Submicron Particles. *Langmuir* **1996**, *12*, 4611–4613.
40. Gustavsson, J.; Ljusberg-Wahren, H.; Almgren, M.; Larsson, K. Submicron Particles of Reversed Lipid Phases in Water Stabilized by a Nonionic Amphiphilic Polymer. *Langmuir* **1997**, *13*, 6964–6971.
41. Barauskas, J.; Johnsson, M.; Joabsson, F.; Tiberg, F. Cubic Phase Nanoparticles (Cubosome): Principles for Controlling Size, Structure, and Stability. *Langmuir* **2005**, *21*, 2569–2577.
42. Spicer, P. T. Progress in Liquid Crystalline Dispersions: Cubosomes. *Curr. Opin. Colloid Interfac. Sci.* **2005**, *10*, 274–279.
43. Israelachvili, J. N. *Intermolecular and Surface Forces*, 3rd Ed.; Academic Press; Amsterdam, 1992.
44. Israelachvili, J. N.; Mitchell, D. J.; Ninham, B. W. Theory of Self-Assembly of Hydrocarbon Amphiphiles into Micelles and Bilayers. *J. Chem. Soc., Faraday Trans. 2* **1976**, *72*, 1525–1568.
45. Zhang, L.; Eisenberg, A. Multiple Morphologies of "Crew-Cut" Aggregates of Polystyrene-b-poly(acrylic acid) Block Copolymers. *Science* **1995**, *268*, 1728–1731.

46. van Hest, J. C. M.; Delnoye, D. A. P.; Baars, M. W. P. L.; van Genderen, M. H. P.; Meijer, E. W. Polystyrene-Dendrimer Amphiphilic Block Copolymers with a Generation-Dependent Aggregation. *Science* **1995**, *268*, 1592–1595.
47. Discher, D. E.; Eisenberg, A. Polymer Vesicles. *Science* **2002**, *297*, 967.
48. Yang, D.; Armitage, B.; Marder, S. R. Cubic Liquid-Crystalline Nanoparticles. *Angew. Chem., Int. Ed.* **2004**, *43*, 4402–4409.
49. McKenzie, B. E.; Nudelman, F; Bomans, P. H. H.; Holder, S. J.; Sommerdijk, N. A. J. M. Temperature-Responsive Nanospheres with Bicontinuous Internal Structures from a Semicrystalline Amphiphilic Block Copolymer. *J. Am. Chem. Soc.* **2010**, *132*, 10256–10259.
50. Parry, A. L.; Bomans, P. H. H.; Holder, S. J.; Sommerdijk, N. A. J. M.; Biagini, S. C. G. Cryo Electron Tomography Reveals Confined Complex Morphologies of Tripeptide-Containing Amphiphilic Double-Comb Diblock Copolymers. *Angew. Chem., Int. Ed.* **2008**, *47*, 8859–8862.
51. McKenzie, B. E.; Friedrich, H.; Wirix, M. J. M.; de Visser, J.; Monaghan, O. R.; Bomans, P. H. H.; Nudelman, F.; Holder, S. J.; Sommerdijk, N. A. J. M. Controlling Internal Pore Sizes in Bicontinuous Polymeric Nanospheres. *Angew. Chem., Int. Ed.* **2015**, *54*, 2457–2461.
52. McKenzie, B. E.; de Visser, J. F.; Friedrich, H.; Wirix, M. J. M.; Bomans, P. H. H.; de With, G.; Holder, S. J.; Sommerdijk, N. A. J. M. Bicontinuous Nanospheres from Simple Amorphous Amphiphilic Diblock Copolymers. *Macromolecules* **2013**, *46*, 9845–9848.
53. Holder, S. J.; Woodward, G.; McKenziea, B.; Sommerdijk, N. A. J. M. Semi-Crystalline Block Copolymer Bicontinuous Nanospheres for Thermoresponsive Controlled Release. *RSC Adv.* **2014**, *4*, 26354–26358.
54. McKenzie, B. E.; Holder, S. J.; Sommerdijk, N. A. J. M. Assessing Internal Structure of Polymer Assemblies from 2D to 3D CryoTEM: Bicontinuous Micelles. *Curr. Opin. Colloid Interfac. Sci.* **2012**, ***17***, 343–349.
55. Hales, K.; Chen, Z.; Wooley, K. L.; Pochan, D. J. Nanoparticles with Tunable Internal Structure from Triblock Copolymers of PAA-*b*-PMA-*b*-PS. *Nano Lett.* **2008**, *8*, 2023–2026.
56. Zhang, L.; Bartels, C.; Yu, Y.; Shen, H.; Eisenberg, A. Mesosized Crystal-like Structure of Hexagonally Packed Hollow Hoops by Solution Self-Assembly of Diblock Copolymers. *Phys. Rev. Lett.* **1997**, *79***,** 5034–5037.
57. Yu, K.; Bartels, C.; Eisenberg, A. Trapping of Intermediate Structures of the Morphological Transition of Vesicles to Inverted Hexagonally Packed Rods in Dilute Solutions of PS-*b*-PEO. *Langmuir* **1999**, *15*, 7157–7167.

58. Yu, K.; Bartels, C.; Eisenberg, A. Vesicles with Hollow Rods in the Walls: A Trapped Intermediate Morphology in the Transition of Vesicles to Inverted Hexagonally Packed Rods in Dilute Solutions of PS-*b*-PEO. *Macromolecules* **1998**, *31*, 9399–9402.

59. Cai, H.; Jiang, G.; Shen, Z.; Fan, X. Solvent-Induced Hierarchical Self-Assembly of Amphiphilic PEG(G_m)-*b*-PS Dendritic-Linear Block Copolymers. *Soft Matter* **2013**, *9*, 11398–11404.

60. Cai, H.; Jiang, G.; Chen, C.; Li, Z.; Shen, Z.; Fan, X. New Morphologies and Phase Transitions of Rod–Coil Dendritic–Linear Block Copolymers Depending on Dendron Generation and Preparation Procedure. *Macromolecules* **2014**, *47*, 146–151.

61. Percec, V.; Wilson, D. A.; Leowanawat, P.; Wilson, C. J.; Hughes, A. D.; Kaucher, M. S.; Hammer, D. A.; Levine, D. H.; Kim. A. J.; Bates, F. S.; Davis, K. P.; Lodge, T. P.; Klein, M. L.; DeVane, R. H.; Aqad, E.; Rosen, B. M.; Argintaru, A. O.; Sienkowska, M. J.; Rissanen, K.; Nummelin, S.; et al. Self-Assembly of Janus Dendrimers into Uniform Dendrimersomes and Other Complex Architectures. *Science* **2010**, *328*, 1009–1014.

62. Percec, V.; Leowanawat, P.; Sun, H.-J.; Kulikov, O.; Nusbaum, C. D.; Tran, T. M.; Bertin, A.; Wilson, D. A.; Peterca, M.; Zhang, S.; Kamat, N. P.; Vargo, K.; Moock, D.; Johnston, E. D.; Hammer, D. A.; Pochan, D. J.; Chen, Y.; Chabre, Y. M.; Shiao, T. C.; Bergeron-Brlek, M.; et al. Modular Synthesis of Amphiphilic Janus Glycodendrimers and Their Self-Assembly into Glycodendrimersomes and Other Complex Architectures with Bioactivity to Biomedically Relevant Lectins. *J. Am. Chem. Soc.* **2013**, *135*, 9055–9077.

63. Opsteen, J. A.; van Hest, J. C. M. Modular Synthesis of Block Copolymers *via* Cycloaddition of Terminal Azide and Alkyne Functionalized Polymers. *Chem. Commun.* **2005**, 57–59.

64. Jeong, M. G.; van Hest, J. C. M.; Kim, K. T. Self-Assembly of Dendritic-Linear Block Copolymers with Fixed Molecular Weight and Block Ratio. *Chem. Commun*. **2012**, *48*, 3590–3592.

65. Schröder-Turk, G. E.; Wickham, S.; Averdunk, H.; Brink, F.; Fitz Gerald, J. D.; Poladian, L.; Large, M. C. J.; Hyde, S. T. The Chiral Structure of Porous Chitin within the Wing-Scales of Callophrys rubi. *J. Struc. Biol.* **2011**, *174*, 290–295.

66. Saranathan, V.; Osuji, C. O.; Mochrie, S. G. J.; Noh, H.; Narayanan, S.; Sandy, A.; Dufresne, E. R.; Prum, R. O. Structure, Function, and Self-Assembly of Single Network Gyroid ($I4_132$) Photonic Crystals in Butterfly Wing Scales. *Proc. Natl. Acad. Sci. USA* **2010**, *107*, 11676–11681.

67. Sauranthan, V.; Seago, A. E.; Sandy, A.; Narayanan, S.; Mochrie, S. G. J.; Dufresne, E. R.; Cao, H.; Osuji, C. O.; Prum, R. O. Structural Diversity of Arthropod Biophotonic Nanostructures Spans Amphiphilic Phase-Space. *Nano Lett.* **2015**, *15*, 3735–3742.

68. Negrini, R.; Mezzenga, R. Correction to Diffusion, Molecular Separation, and Drug Delivery from Lipid Mesophases with Tunable Water Channels. *Langmuir* **2012**, *28*, 16455–16462.

69. Tyler, I. I. A.; Barriga, H. M. G.; Parsons, E. S.; McCarthy, N. L. C.; Ces, O.; Law, R. V.; Seddon, J. M.; Brooks, N. J. **Electrostatic Swelling of Bicontinuous Cubic Lipid Phases.** *Soft Matter* **2015**, *11*, 3279–3286.

70. Barriga, H. M. G.; Tyler, A. I. I.; McCarthy, N. L. C.; Parsons, E. S.; Ces, O.; Law. R. V.; Seddon, J. M.; Brooks, N. J. Temperature and Pressure Tuneable Swollen Bicontinuous Cubic Phases Approaching Nature's Length Scales. *Soft Matter* **2015**, *11*, 600–607.

Chapter 3. Mix-and-Match Assembly of Block Copolymer Blends in Solution

3.1 Abstract

The chemical structure of a block copolymer (BCP) dictates the size, shape, and function of its self-assembled structure in solution. This direct correspondence demands precision synthesis of a specific BCP with optimized structural parameters to obtain the desired nanostructures with structural and functional complexity by solution self-assembly. Here we show that the binary blends of BCPs self-assemble into the desired nanostructure in solution by adjusting the composition of the blend. By modifying the structural parameters of a binary BCP blend through control of the composition, two BCPs sharing the repeating units in both polymer blocks coassemble into the desired structures, which range from spherical micelles to inverse cubic and hexagonal mesophases. These BCP blends not only allow the direct creation of complex periodic mesoporous structures of the desired periodicity and pore size but also provide nanostructures of unprecedented morphology by simple solution self-assembly without relying on the synthesis of correspondingly designed BCPs.

3.2 Introduction

The structural analogy between amphiphilic block copolymers (BCPs)[1] and lipids has enabled the chemical structures of BCPs to be systematically designed and synthesized, resulting in self-assembled structures in solution whose morphology can be precisely controlled in accordance to their structural parameters.[2,3] Depending primarily on structural parameters such as the molecular weight and ratio between the molecular weights of the constituent polymer blocks (block ratio), the morphology of the self-assembled BCP structure in solution switches between three basic shapes (sphere, cylinder, and bilayers).[4] This block-ratio-dependent behavior of the self-assembly of BCPs in solution has recently been demonstrated by polymerization-induced self-assembly (PISA), which is based on the in situ alteration of the block ratio of BCPs during controlled polymerization of the hydrophobic polymer block initiated by water-soluble macromolecular initiators.[5] In addition, nanostructures with structural and functional complexity have also been realized by the solution self-assembly of well-defined BCPs with unusual chemical structures and architectures, such as multiblock copolymers, miktoarm copolymers, metal-containing polymers, and cyclic polymers. These include micellar networks, toroids, patch micelles, block comicelles, and their assemblies.[6–11]

Lipid cubic mesophases arise in solution when the packing parameter (P) of the lipid exceeds unity.[12–14] The packing parameter is expressed by the equation $P = V/a_0 l_c$, where V is the volume of the hydrophobic domain, a_0 is the surface area of the hydrophilic headgroup projected onto the interface,

and l_c is the critical length of the hydrophobic chain.[15] In nature, these three-dimensionally (3D) periodic structures of lipid bilayers are responsible for the formation of highly ordered periodic structures such as the endoplasmic reticulum, butterfly wing scales, and exoskeletons of insects.[16−18] Analogously, inverse mesophases of BCPs may emerge from the solution self-assembly if the *P* value of a BCP is larger than 1. The structural similarity between lipids and BCPs suggests that the high asymmetry of the block ratio (e.g., a very large hydrophobic polymer block compared to the size of a hydrophilic block) warrants the high *P* value (>1) of the BCP. However, such asymmetric BCPs rarely self-assembled into well-defined cubic mesophases in solution because the high molecular weight of a hydrophobic polymer block allows the BCPs to be easily trapped in the local energy minima during self-assembly, resulting in the formation of nonequilibrium structures.[19]

We have shown that the individual structural parameters of a BCP should be carefully adjusted to increase its *P* value above unity so that the BCP can preferentially self-assemble into inverse bicontinuous cubic mesophases without being trapped in nonequilibrium structures in a dilute solution.[20,21] The resulting well-defined 3D structures consisted of the periodic minimal surfaces of BCP bilayers, which possessed internal networks of mesoscale water channels arranged in a long-range crystalline order. These highly organized periodic structures have attracted recent attention because they are physically robust, highly functional, and could thus be directly used as functional platforms for chemical transformation, separation, and nanotemplating.[20−25] Although few BCPs and dendrimer amphiphiles have been shown to form well-defined inverse mesophases in solution,[4,26−31] the direct correspondence of the BCP structure to the outcome of its self-assembly makes it imperative that individual BCPs must be precisely synthesized with the desired architecture and structural parameters in order to obtain the targeted morphology and phase of the self-assembled structures available from the solution self-assembly of BCPs.

Physical and chemical properties of commodity polymers can be readily modified by mixing chemically distinct polymers (polymer blends) without synthesizing new polymers or copolymers.[32] The self-assembly of the binary blends of BCPs of same chemical structures but different molecular weights and block ratios was investigated in bulk.[33−35] Selfassembly of BCP blends has recently emerged as a means to create and fine-tune the resulting nanostructures in solution without relying on the synthesis of a specific BCP.[36−39] We imagined that mixing two BCPs, each representing the low and high *P* value, might be a nonsynthetic method to modulate the *P* value of the resulting binary blend in accordance with the composition of constituent BCPs. When two BCPs share the chemical structures of the repeating units for the constituent polymer blocks, but differ only in the block ratio, we presumed that the resulting binary BCP blends of varying compositions would self-assemble in solution without experiencing phase separation. In this case, the phase and morphology of the self-assembled

nanostructures of each BCP blend should be dictated by the P value, which would be decided by the composition of two BCPs (Figure 3-1).

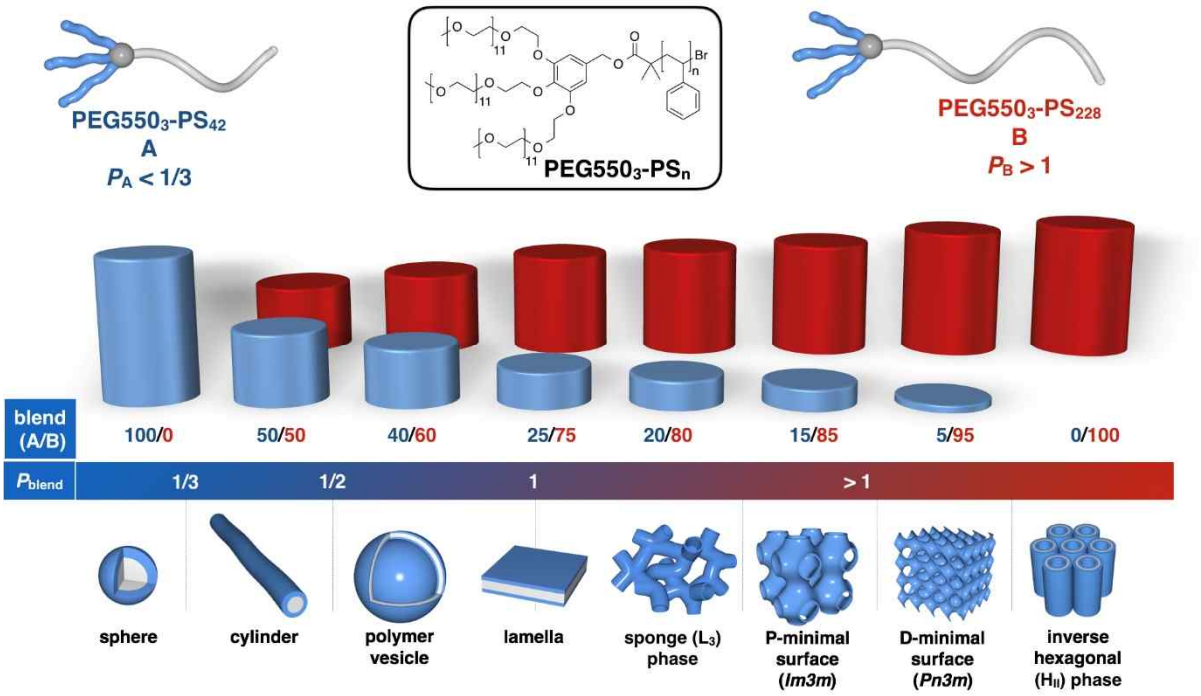

Figure 3-1. Schematic diagram illustrating the mix-and-match process. The BCP blends were composed of two BCPs, one with a low and the other with a high *P* value. The composition of the BCPs determines the *P* value of the binary blend (P_{blend}), which dictates the morphology and phase of the resulting self-assembled structures.

Here we show that the binary blends of BCPs self-assemble into the desired nanostructure in solution by adjusting the composition of two BCPs, representing smaller and larger *P* values, respectively. By modifying the *P* value of a binary BCP blend through control of the composition, two BCPs sharing the repeating units in both polymer blocks coassemble into the desired structures, which range from spherical micelles to inverse cubic and hexagonal mesophases. We demonstrate that these BCP blends directly form complex periodic mesoporous structures of the desired periodicity and pore size but also provide nanostructures of unprecedented morphology by simple solution self-assembly without relying on the synthesis of correspondingly designed BCPs.

3.3 Results and discussion

Mix-and-match self-assembly of branched-linear BCP blends in solution.

To test our concept of the solution self-assembly of BCP blends, we synthesized amphiphilic BCPs by atom-transfer radical polymerization (ATRP) of styrene in the presence of a branched hydrophilic macroinitiator with three peripheral poly(ethylene glycol) (PEG, number-averaged molecular weight (M_n) of 550 g mol^{-1}) chains (Figure 3-1 and Table 3-1). Previously, we showed that the resulting branched-linear BCPs, PEG550$_3$−PS$_n$ (the subscript n denotes the number-average degree of polymerization (DP_n) of polystyrene), exhibited a large molecular area at the air-water interface due to the presence of the branched PEG hydrophilic block compared to that of the BCPs having a linear PEG block with the same molecular weight and block ratio.[20,21] From this enlarged molecular area of the BCP at the air-water interface, we inferred that the interfacial surface area of the hydrophilic block (a_0) of the braned-linear BCP would force the hydrophobic PS block to adopt a less stretched conformation, resulting in a reduced critical chain length (l_c) upon self-assembly. [21] These structural characteristics of PEG550$_3$-PS$_n$ yielded the P value of the BCP to be greater than 1 when the volume of the PS block (V) was sufficiently large, and consequently, the block ratio of the BCP, defined by the molecular weight fraction of the PEG chains (w_{PEG}), was small (<9%). All BCPs were subjected to self-assemble in aqueous solution. Self-assembled structures were formed by the addition of water, a selective solvent for the PEG polymer domain, at a rate of 1 mL h^{-1} into a dioxane solution of the BCP (1 wt %), followed by removal of the organic solvent by dialysis against water. The morphology of the self-assembled structures of the BCP was used for estimating the P value of the BCP (Table 3-1).

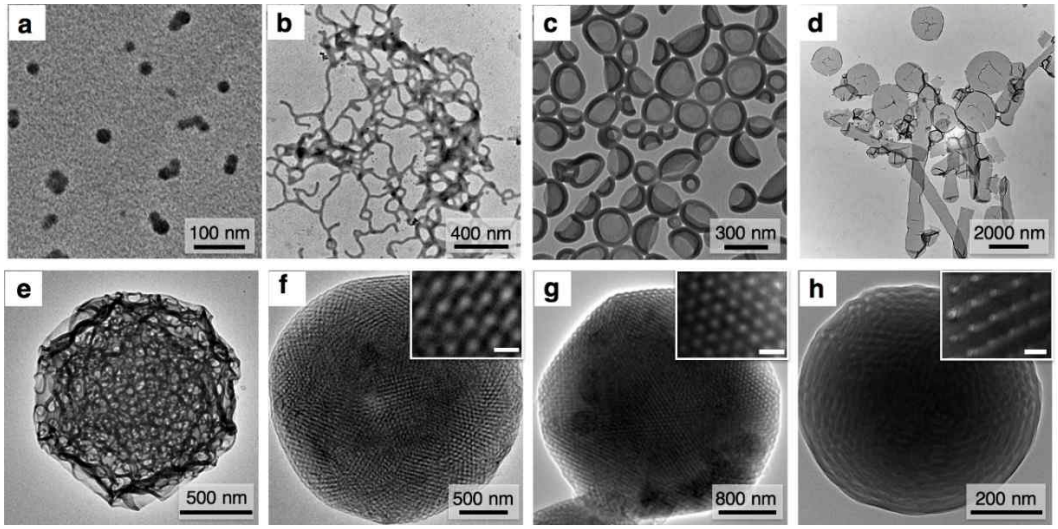

Figure 3-2. Transition of morphology of the self-assembled structure of BCP blends. (a−h) Representative TEM images of the self-assembled structures of the BCP blends, $PEG550_3$-PS_{42}-$PEG550_3$-PS_{228} with varying compositions: (a) Spherical micelles ($PEG550_3$-PS_{42}: $PEG550_3$-PS_{228} = 100:0, w/w). (b) Cylindrical micelles (50:50). (c) Polymer vesicles (40:60). (d) Flat bilayers (25:75). (e) Sponge phase particles (20:80). (f) Polymer cubosomes of Schwarz P-surfaces (15:85). The inset shows a (100) plane of the P-surface (scale bar = 50 nm). (g) Polymer cubosomes of Schwarz D-surfaces (5:95). The inset shows a (100) of the D-surface (scale bar = 50 nm). (h) Polymer hexasomes (0:100). The inset shows a (110) plane of the HII phase (scale bar = 20 nm).

For the preparation of the binary BCP blends, we chose two BCPs, $PEG550_3$-PS_{42} and $PEG550_3$-PS_{228}, which possess an identical branched PEG hydrophilic block attached to hydrophobic PS blocks of different molecular weights. $PEG550_3$-PS_{42}, representing a BCP having a smaller *P* value (component A in Figure 3-1), self-assembled to form spherical micelles in solution, which was confirmed by transmission electron microscopy (TEM) and dynamic light scattering (DLS) (Figure 3-2A and Figure 3-3). From this result, we inferred that the *P* value of $PEG550_3$-PS_{42} should be smaller than 1/3.[2,3,14] Under the same conditions, $PEG550_3$-PS_{228}, representing a BCP with a larger *P* value (component B in Figure 3-1), only self-assembled into large particles with an internal inverse hexagonal structure (hexasomes, H_{II} phase), which suggests that its *P* value should be greater than 1 (Figure 3-2h).[4,13,25] The solution blends of these two BCPs were prepared by dissolving them in dioxane (1 wt %) with varying compositions, followed by equilibration for 24 h at room temperature. Gel permeation chromatography (GPC) of these blends showed two separate peaks in the chromatograms corresponding to the values of M_n of the constituent BCPs, which distinguished the BCP blend from a single BCP with a unimodal and broad size distribution (Figure 3-4).

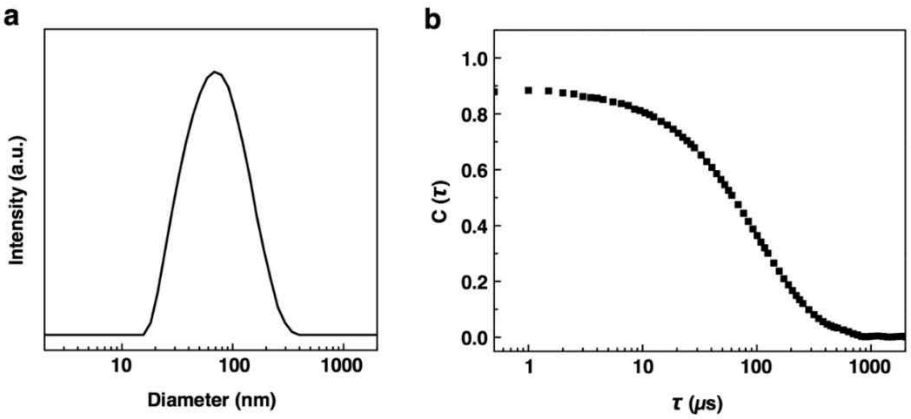

Figure 3-3. DLS results of micellar solution of $PEG550_3$-PS_{42}. (a) Size distributions and (b) autocorrelation functions of spherical micelle. The average diameters of $PEG550_3$-PS_{42} were 62.42 nm (dispersity 0.27).

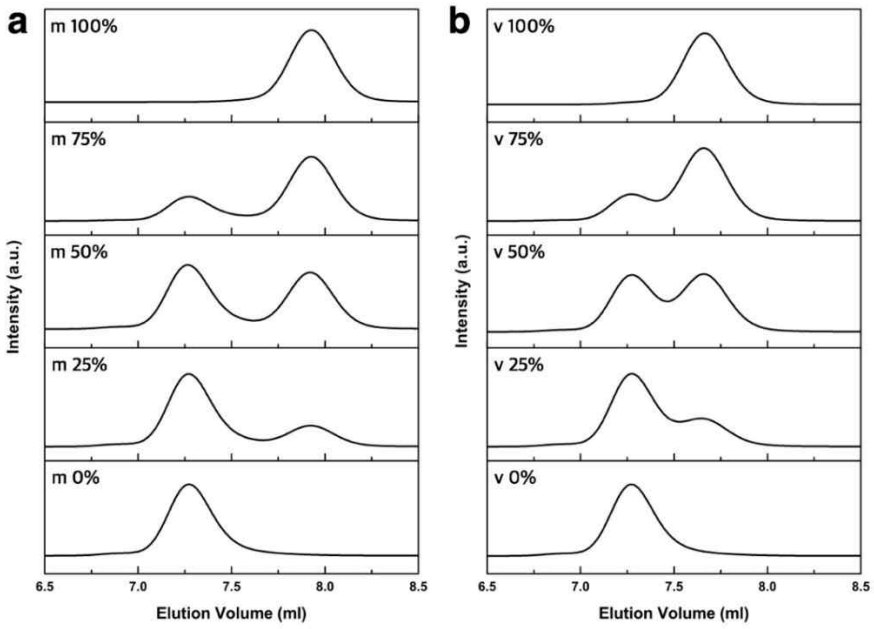

Figure 3-4. Gel permeation chromatography (GPC) results of polymer blends of (a) $PEG550_3$-PS_{42} (M_n = 6800 g mol^{-1}, $Đ$ = 1.06) and $PEG550_3$-PS_{228} (M_n = 23000 g mol^{-1}, $Đ$ = 1.07); (b) $PEG550_3$-PS_{105} (M_n = 7700 g mol^{-1}, $Đ$ = 1.06) and $PEG550_3$-PS_{228} (M_n = 23000 g mol^{-1}, $Đ$ = 1.07). (m = $PEG550_3$-PS_{42}, micelle; v = $PEG550_3$-PS_{105}, vesicle; wt%).

These BCP blend solutions were allowed to self-assemble under the same condition for the self-assembly of an individual BCP. When we used TEM to study the resulting aqueous suspensions of the BCP blends, we found that the morphology of the structure transformed from spherical micelles of pure $PEG550_3$-PS_{42} to cylindrical micelles and vesicles in the presence of 50 and 60 wt %, respectively, of $PEG550_3$-PS_{228} in the BCP blend (Figure 3-2a−c). When the fraction of $PEG550_3$-PS_{228} was increased to 75%, the morphology turned to flat lamella, suggesting that the *P* value of the BCP blend was close to unity (Figure 3-2d and Figure 3-5). When the fraction of $PEG550_3$-PS_{228} exceeded 75%, the resulting BCP blends self-assembled into inverse mesophase structures with a negative Gaussian curvature along the surface.[13,14] As the fraction of $PEG550_3$-PS_{228} continued to increase, the inverse phase structures transformed from sponge phase (L_3) particles (Figure 3-2e and Figure 3-6) to colloidal particles composed of periodic minimal surfaces (polymer cubosomes), of which the internal structure had a primitive cubic crystalline lattice (Figure 3-2f) and a double diamond lattice (Figure 3-2g). When the fraction of $PEG550_3$-PS_{228} in the binary blend exceeded 95%, only hexasomes (H_{II} phase) were observed by TEM (Figure 3-2h).

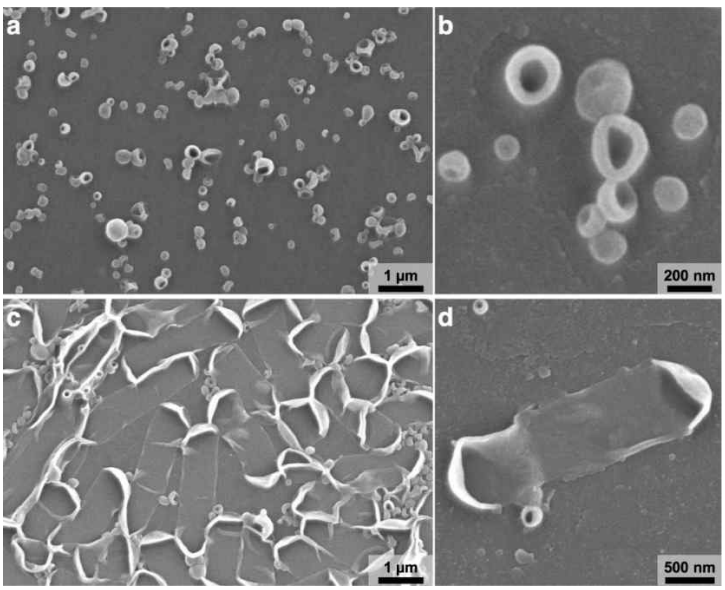

Figure 3-5. SEM image of (a and b) polymer vesicles of the BCP blend of $PEG550_3$-PS_{42}–$PEG550_3$-PS_{228} (40:60, w/w) and (c and d) flat bilayers (25:75, w/w).

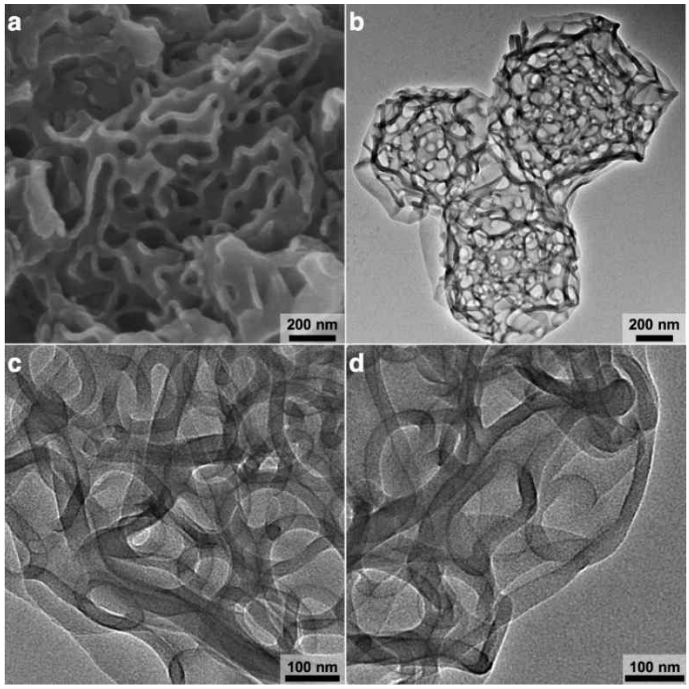

Figure 3-6. SEM and TEM images of irregular sponge (L_3) phase of the BCP blend of PEG550$_3$-PS$_{42}$–PEG 550$_3$-PS$_{228}$ (20/80, w/w). (a) SEM image of internal structure of irregular sponge phase. TEM image of representative irregular sponge phase (b) and its internal structures (c and d).

We used scanning electron microscopy (SEM) to further investigate the phase transitions, triggered by changes in the BCP composition, of inverse mesophases of the BCP blends. As the fraction of PEG550$_3$-PS$_{228}$ was gradually increased from 80 to 95%, SEM images of the dried self-assembled structures of the PEG550$_3$-PS$_{42}$-PEG550$_3$-PS$_{228}$ blends clearly showed the phase transition of inverse mesophases of the BCP blends from the irregular sponge (L_3) phase to the polymer cubosomes composed of a Schwarz P-minimal surface with a primitive cubic lattice (Figure 3-7a−d) and polymer cubosomes constructed of a Schwarz D-surface with a double diamond lattice (Figure 3-7e−h). The internal structures eventually transformed to inverse hexagonal structures (H_{II} phase) when the fraction of PEG550$_3$-PS$_{228}$ was higher than 95% in the BCP blend (Figure 3-7i−k). Synchrotron small-angle X-ray scattering (SAXS) results of these structures confirmed the observed phase transition from the sponge phase to the Schwarz P-surface (Figure 3-7l; *Im3m*, lattice constant (a) = 60.4 nm) and the Schwarz D-surface (Figure 3-7M; *Pn3m*, a = 42.8 nm) and the inverse hexagonal phase (Figure 3-7n; *P6mm*, a = 30.2 nm) as the composition of the BCP blend was varied. Remarkably, the BCP blends did not show any formation of spherical micelles and hexasomes arising from the self-assembly of the individual BCPs with a wide range of compositions, indicating that no phase separation occurred between the BCPs during self-assembly (Figure 3-8).

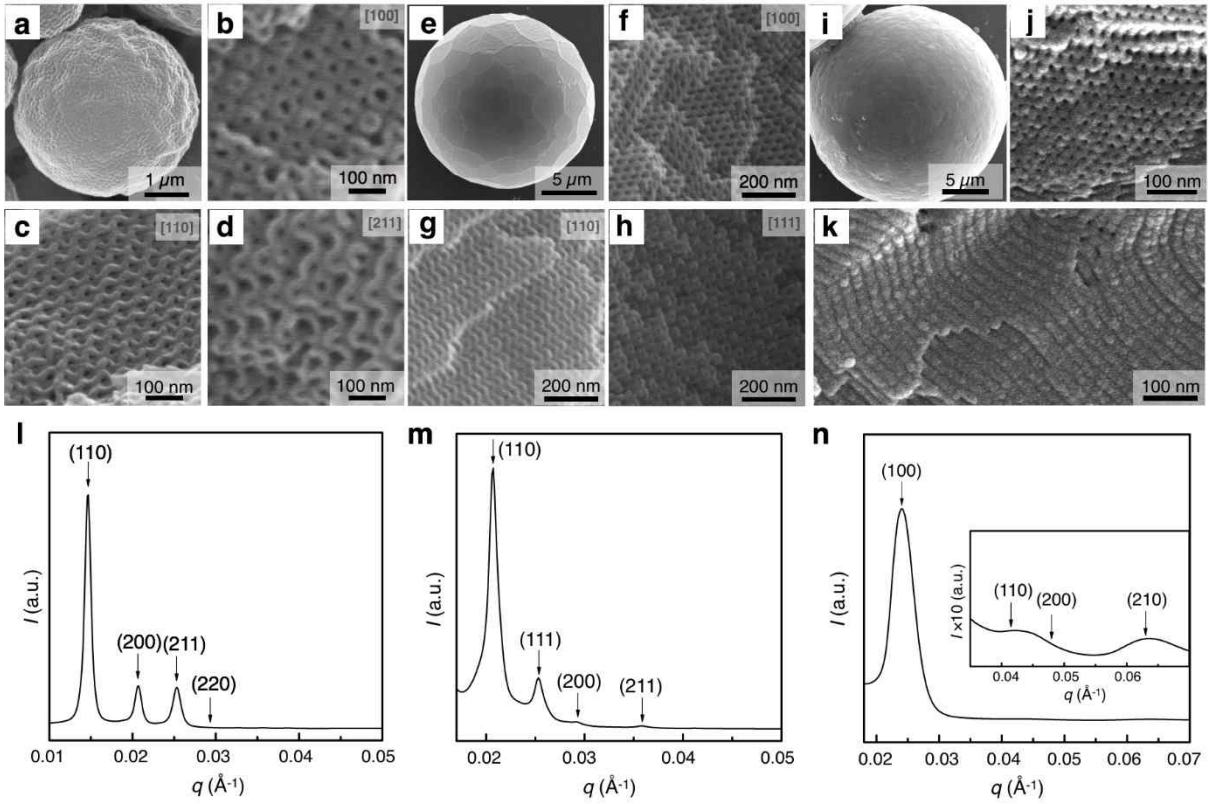

Figure 3-7. Internal structures of polymer cubosomes and hexasomes of the BCP blends. (a−d) SEM images of the polymer cubosomes of the BCP blend of $PEG550_3$-PS_{42} and $PEG550_3$-PS_{228} (15:85, w/w), showing a Schwarz P-minimal surface of BCP bilayers viewed along the (b) [100], (c) [110], and (d) [211] directions. (e−h) SEM images of the polymer cubosomes of a $PEG550_3$-PS_{42}-$PEG550_3$-PS_{228} blend (5:95, w/w) showing a Schwarz D-minimal surface viewed along the (f) [100], (g) [110], and (h) [111] directions. (i−k) SEM images of the polymer hexasomes of $PEG550_3$-PS_{228} showing H_{II} phase. (l) SAXS result of the dried polymer cubosomes of a $PEG550_3$-PS_{42}-$PEG550_3$-PS_{228} (15:85, w/w) blend assigned to primitive cubic symmetry (*Im3m* space group, a = 60.4 nm). (m) SAXS result of the dried polymer cubosomes of a $PEG550_3$-PS_{42}-$PEG550_3$-PS_{228} (5:95, w/w) blend assigned to double diamond symmetry (*Pn3m* space group, a = 42.8 nm). (n) SAXS result of the dried polymer hexasomes of $PEG550_3$-PS_{228} showing the H_{II} phase (*P6mm* space group, a = 30.2 nm).

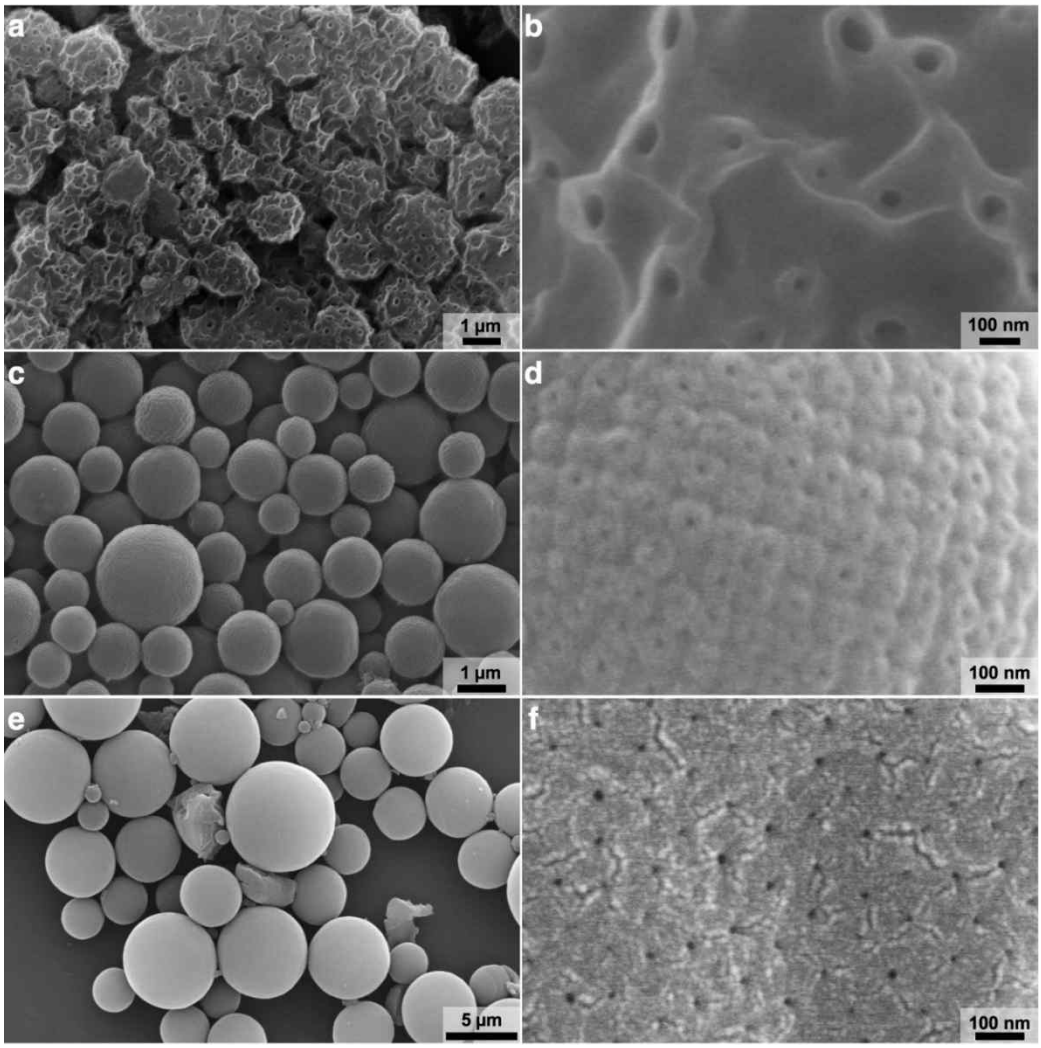

Figure 3-8. Phase transition of inverse mesophases of block copolymer blends of $PEG550_3$-PS_{42} and $PEG\ 550_3$-PS_{228}. SEM image of (a and b) sponge phase particles, (c and d) polymer cubosomes with primitive cubic (*Im3m*) symmetry, and (e and f) polymer cubosomes with double diamond (*Pn3m*) symmetry.

To investigate the generality of our approach of mixing two BCPs with distinct *P* values to modulate the *P* value of the BCP mixture, we performed the same experiments with a pair of BCPs, $PEG550_3$-PS_{56} ($1/3 < P < 1/2$) and the $PEG550_3$-PS_{228} ($P > 1$). The same transitions of phase and morphology were observed from the self-assembly of the binary blends of $PEG550_3$-PS_{56} ($1/3 < P < 1/2$) and the $PEG550_3$-PS_{228} ($P > 1$), showing all the morphologies and phases that existed between the cylindrical micelles and hexasomes (Figures 3-9 and Figures 3-10). These results agree with the phase transition observed in the solution self-assembly of a series of branched−linear BCPs with increasing the M_n of

the hydrophobic PS block.[23] Considering the findings of previous studies on the relationship between the structure of a lipid and its assemblies,[14,40] our results strongly suggest that the *P* value of the binary BCP blend was proportionally increased with respect to the fraction of the constituent BCP with the higher *P* value. As a result, the phase and morphology of the self-assembled structures of the BCP blend could be controlled simply by adjusting the composition of the two constituent BCPs, without relying on the precise synthesis of a correspondingly designed BCP. Accordingly, we have named our method the "mix-and-match" approach to self-assembly.

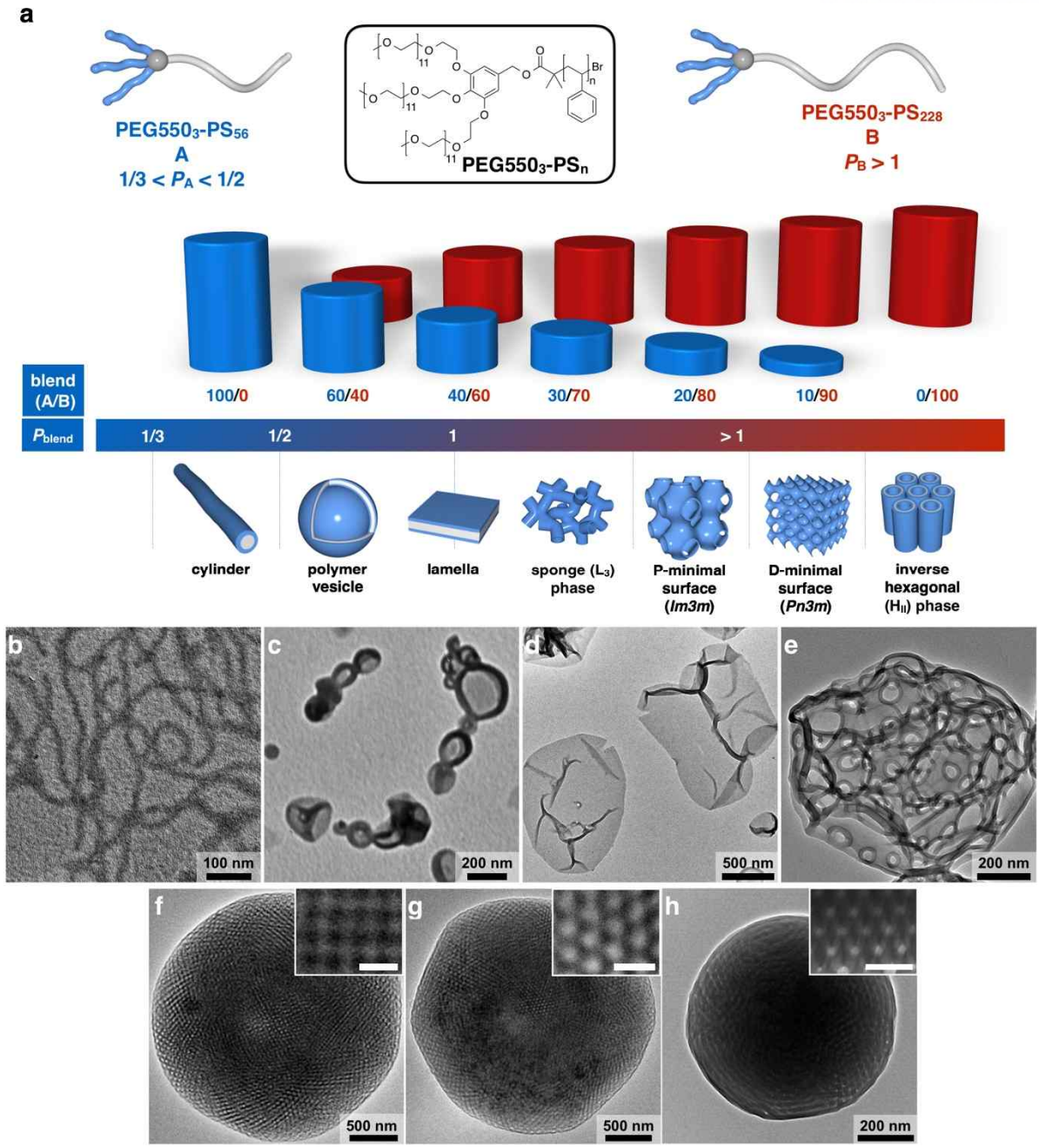

Figure 3-9. (a) Schematic diagram illustrating another mix-and-match process between PEG550$_3$-PS$_{56}$ and PEG 550$_3$-PS$_{228}$. (b–h) Representative TEM images of the self-assembled structures of the BCP blends, PEG550$_3$-PS$_{56}$–PEG550$_3$-PS$_{228}$ with varying compositions. (b) cylindrical micelles (PEG550$_3$-PS$_{56}$–PEG550$_3$-PS$_{228}$ = 100/0, w/w); (c) polymer vesicles (60/40, w/w); (d) flat bilayers (40/60, w/w); (e) sponge phase particles (30/70, w/w); (f) polymer cubosomes of Schwarz P-surfaces (20/80, w/w); (g) polymer cubosomes of Schwarz D-surfaces (10/90, w/w); (h) polymer hexasomes (0/100, w/w). The scale bars in the insets are 50 nm.

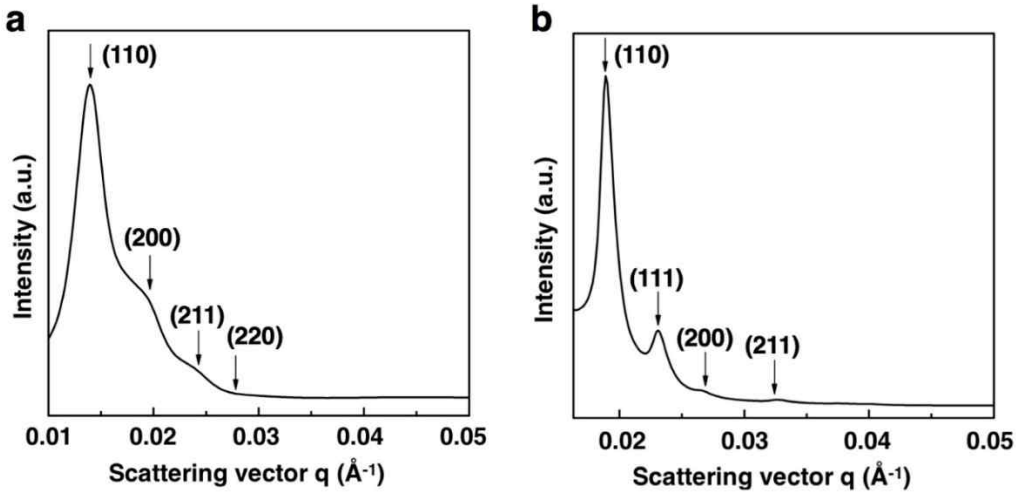

Figure 3-10. SAXS result of (a) polymer cubosomes of the BCP blend of $PEG550_3$-PS_{56}–$PEG550_3$-PS_{228} (20:80, w/w). The peaks were assigned to *Im3m* space group (a = 63.8 nm) and (b) polymer cubosomes of the BCP blend with a composition of 10:90 (w/w). The peaks were assigned to *Pn3m* space group (a = 47.0 nm).

Contol of Pore Size and Periodicity of Polymer Cubosomes by Mix-and-Match Assembly.

Solution self-assembly of BCP blends into periodic minimal surfaces of BCP bilayers offers a direct route to prepare physically robust mesoporous polymers, which possess diverse functional groups throughout the surface of the 3D defined networks of internal water channels. The ability to control the lattice, periodicity, and pore size of the mesoporous networks within the minimal surfaces could yield tailor-made mesoporous structures for separation and nanotemplating.[41−44] Therefore, we investigated the possibility of our mix-and-match approach of self-assembly to provide such controls by simply adjusting the composition of BCP blends. We found that the BCP blends of $PEG550_3$-PS_{105} and $PEG550_3$-PS_{228} only self-assembled to form the polymer cubosomes when the fraction of $PEG550_3$-PS_{105}, only forming polymer vesicles ($1/2 < P < 1$), was in a range of 15−27% (Figure 3-11). SEM images of the dried polymer cubosomes of the BCP blends clearly showed that the lattice of the polymer cubosomes retained the double diamond structure, but the periodicity of the polymer cubosomes gradually increased as the fraction of $PEG550_3$-PS_{105} increased from 15 to 27% (Figure 3-12a−c). SAXS results of the dried polymer cubosomes of the BCP blends corroborated the SEM results, which showed that the symmetry of the crystalline lattice of the periodic minimal surface was preserved in the double diamond lattice (*Pn3m*), but the a value was gradually increased from 32.6 to 58.4 nm in proportion to the increase in the fraction of $PEG550_3$-PS_{105} from 15 to 27% in the BCP blend (Figure 3-12d).

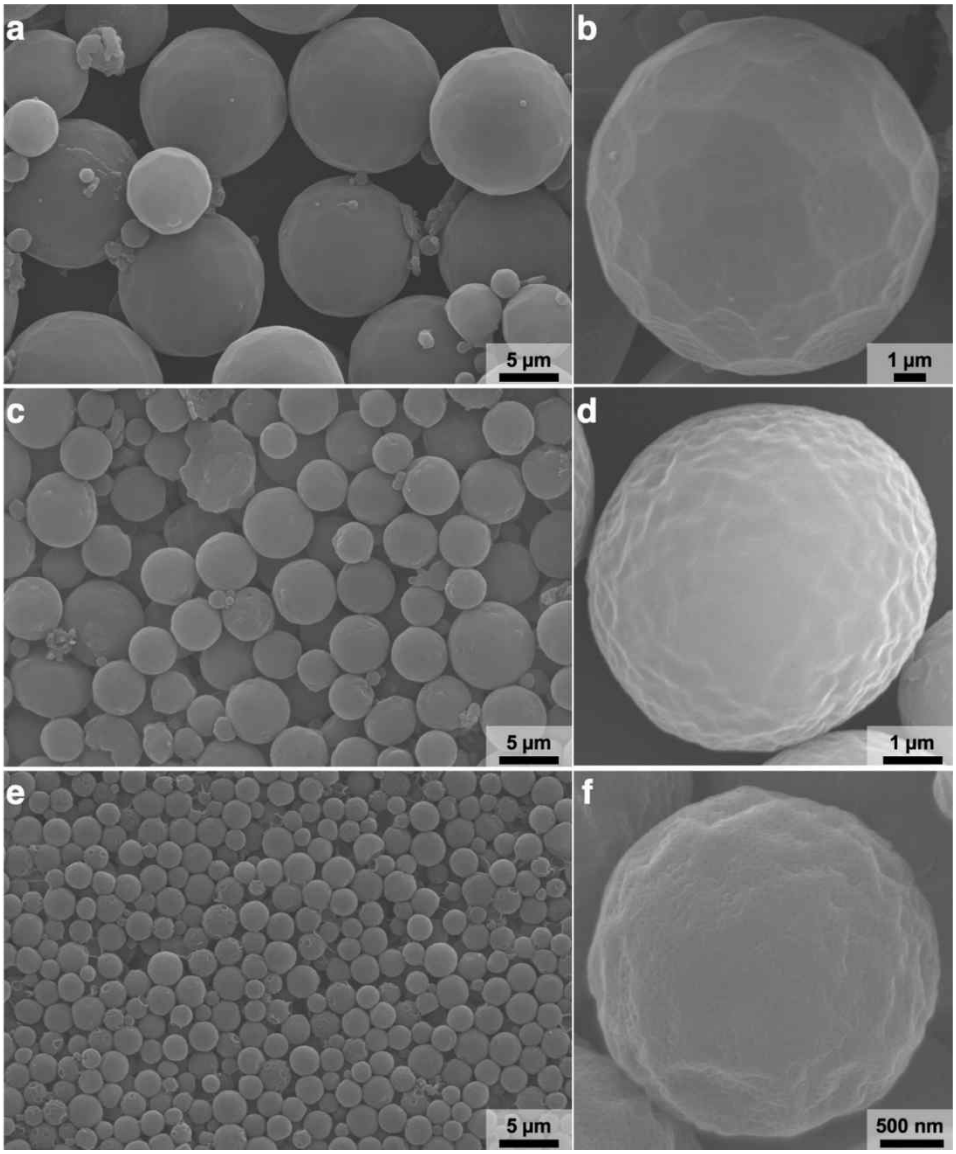

Figure 3-11. Representative SEM images of polymer cubosomes of BCP blends of $PEG550_3$-PS_{105} and $PEG550_3$-PS_{228} with the ratio of (a and b) 15/85, w/w; (c and d) 23/77, w/w; and (e and f) 27/73, w/w.

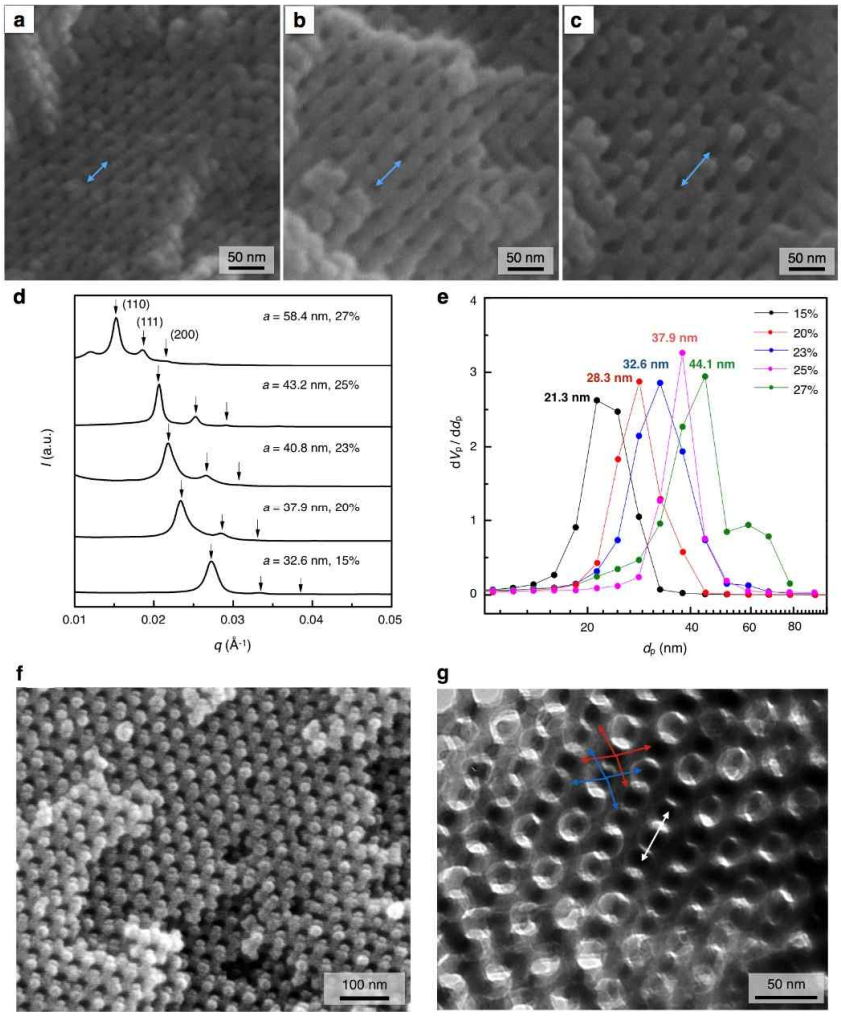

Figure 3-12. Control of the periodicity and pore size of water channel networks among polymer cubosomes of BCP blends. (a−c) SEM images showing the (111) plane of the lattice of the Schwarz D-surface of polymer cubosomes of BCP blends of $PEG550_3$-PS_{105}-$PEG550_3$-PS_{228} with the composition of (a) 15:85, w/w, pore distance (d) = 36.4 nm; (b) 23:77, w/w, d = 51.0 nm; and (c) 27:73, w/w, d = 62.8 nm. (d) SAXS results of these polymer cubosomes showing double diamond symmetry (*Pn3m* space group). The a value of the polymer cubosomes was gradually increased from 32.6 nm for the blend of $PEG550_3$-PS_{105}-$PEG550_3$-PS_{228} with the composition of 15:85, w/w, to 58.4 nm with the composition of 27:73, w/w. (e) The BJH pore size distributions of the polymer cubosomes of the blends of $PEG550_3$-PS_{105}-$PEG550_3$-PS_{228} with different compositions. (f) SEM image of the silica replica of the internal water channels of the polymer cubosomes of the BCP blend of $PEG550_3$-PS_{105}-$PEG550_3$-PS_{228} (23:77, w/w). (g) TEM image of the silica replica shows two noninterpenetrating single diamond networks (*Fd3m* space group), which are marked by red and blue arrows, respectively. The distance between 4-folded junctions of the diamond network was 43.5 nm (white line).

The thickness of a BCP bilayer scales in proportion to the square root of the molecular weight of a hydrophobic polymer block.[4,45] Therefore, the molecular weight of the BCP should be substantially larger for the formation of periodic minimal surfaces with higher periodicity.[22] Given the constant thickness of the BCP bilayers (~16 nm, Figure 3-13) observed in the TEM images of the polymer cubosomes of BCP blends, the increase in periodicity of the polymer cubosomes strongly suggests that the diameter of the water channels weaving through the periodic minimal surfaces could also be increased in accordance with the change in composition of the BCP blends.46 We measured the distribution of the diameter of water channels of the polymer cubosomes of the BCP blends from the Barret−Joyner−Halenda (BJH) pore-size distribution curves obtained from N_2 adsorption−desorption isotherms of the polymer cubosomes at 77 K. As the fraction of $PEG550_3$-PS_{105} was increased from 15 to 27 wt % in the BCP blend, the average pore size of the networks of water channels in the polymer cubosomes was proportionally enlarged from 21 to 44 nm (Figure 3-12e). The Brunauer−Emmett−Teller (BET) surface areas of the polymer cubosomes of the BCP blend remained at ~130 m^2 g^{-1} (Figure 3-14).

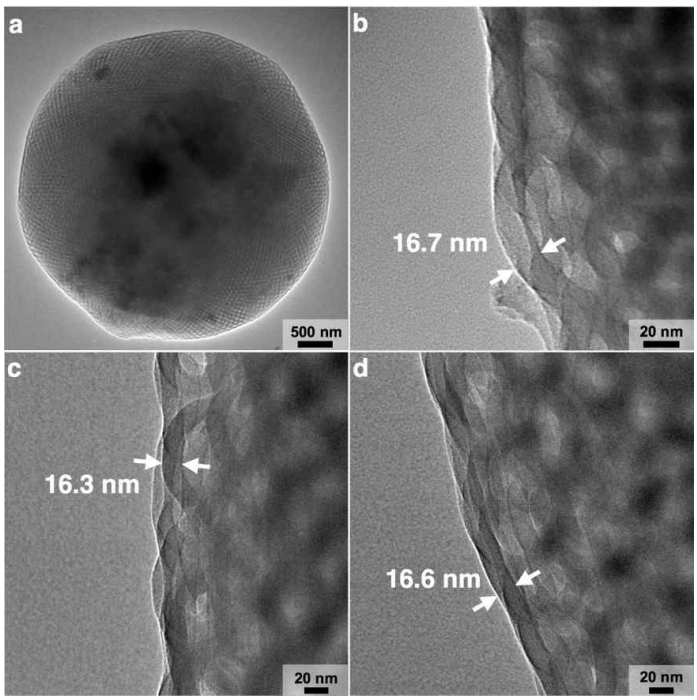

Figure 3-13. TEM images of the polymer cubosomes of BCP blends of $PEG550_3$-PS_{105} and $PEG550_3$-PS_{228} with a composition of (a) 23/77, w/w; (b) 15/85, w/w; (c) 23/77, w/w; (d) 27/73, w/w. (b–c) Arrows indicate the thickness of the bilayer shells of the polymer cubosomes (16.7 nm in b, 16.3 nm in c, 16.6 nm in d).

To visualize the pore networks within the polymer cubosomes of the BCP blend, we synthesized the skeletal replica of the pore network by sol−gel reaction of backfilled tetraethyl orthosilicate (TEOS) under acidic conditions. Using the polymer cubosome of the BCP blend of $PEG550_3$-PS_{105} and $PEG550_3$-PS_{228} (23:77 w/w) as a template, cross-linking of backfilled TEOS and calcination at 500 °C gave spherical replica of the polymer cubosomes (Figure 3-15). SEM image of the fractured silica replica of the polymer cubosomes showed the skeletal networks formed within the water channel networks residing in the double diamond structure of the BCP bilayers (Figure 3-12f). TEM image of the skeletal replica also showed the presence of two noninterpenetrating skeletal networks (labeled with red and blue arrows, respectively). The distance between two adjacent 4-fold functions of the single skeletal network was measured to be 43.5 nm (Figure 3-12g), which was reduced from the distance between two adjacent channels (51 nm) measured from the SEM image of the polymer cubosome template (blue arrow in Figure 3-12b). This was attributed to the shrinkage of the silica skeletal networks during the calcination. These results suggest that the mix-and-match self-assembly of BCP blends could be a means to tailor the periodicity and pore size of the periodic minimal surfaces of BCP bilayers to the levels routinely observed in periodic biological structures without significantly altering the molecular weights of BCPs.[16−18]

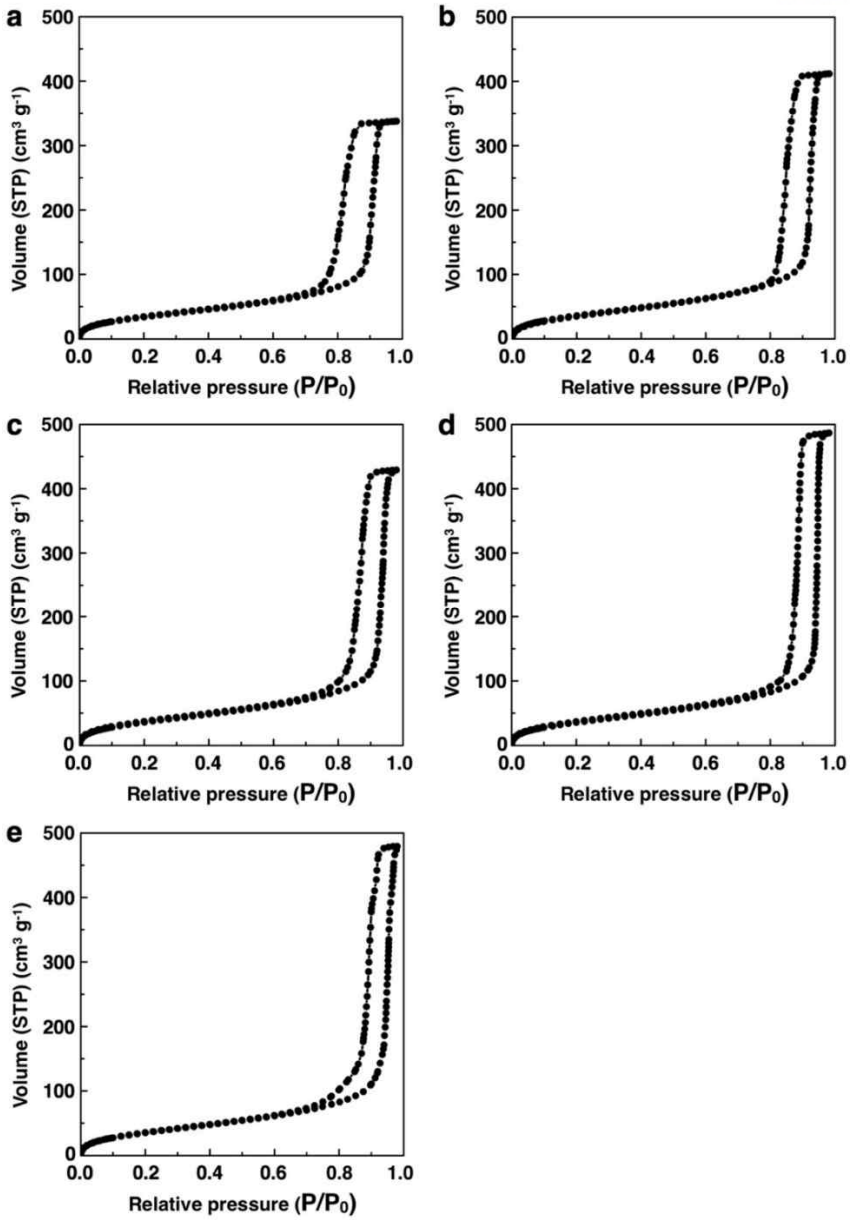

Figure 3-14. N_2 adsorption–desorption isotherms measured at 77 K of the polymer cubosomes of the BCP blends of $PEG550_3$-PS_{105}–$PEG550_3$-PS_{228} with a composition of (a) 15/85 (w/w); (b) 20/80 (w/w); (c) 23/77 (w/w); (d) 25/75 (w/w); (e) 27/73 (w/w). The BET surface area and pore volume are (a) 130 $m^2\ g^{-1}$ / 0.52 $cm^3\ g^{-1}$, (b) 138 $m^2\ g^{-1}$ / 0.64 $cm^3\ g^{-1}$ (c) 138 $m^2\ g^{-1}$, 0.66 $cm^3\ g^{-1}$, (d) 137 $m^2\ g^{-1}$, 0.75 $cm^3\ g^{-1}$, and (e) 136 $m^2\ g^{-1}$, 0.74 $cm^3\ g^{-1}$.

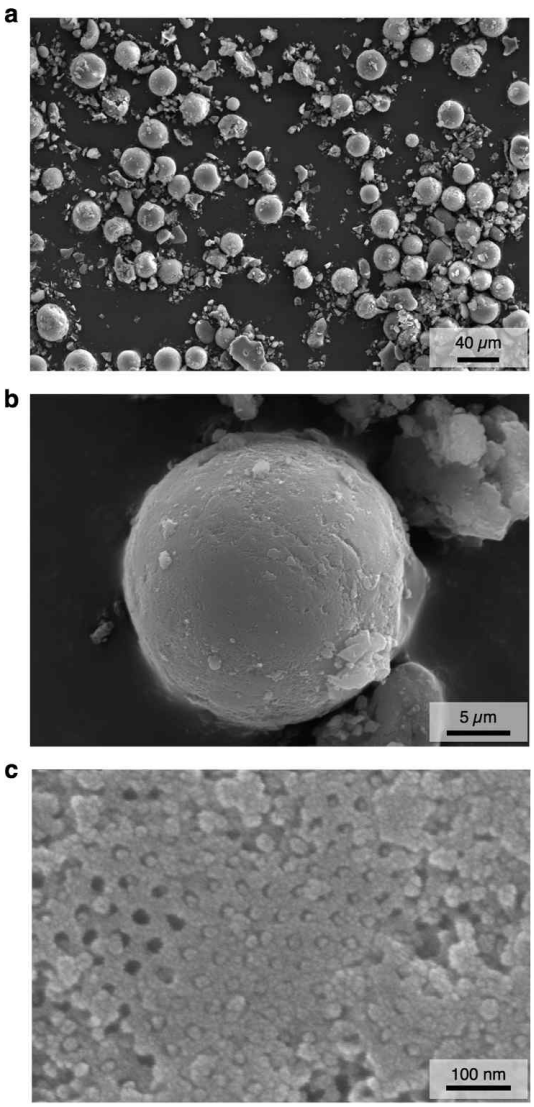

Figure 3-15. (a–c) SEM images of the silica replica of the polymer cubosomes of the BCP blend of $PEG550_3$-PS_{105} and $PEG550_3$-PS_{228} (23:77 w/w). The silica replica was synthesized by sol-gel reaction of TEOS under acidic condition using the polymer cubosome as a template.

Formation of Hexasome Flowers.

The mix-and-match approach to solution self-assembly of BCP blends not only allowed us to transform the morphologies of self-assembled nanostructures without synthesizing new BCPs but also provided a chance to discover new nanostructures. Previously, we prepared BCP blends composed of a branched−linear BCP, $PEG550_3$-PS_{231}, and a α-functionalized linear BCP, NH_2-PEG2000-PS_{210}. When used as a minor component (<12 wt %), the increasing presence of NH_2-PEG2000-PS_{210} in the BCP

blend induced a phase transition of the polymer cubosomes from a double diamond phase (*Pn3m*) to a primitive cubic phase (*Im3m*).[21] In addition, the entire surface of each resulting polymer cubosome was decorated with amino groups, which resulted from the homogeneous distribution of the end-functionalized linear BCP throughout the bilayer of the BCP blend. Surface functional groups protruding from the surface of the internal networks of water channels within the polymer cubosomes could anchor large guest molecules such as proteins and their complexes.[20,25]

We extended this mix-and-match strategy to the preparation of BCP blends of $PEG550_3$-PS_{251} ($P > 1$) and NH_2-PEG2000-PS_{184}. Contrary to our expectation of a gradual phase transition from inverse hexagonal to bicontinuous cubic phases with increasing fraction of NH_2-PEG2000-PS_{184} in the blend, the self-assembled structures of the BCP blend did not undergo phase transition from hexasomes to flat bilayers and polymer vesicles until the fraction of the linear BCP reached to 70 wt %. Surprisingly, SEM and TEM images of the self-assembled structures of the BCP blends showed that as the fraction of NH_2-PEG2000-PS_{184} in the BCP blend increased, the outermost bilayers of the hexasomes gradually loosened to form polymer vesicles tethered to the hexasome core (Figure 3-16a−d). As Figure 3-16e shows, TEM image of the self-assembled structures, hereafter referred to as hexasome flowers, revealed that the core of the structure possessed hexasome-like internal structures. We used these hexasome flowers as templates for the sol−gel synthesis of silica. After cross-linking of infiltrated TEOS under acidic condition, followed by removal of the hexasome flower templates in THF, we observed bundles of silica cylinders (Figure 3-16f and Figure 3-17), which were replicas of hexagonally packed water channels within the inverse hexagonal core of the hexasome flower. This observation corroborated that the internal phase of the hexasome core was indeed inverse hexagonal phase rather than bicontinuous structures.

Because the linear BCP NH_2-PEG2000-PS_{184} only self-assembled into polymer vesicles in an aqueous solution ($1/2 < P < 1$) (Figure 3-18), we suspected that the blossoming of the hexasomes of the BCP blend into hexasome flowers in the presence of the linear BCP might have originated from the phase separation of the linear BCP from the branched−linear BCP forming the hexasome core, which would have increased the amount of the linear BCP on the crust of the hexasome. To investigate this possibility, we labeled the surface amino groups protruding from the BCP bilayers consisting of the hexasome flowers with fluorescamine, a pro-fluorescent dye that only fluoresces upon reaction with amine.

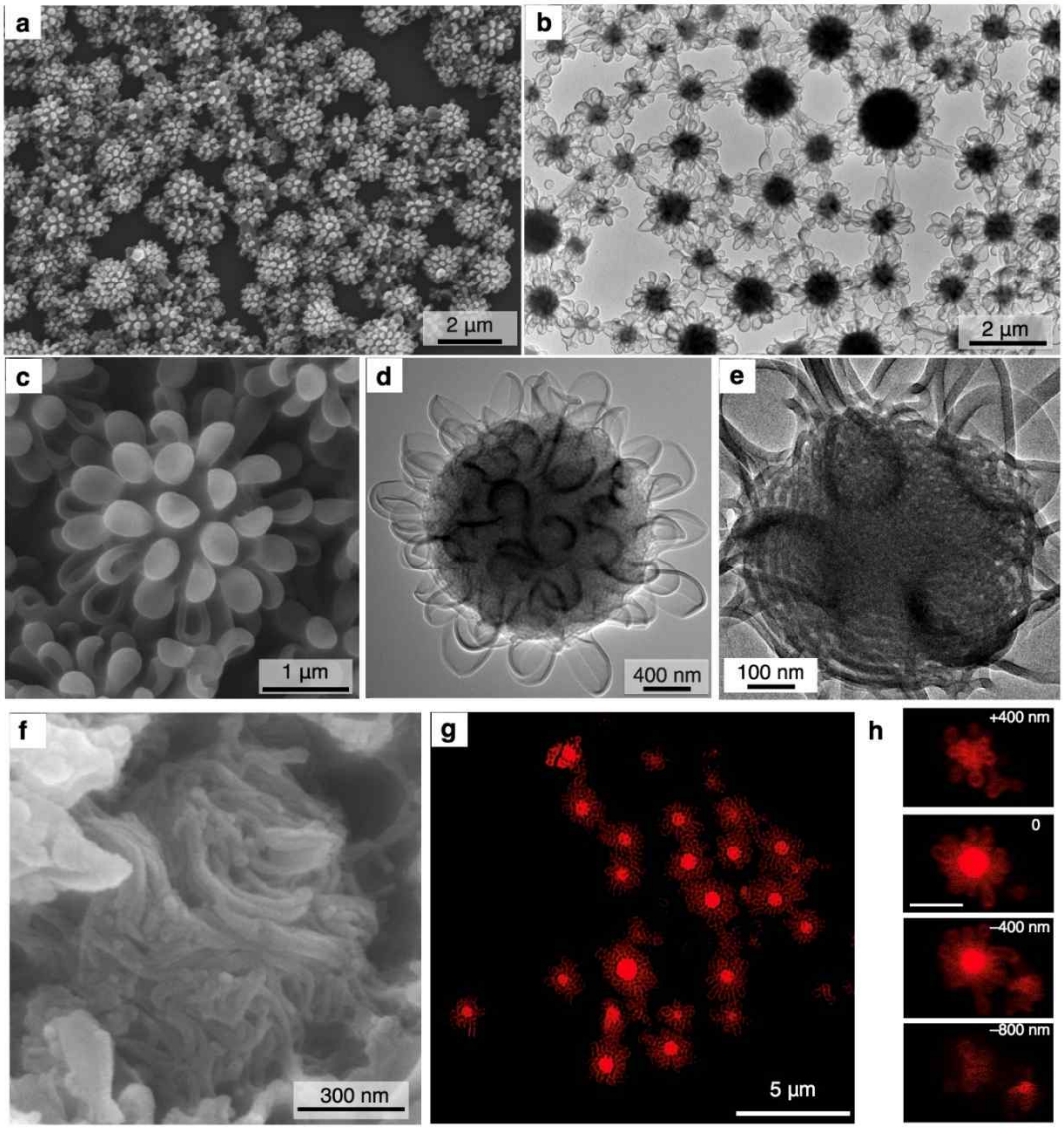

Figure 3-16. Hexasome flowers of the BCP blends. (a, b) Low magnification (a) SEM and (b) TEM image of the hexasome flowers of the BCP blends of NH_2-PEG2000-PS_{184}-PEG550_3-PS_{251} at the composition of 30:70 (w/w). (c, d) High magnification images showed the vesicular petals tethered to the hexasome core. (e) TEM image of the hexasome flower of NH_2-PEG2000-PS_{184}-PEG550_3-PS_{251} (50:50, w/w) showing the inverse hexagonal phase of the core. (f) SEM image of collapsed silica cylinders synthesized by sol−gel reaction of TEOS using the hexasome flowers as templates, followed by removal of polymer templates. (g) SIM image of the rhodamine-labeled hexasome flowers of NH_2-PEG2000-PS_{184} and PEG550_3-PS_{251} at the composition of 50:50 (w/w). Surface amino groups were labeled with rhodamine−N-hydroxysuccinic anhydride. (h) Cross-sectional CLSM images of the rhodamine-labeled hexasome flower captured at different focal planes show the accessibility of the core.

Confocal laser scanning microscopy (CLSM) of the fluorescamine-labeled hexasome flowers showed that the surface amino groups were dispersed in the vesicular petals as well as the inverse hexagonal core (Figure 3-19). The unique morphology of the rhodamine-labeled hexasome flowers was clearly observed from structured illumination miscoscopy (SIM) and CLSM, which showed the presence of vesicular petals blooming from the hexasome core (Figure 3-16g,h). This result strongly suggested that the linear BCP was evenly distributed in the BCP bilayer composing the vesicular petals and the inverse hexagonal core, which ruled out the possibility of the phase separation of the two BCPs upon self-assembly.

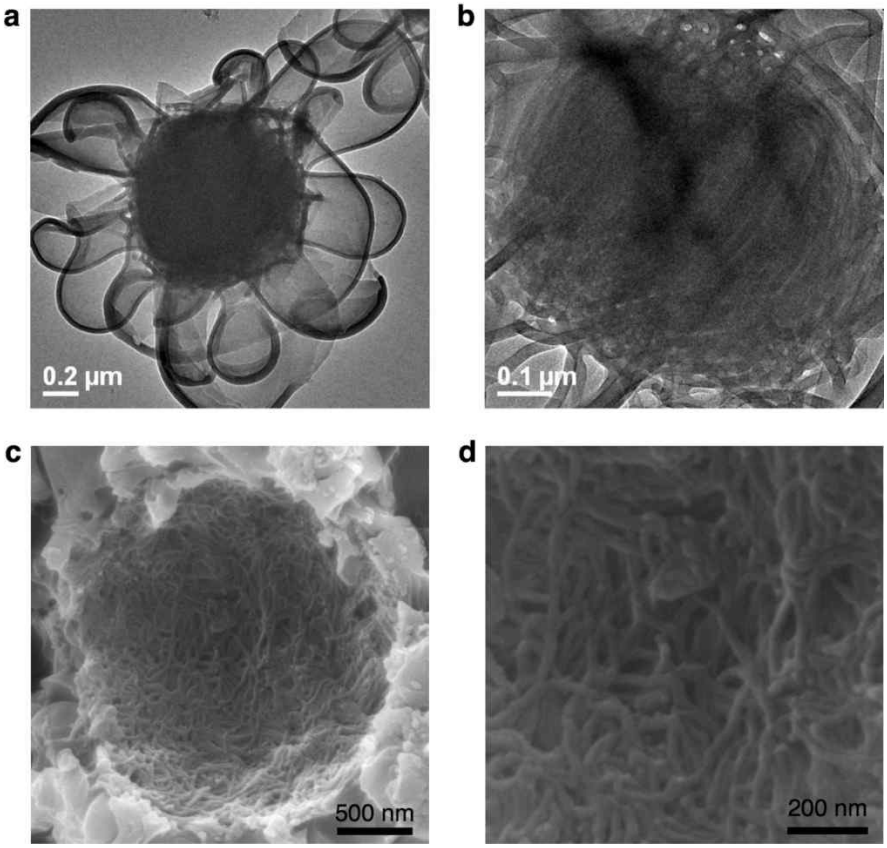

Figure 3-17. (a and b) TEM images of the hexasome flower of the BCP blend of NH_2-PEG2000-PS_{184}–PEG550_3-PS_{251} (50/50, w/w). (c and d) Silica replica synthesized by sol-gel reaction of tetraethoxysilicate (TEOS) using the hexasome flower as a template. Silica cylinders were created from the crosslinking of TEOS within the hexagonally packed cylindrical channels within the hexasome flower. D shows the collapsed silica cylinders after removing the hexasome flower template in THF.

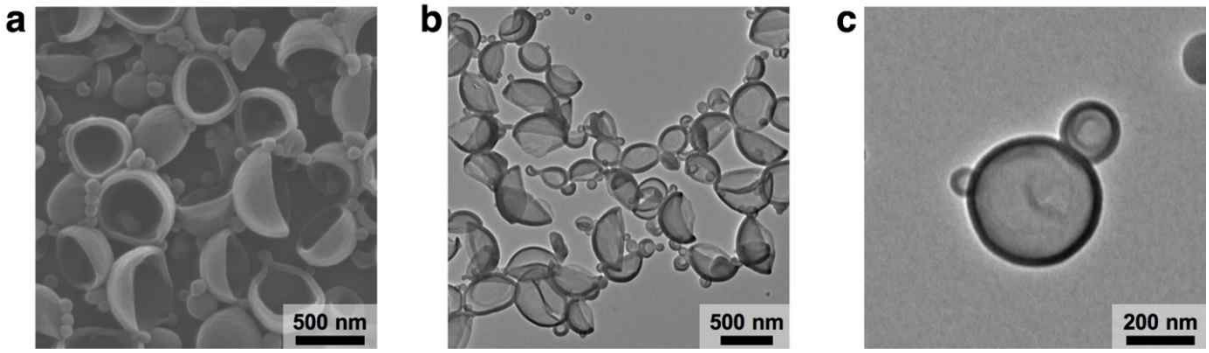

Figure 3-18. SEM (a) and TEM (b and c) images of the polymer vesicles of NH_2-PEG2000-PS_{184}.

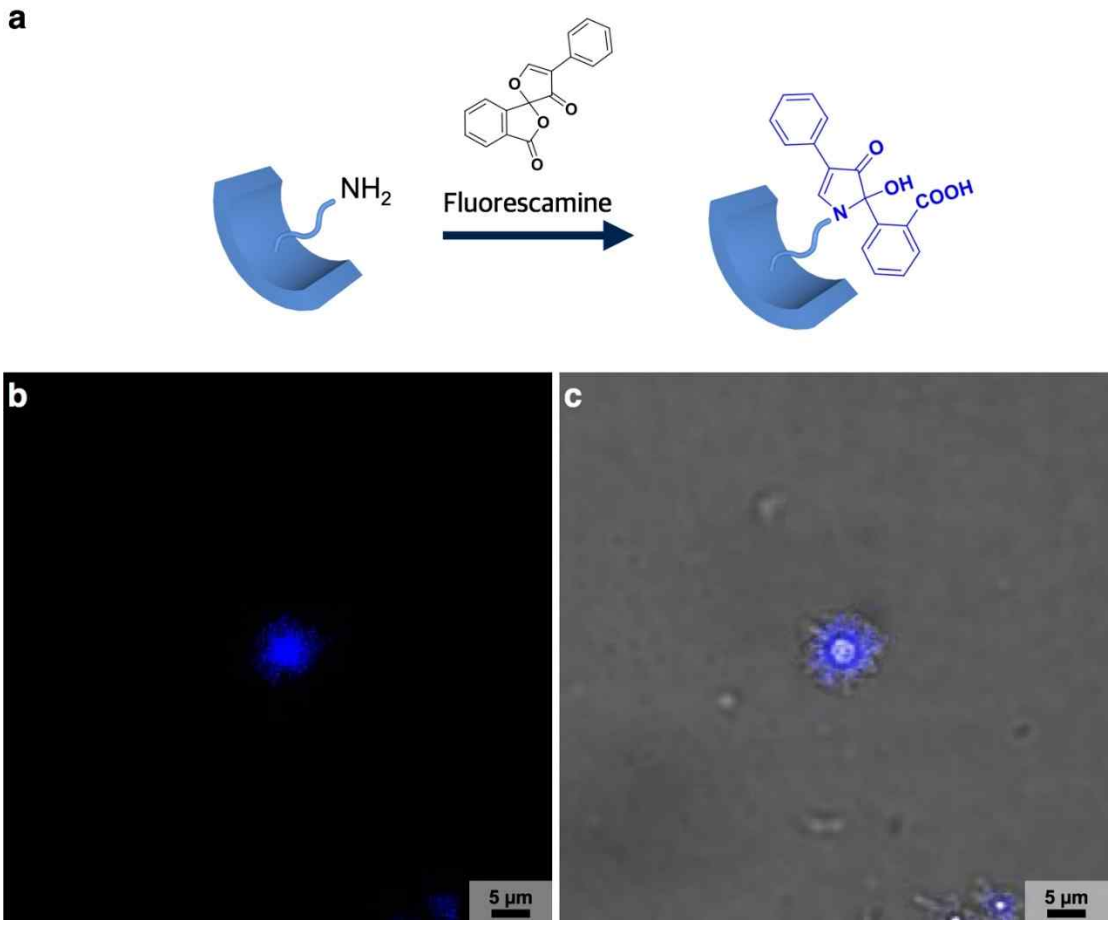

Figure 3-19. (a) Surface functionalization of polymer cubosomes with fluorescamine. (b and c) CLSM image of the fluorescamine-labeled hexasome flowers of the blend of NH_2-PEG2000-PS_{184}–PEG550$_3$-PS_{251} (50/50, w/w).

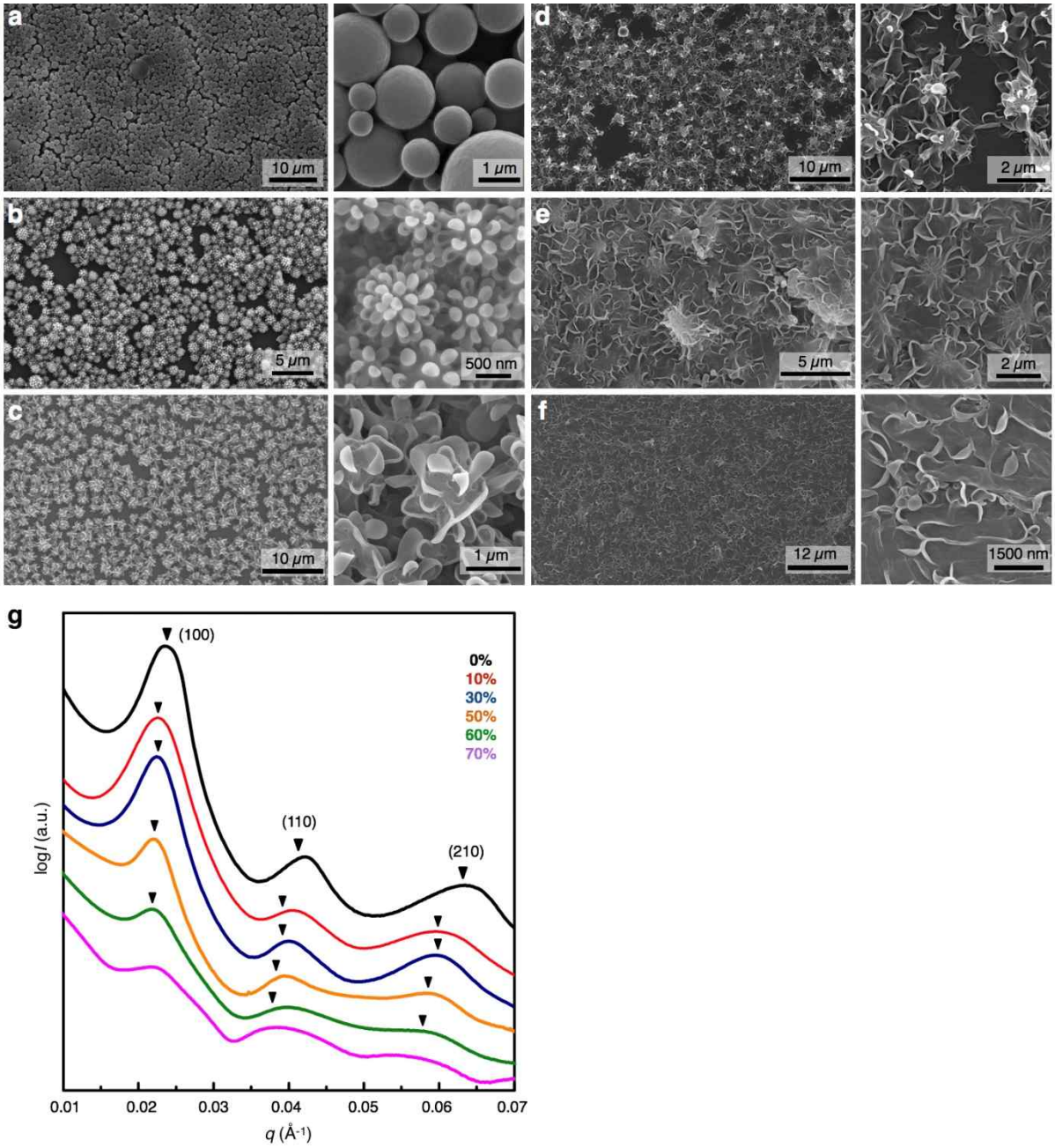

Figure 3-20. 3-D growth of vesicular petals of hexasome flowers of BCP blends. (a−f) SEM images of the hexasome flowers of the BCP blends of NH_2-PEG2000-PS_{184}-PEG550_3-PS_{251} with the composition of (a) 10:90, w/w; (b) 30:70, w/w; (c) 50:50, w/w; (d) 60:40, w/w; (e) 67:33, w/w; and (f) 70:30, w/w. (g) SAXS results of the hexasome flowers of the BCP blends with increasing the fraction of NH_2-PEG2000-PS_{184}. Peaks were assigned to *P6mm* symmetry.

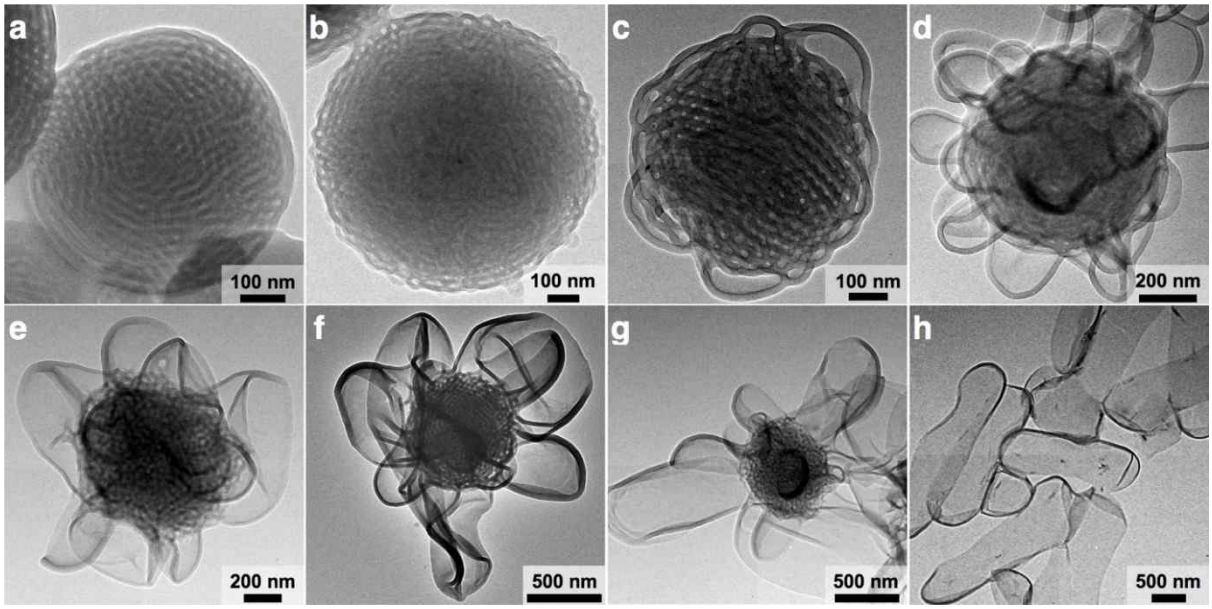

Figure 3-21. TEM images showing the evolution of the hexasome flowers of the BCP blends of NH_2-PEG2000-PS_{184}–PEG550_3-PS_{251} upon increasing the fraction of the linear BCP. (a) 0/100, w/w; (b) 10/90, w/w; (c) 20 /80, w/w; (d) 30/70, w/w; (e) 40/60, w/w; (f) 50/50, w/w; (g) 60/40, w/w; (h) 70/30, w/w.

Upon the increase in fraction of the linear BCP in the blend from 30 to 70%, the vesicular petals gradually grew from spherical vesicular buds to large irregular sacs tethered to the hexasome core (Figure 3-20 and Figure 3-21). SAXS results of the dried structures revealed that the *P6mm* symmetry (H_{II} phase) of the lattice of the internal core remained until the complete disappearance of the core and emergence of flat bilayers when the fraction of the linear BCP exceeded 70% (Figure 3-20g). To understand the mechanism of the formation of vesicular petals of hexasome flowers, we investigated the blooming of the polymer hexasomes into hexasome flowers by time-interval quenching experiments of the self-assembly of the BCP blend of PEG550_3-PS_{251} and NH_2-PEG2000-PS_{184}. (30:70, w/w) during addition of water at a rate of 1 mL h^{-1}. An aliquot (~ 10 μL) of suspension solution at the targeted water content was taken and diluted in 1 mL of water, which would freeze the self-assembled structure by vitrification of PS blocks. SEM images of the quenched particles revealed that corrugation of the surface bilayers of the hexasome core was followed by budding of vesicular petals in an early stage of water addition (15 vol %). The fully bloomed hexasome flowers were observed after 30% of water content in the suspension (Figure 3-22). The reduced rate of water addition (0.5 mL h^{-1}) did not affect the size of the vesicular petals, suggesting that the development of the vesicular petals was dependent on the fraction of the linear BCP in the blend.

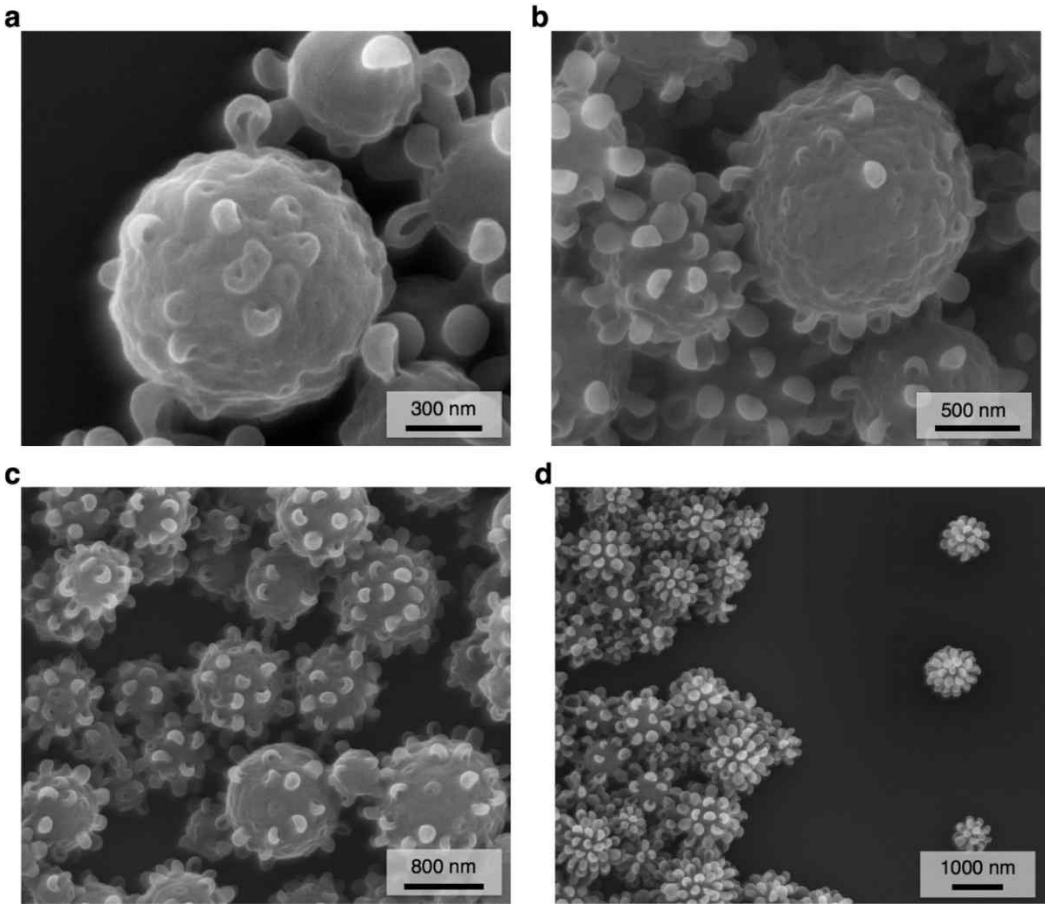

Figure 3-22. Evolution of hexasome flowers of the BCP blend of NH_2-PEG2000-PS_{184}–PEG550_3-PS_{251} (30:70, w/w) with captured by time-interval quenching experiments. SEM images of the quenched structure captured at the water content of (**a**) 15%; (**b**) 20%; (**c**) 30%, and (**d**) 50%. The rate of water addition was 1 mL h^{-1}. The volume of dioxane solution of the BCP blend was 2 mL.

The formation of hexasome flowers of BCP blends upon increasing the fraction of linear BCP is reminiscent of instability-induced budding of BCP bilayers into polymer vesicles, previously reported by Hayward and co-workers.[47] However, our results suggest that the formation of hexasome flowers could be a consequence of thermodynamics rather than kinetic manipulation caused from instability[47,48] The hexasome flowers described here have not been previously observed in solution self-assembly of BCPs in solution.

3.4 Summary

In summary, we showed that the binary blends of BCPs self-assemble into the desired nanostructure in solution by adjusting the composition of two BCPs. When two BCPs share the chemical structures of the repeating units for the constituent polymer blocks, but differs only in the block ratio, the resulting binary BCP blends of varying compositions would self-assemble in solution without experiencing phase separation. Our results strongly suggested that the *P* value of the binary BCP blend was proportionally increased with respect to the fraction of the constituent BCP with the higher *P* value. As a result, the phase and morphology of the self-assembled structures of the BCP blend could be controlled simply by adjusting the composition of the two constituent BCPs, without relying on the precise synthesis of a correspondingly designed BCP. Our results suggest that the mix-and-match approach to self-assembly of BCP blends is not only a nonsynthetic strategy to generate and fine-tune the phase and morphology allowed for the solution self-assembly of BCPs but also a way to create new nanostructures with unprecedented structural complexity that have not been available via conventional solution self-assembly of BCPs.

3.5 Experimental

Characterization

^{1}H NMR spectra were recorded on Agilent 400-MR DD2 spectrometer using CD_2Cl_2 and $CDCl_3$ as solvents. Dynamic light scattering (DLS) was performed at a Malvern Zetasizer Nano-S.

Scanning electron microscopy (SEM) was performed on Hitachi S-4300 at an acceleration voltage of 15 kV. Self-assembled structures were dried on a conductive carbon tape and then coated with Pt by using Hitachi E-1030 ion sputter (20 mA, 60s).

Transmission electron microscopy (TEM) was recorded on JEOL JEM-2100 microscpe at 200 kV and Hitachi 7600 at 100 kV. Specimens were prepared by placing a drop of the suspension of self-assembled structures on a carbon-coated Cu grid (200 mesh, EM science). After 30 min, remaining solution on a grid was removed with a filter paper, and the grid was air-dried overnight.

Synchrotron small angle X-ray scattering data were obtained on the SAXS beam line (PLS- II 6D, 11.18 keV, 6.5 m) at Pohang acceleration laboratory (Pohang, Korea). The concentrated suspension of the self-assembled aggregates was dried for 2 days in freeze dryer. The resulting powder was placed on a customized holder. Ti-SBA standard was used and X-ray irradiation time was 2~10 seconds depend on the saturation level of the detector.

The porous structures of the polymer cubosomes were analyzed by a nitrogen adsorption experiment at -196 °C using a BEL BELSORP-Max system. The surface areas and pore size distributions of the

samples were calculated by using the Brunauer–Emmett–Teller (BET) equation and the Barrett–Joyner–Halenda (BJH) method, respectively.

CLSM image of fluorescently labeled hexasome flowers of BCP blends with fluorescamine (Sigma Aldrich, λ_{Ex} = 390 nm, λ_{Em} = 495 nm) and NHS-rhodamine (Thermno scientific, λ_{Ex} = 552 nm, λ_{Em} = 575 nm) were obtained using Leica SP8 X Confocal Microscope and Nikon N-SIM Super-Resolution Microscope System. 5-10 μL of concentrated suspension of the fluorescently labeled hexasome flowers was placed on a slide glass and sealed with cover glass. Residual solution was removed by filter paper and cover glass was fixed with sealant.

Polymer Synthesis

Block copolymers used in this study were synthesized as previously reported (*21*). Molecular weights and polydispersity indices of block copolymers were measured by gel permeation chromatography (GPC) (Agilent 1260 Infinity) equipped with a PL gel 5 μm mixed D column (Agilent Technologies) and differential refractive index detectors. THF was used as an eluent with a flow rate of 0.3 mL min^{-1} at 35 °C. A PS standard (Agilent Technologies) was used for calibration. The degree of polymerization of a PS block was estimated by comparing the ^{1}H NMR integration of the peaks corresponding to the PS block in the BCP with the integration of the peaks of the PEG block.

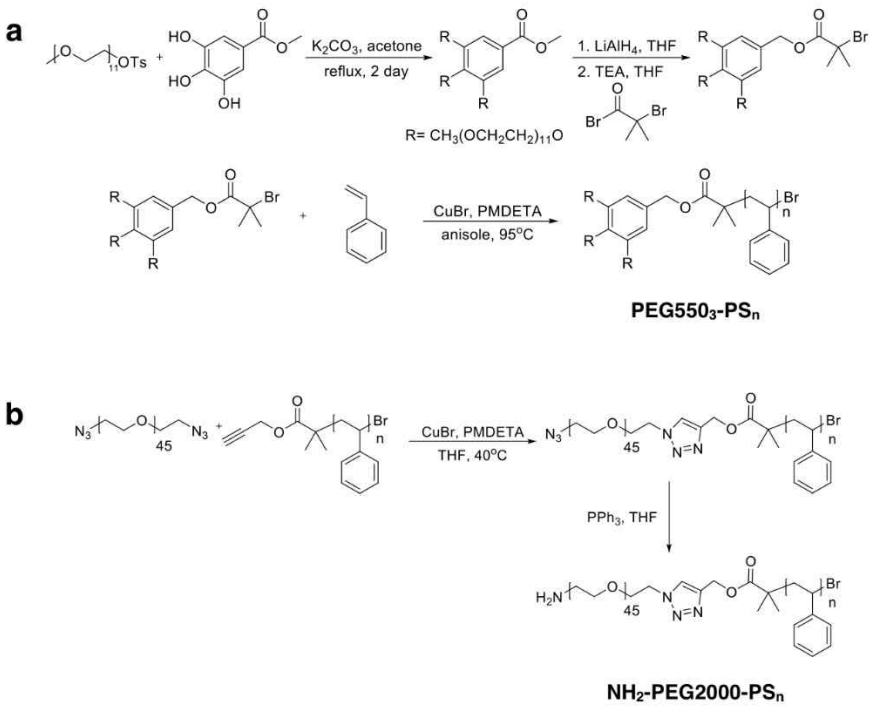

Scheme 3-1. Synthetic scheme of BCP of (a) PEG550$_3$-PS$_n$ and (b) NH_2-PEG2000-PS$_n$.

Table 3-1. Characterization of block copolymers.

Sample	M_n (g mol^{-1})[a]	$Đ$[a]	DP_n (PS)[b]	f_{PEG} (%)[c]	*Phase*[d]
PEG550$_3$-PS$_{42}$	6 800	1.06	43	36.9	sm
PEG550$_3$-PS$_{56}$	7 700	1.06	56	28.3	cm
PEG550$_3$-PS$_{105}$	9 900	1.06	105	15.1	v
PEG550$_3$-PS$_{228}$	23 000	1.07	228	7.0	hx
PEG550$_3$-PS$_{251}$	25 000	1.08	297	5.3	hx
NH$_2$-PEG2000-PS$_{184}$	22 000	1.09	184	10.5	v

[a]The number average molecular weight and molecular weight distribution determined by GPC (THF, 35 °C, 0.3 mL min^{-1} flow rate) using PS standards. [b]DP_n determined by ^{1}H NMR integration. [c]The molecular weight ratio of the PEG domain to that of the PS block. (1650 g mol^{-1} for PEG550$_3$-PS$_n$, and 2000 g mol^{-1} for PEG2000-PS$_n$). [d]Observed morphology of self-assembled structures of the suspension solution prepared from a dioxane solution of the BCP (1 wt%). sm:spherical micelle, cm:cylindrical micelle, v:vesicle, hx:hexasomes.

Self-assembly of block copolymer blends

A 1,4-dioxane solution of the mixture of two block copolymers was prepared by mixing two stock solutions (concentration of 10 mg mL^{-1}) of the block copolymers. The resulting solution of BCP mixture was allowed to equilibrate for 24 h at room temperature. The BCP blend (20 mg) was initially dissolved in 1,4-dioxane (total 2 mL, 1 wt %) in a capped vial and the solution was stirred for 24 h at room temperature. Water (total 2 mL) was added at a controlled rate (1 mL h^{-1}) to the solution via a syringe pump with vigorous stirring (850 rpm). The resulting suspension was dialyzed (molecular weight cutoff (MWCO) = 12-14 kDa, SpectraPor) against water for 1 day to remove the organic solvent.

Dye labeling of surface functional group of hexasome flowers of the BCP blends

Hexasome flowers (10 mg mL^{-1}, PEG550$_3$-PS$_{251}$/NH$_2$-PEG2000-PS$_{184}$) in PBS (pH 7.4) were mixed with dye solution (Fluorescamine in methanol, Sigma Aldrich, 200 eq. to NH$_2$ groups). The mixtures were aged at room temperature for 24 h. The residual reagent was removed by centrifugation and diluted with water. The same procedure was used for labeling the hexasome flowers with rhodamine-N-hydroxysuccinimide (Sigma).

Synthesis of Silica Replica of Polymer Cubosomes and Hexasome Flowers

A humidity chamber filled with HCl vapor was prepared by placing 5 M HCl aqueous solution (50 mL) in a 100 mL vial equipped with a cylinder to place a glass substrate. Tetraethyl orthosilicate (TEOS) solution was prepared by refluxing a mixture of TEOS, ethanol, water, and HCl (molar ratio, 1:3:1:5 × 10−5) at 60 °C for 90 min. Dried polymer cubosomes or hexasome flowers (～10 mg) were impregnated with the TEOS sol. The suspension was then centrifuged and exchanged several times with fresh TEOS sol. After aging at 40 °C for 30 min, the concentrated suspension of polymer cubosomes or hexasome flowers were cast on the glass slide (1 cm × 1 cm). Residual sol was removed by using a filter paper and the substrate was rapidly placed on the cylinder in the HCl chamber. After 8 h, the polymer template was removed by calcination at 500 °C under air or dissolution of BCPs in THF.

3.6 Reference

1. Hamley, I. W. *Block Copolymers in Solutions: Fundamentals and Applications*; Wiley: Chichester, 2005.
2. Zhang, L. & Eisenberg, A. Multiple morphologies of "crew-cut" aggregates of polystyrene-*b*-poly(acrylic acid) block copolymers. *Science* **268**, 1728–1731 (1995).
3. van Hest, J. C. M., Delnoye, D. A. P., Baars, M. W. P. L., van Genderen, M. H. P. & Meijer, E. W. Polystyrene-dendrimer amphiphilic block copolymers with a generation-dependent aggregation. *Science* **268**, 1592–1595 (1995).
4. Mai, Y. & Eisenberg, A. Self-assembly of block copolymers, *Chem. Soc. Rev.* **41**, 5969–5985 (2012).
5. Warren, N. J. & Armes, S. P. Polymerization-induced self-assembly of block copolymer nanoobjects via RAFT aqueous dispersion polymerization. *J. Am. Chem. Soc.* **136**, 10174–10185 (2014).
6. Li, Z., Kesselman, E., Talmon, Y., Hillmyer, M. A. & Lodge, T. P. Multicompartment micelles from ABC miktoarm stars in water. *Science* **306**, 98–101 (2004).
7. Jain, S. & Bates, F. S. On the origins of morphological complexity in block copolymer surfactants. *Science* **300**, 460–464 (2003).
8. Pochan, D. J. *et al.* Toroidal triblock copolymer assemblies. *Science* **306**, 94–97 (2004).
9. Holder, S. J. & Sommerdijk, N. A. J. M. New micellar morphologies from amphiphilic block copolymers: disks, toroids, and bicontinuous micelles. *Polym. Chem*. **2**, 1018–1028 (2011).
10. Gröschel, A. H. *et al.* Guided hierarchical co-assembly of soft patchy nanoparticles. *Nature* **503**, 247–251 (2013).
11. Wang, X. *et al*. Cylindrical block copolymer micelles and co-micelles of controlled length and architecture. *Science* **317**, 644–647 (2007).
12. Almsherqi, Z. A., Kohlwein, S. D. & Deng, Y. Cubic membranes: a legend beyond the flatland of cell membrane organization. *J. Cell Biol.* **173**, 839–844 (2006).
13. Larsson, K. Cubic lipid-water phases: structures and biomembrane aspects. *J. Phys. Chem.* **93**, 7304–7314 (1989)
14. Kulkarni, C. V., Wachter, W., Iglesias-Salto, G., Engelskirchen, S. & Ahualli, S. Monoolein: a magic lipid? *Phys. Chem. Chem. Phys.* **13**, 3004–3021 (2011).

15. Israelachvili, J. N. *Intermolecular and Surface Forces*, 3rd edn. (Academic Press, 2011).

16. Vukusic, P. & Sambles, J. R. Photonic structures in biology. *Nature* **424**, 852–855 (2003).

17. Schröder-Turk, G. E. *et al.* The chiral structure of porous chitin within the wing-scales of callophrys rubi. *J. Struct. Biol.* **174**, 290–295 (2011).

18. Saranathan, V. *et al.* Structure, function, and self-assembly of single network gyroid ($I4_132$) photonic crystals in butterfly wing scales. *Proc. Natl. Acad. Sci. U. S. A.* **107**, 11676–16462 (2010).

19. Hayward, R. C. & Pochan, D. J. Tailored assemblies of block copolymers in solution:it is all about the process. *Macromolecules* **43**, 3577–3584 (2010).

20. La, Y. *et al.* Colloidal inverse bicontinuous cubic membranes of block copolymers with tunable surface functional groups. *Nat. Chem.* **6**, 534–541 (2014).

21. An, T. H. *et al*. Solution self-assembly of block copolymers containing a branched hydrophilic block into inverse bicontinuous cubic mesophases. *ACS Nano* **9**, 3084–3096 (2015).

22. Cho, A., La, Y., Shin, T. J., Park, C. & Kim, K. T. Structural requirements of block copolymers for self-assembly into inverse bicontinuous cubic mesophases in solution. *Macromolecules* **49**, 4510–4519 (2016).

23. La, Y., An, T. H., Shin, T. J., Park, C. & Kim, K. T. A morphological transition of inverse mesophases of a branched-linear block copolymer guided by using cosolvents. *Angew. Chem. Int. Ed.* **54**, 10483–10487 (2015).

24. Jeong, M. G. & Kim, K. T. Covalent stabilization of inverse bicontinuous cubic structures of block copolymer bilayers by photodimerization of indene pendant groups of polystyrene hydrophobic blocks. *Macromolecules* **50**, 223–234 (2017).

25. Park, C. *et al.* Mesoporous monoliths of inverse bicontinuous cubic phases of block copolymer bilayers. *Nat. Commun.* **6**, 6392 (2015).

26. Yu, H., Qiu, X., Nunes, S. P. & Peinemann, K.-V. Biomimetic block copolymer particles with gated nanopores and ultrahigh protein sorption capacity. *Nat. Commun.* **5**, 4110 (2014).

27. Zhang, L., Bartels, C. & Eisenberg, A. Mesosized crystal-like structure of hexagonally packed hollow hoops by solution self-assembly of diblock copolymers. *Phys. Rev. Lett.* **79**, 5034–5037 (1997).

28. McKenzie, B. E. *et al.* Temperature-responsive nanospheres with bicontinuous internal structures from a semicrystalline amphiphilic block copolymer. *J. Am. Chem. Soc.* **132,** 10256–10259 (2010).

29. Hales, K., Chen, Z., Wooley, K. L. & Pochan, D. J. Nanoparticles with tunable internal structure from triblock copolymers of PAA-b-PMA-b-PS. *Nano Lett.* **8,** 2023–2026 (2008).

30. He, K. *et al.* Cubosomes from hierarchical self-assembly of poly(ionic liquid) block copolymers. *Nat. Commun.* **8**, 14057 (2017).

31. Xiao, Q. *et al.* Why do membranes of some unhealthy cells adopt a cubic architecture? *ACS Cent. Sci.* **2**, 943–953 (2016).

32. Robeson, L. M. Applications of polymer blends: emphasis on recent advances. *Polym. Eng. Sci.* **24**, 587–597 (1984).

33. Court, F.; Hashimoto, T. Morphological Studies of Binary Mixtures of Block Copolymers. 1. Corsurfactnat Effects and Composition Dependence of Morphology. *Macromolecules* **2001**, *34*, 2536−2545.

34. Court, F.; Hashimoto, T. Morphological Studies of Binary Court, F.; Hashimoto, T. Morphological Studies of Binary Short Blocks in Lamellar Microdomains and Its Effect on Domain Size and Stability. *Macromolecules* **2002**, *35*, 2566−2575.

35. Chen, F.; Kondo, Y.; Hashimoto, T. Control of Nanostructure in Mixtures of Block Copolymers: Curvature Control via Cosurfactant Effects. *Macromolecules* **2007**, *40*, 3714−3723.

36. Zhu, J., Zhang, S., Zhang, K., Wang, X., Mays, J. W., Wooley, K. L. & Pochan, D. J. Disk-cylinder and disk-sphere nanoparticles via a block copolymer blend solution construction. *Nat. Commun.* **4**, 2291 (2013).

37. Qiu, H. *et al.* Uniform patchy and hollow rectangular platelet micelles from crystallizable polymer blends. *Science* **352**, 697–701 (2016).

38. Jain, S. & Bates, F. S. Consequences of nonergodicity in aqueous binary PEO–PB micellar dispersions. *Macromolecules* **37**, 1511–1523 (2004).

39. Wright D. B. *et al.* The copolymer blending method: a new approach for targeted assembly of micellar nanoparticles. *Macromolecules* **48**, 6516–6522 (2015).

40. Kulkarni, C. V., Tang, T.-Y., Seddon, A. M., Seddon, J. M., Ces, O. & Templer, R. H. Engineering bicontinuous cubic structures at the nanoscale–the role of chain splay. *Soft Matter* **6**, 3191–3194 (2010).

41. Seo, M. & Hillmyer, M. A. Reticulated nanoporous polymers by controlled polymerization-induced mesophase separation. *Science* **336**, 1422–1425 (2012).

42. Sai, H. *et al.* Hierarchical porous polymer scaffolds from block copolymers. *Science* **341**, 530–534 (2013).

43. McKenzie, B. E. *et al.* Controlling internal pore sizes in bicontinuous polymeric nanospheres. *Angew. Chem. Int. Ed.* **54**, 2457–2461 (2015).

44. Yu, H. et al. Self-assembled asymmetric block copolymer membranes: bridging the gap from ultra- to nanofiltration. *Angew. Chem. Int. Ed.* **54**, 13937–13941 (2015).

45. Azzam, T. & Eisenberg, A. Control of vesicular morphologies through hydrophobic block length. *Angew. Chem. Int. Ed.* **45**, 7443–7447 (2006).

46. Negrini, R. & Mezzenga, R. Diffusion, molecular separation, and drug delivery from lipid cubic mesophases with tunable water channels. *Langmuir* **28**, 16455–16462 (2012).

47. Zhu, J. & Hayward, R. C. Hierarchically structured microparticles formed by interfacial instabilities of emulsion droplets containing amphiphilic block copolymers. *Angew. Chem. Int. Ed.* **47**, 2113–2116 (2008).

48. Zhu, J. & Hayward, R. C. Spontaneous generation of amphiphilic block copolymer micelles with multiple morphologies through interfacial instabilities. *J. Am. Chem. Soc.* **130**, 7496–7502 (2008).

Chapter 4. Branched Cylindrical Micelle Structures from the Binary Blended System with High Molecular Weight Difference.

4.1 Abstract

The self-assembly of amphiphilic block copolymers (BCPs) into precisely controlled nanostructure is required in many applications for the intended use. Blending is one of a convenient way to control the nanostructures. Here we show that binary blends of BCPs self-assemble into the various type of micelles. This polymer blending was carried out in a range of molecular weights, which is not covered much in previous studies, and it was possible to observe the unusual structural changes which were not seen at small molecular weight range due to its large molecular weight. These BCP blends not only allow the direct creation of various types of micelles, but also provide nanostructures of unprecedented morphology.

4.2 Introduction

Block copolymers (BCPs) in selective solvent forms nanostructures like micelles upon certain concentration. Such nanostructures are used in many fields such as nanomaterial synthesis, lithography and drug delivery.[1,2] Unlike lipids or surfactants with low molecular weight, BCPs have physical stability, and it is possible to control various structures and functionality by adjusting the composition of polymers. Recently, some studies have been reported to precisely control the structure and size of micelles through the self-assembly of polymers with various architectures. Also, it is possible to form micelles with unique structures such as branched micelles or toroids by blending with polymer having a large molecular weight difference or a small molecules.[3-7]

We have shown that the self-assembly of binary blend not only allow the desired nanostructure by adjusting the composition of two BCPs but also create unusual nanostructures with unprecedented structural complexity. Here we show that the binary blend of BCPs with high molecular weight differences self-assemble into branched networks by adjusting the composition of two BCPs. Increasing the curvature of molecular packing shapes through control of the composition can lead to morphological transition from inverse structures to branched networks and spheres. We demonstrated that micelle structures can be controlled through simple blending methods.

4.3 Result and discussion

We synthesized amphiphilic block copolymers with a molecular weight difference of 10 times in order to observe the self-assembly behavior of these polymer blends. Poly(ethylene glycol)-*b*-polystyrene (PEG-*b*-PS) with high molecular weight was synthesized by atom transfer radical polymerization (ATRP) of styrene initiated from macro-initiator with PEG dendron (3PEG chains, Mn=2000 g mol^{-1}).

Small molecular weight polymers were synthesized via ATRP initiated from the macro-initiator with PEG dendron (3PEG chains, Mn 1000 g mol^{-1}) and Cu(I)-catalyzed azide−alkyne cycloaddition (click chemistry) between PEG dendron (3PEG chains, Mn 1000 g mol^{-1}) linked to focal benzoyl group with three propargyloxy groups and azido polystyrene. Small molecular weight polymers were prepared with branched-linear BCP having the same size as the entire styrene DP of branched-branched BCP (bb-BCP).

The stock solution (10 mg ml^{-1}) of each polymer was prepared, and the mixture was blended in the corresponding ratio. After polymers were sufficiently mixed by stirring for 24 h, polymers were self-assembled under general conditions. The structure of each polymer was confirmed by transmission electron microscopy (TEM). $PEG2000_3$-PS_{2030} (M_n = 176 kg mol^{-1}, $Đ$ = 1.20) showed bicontinuous structures in dioxane, and small molecular weight polymers form spherical micelle ($PEG1000_3$-PS_{118}, M_n = 19 kg mol^{-1}, $Đ$ = 1.09) and vesicles ($PEG1000_3$-(3,4,5)-$(PS_{54})_3$, M_n = 22.5 kg mol^{-1}, $Đ$ = 1.05). (Figure 4-1)

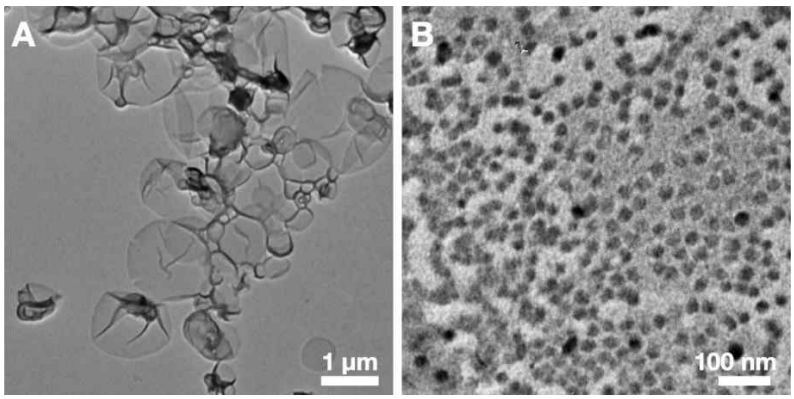

Figure 4-1. Representative TEM image of (A) $PEG1000_3$-(*3,4,5*)-$(PS_{54})_3$ and (B) $PEG1000_3$-PS_{118}.

Self-assembly of blends with small bb-BCP in solution

In the previous blending system, when the ratio of vesicle-forming polymers in the mixture was increased, a lattice change of bicontinuous structure occurred or a morphological transition to the

sponge phase occurred. However, in the blending system of $PEG2000_3$-PS_{2030} and $PEG1000_3$-(*3,4,5*)-$(PS_{54})_3$, completely different structural changes were found unlike expectations.

When a small amount of $PEG1000_3$-(*3,4,5*)-$(PS_{54})_3$ is mixed, more ordered bicnontinuous structure and vesicle were formed, and branched cylinder and its aggregates can be observed at the composition of $PEG2000_3$-PS_{2030} : $PEG1000_3$-(*3,4,5*)-$(PS_{54})_3$ = 80:20. (Figure 4-2) If we had mix more than 20 %, we could observe that number of aggregates decreases and various kinds of cylinders were mixed and eventually all become spheres.

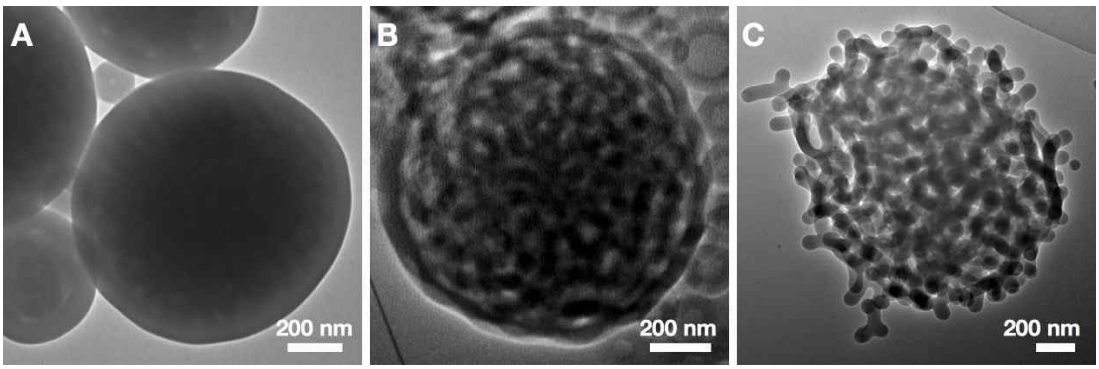

Figure 4-2. (A-C) Representative TEM images of morphological transition induced by curvature change as increase of composition of high curvature molecule. (A) $PEG2000_3$-PS_{2030} (B) $PEG2000_3$-PS_{2030} : $PEG1000_3$-(*3,4,5*)-$(PS_{54})_3$ = 95:5, (C) $PEG2000_3$-PS_{2030} : $PEG1000_3$-(*3,4,5*)-$(PS_{54})_3$ = 80:20.

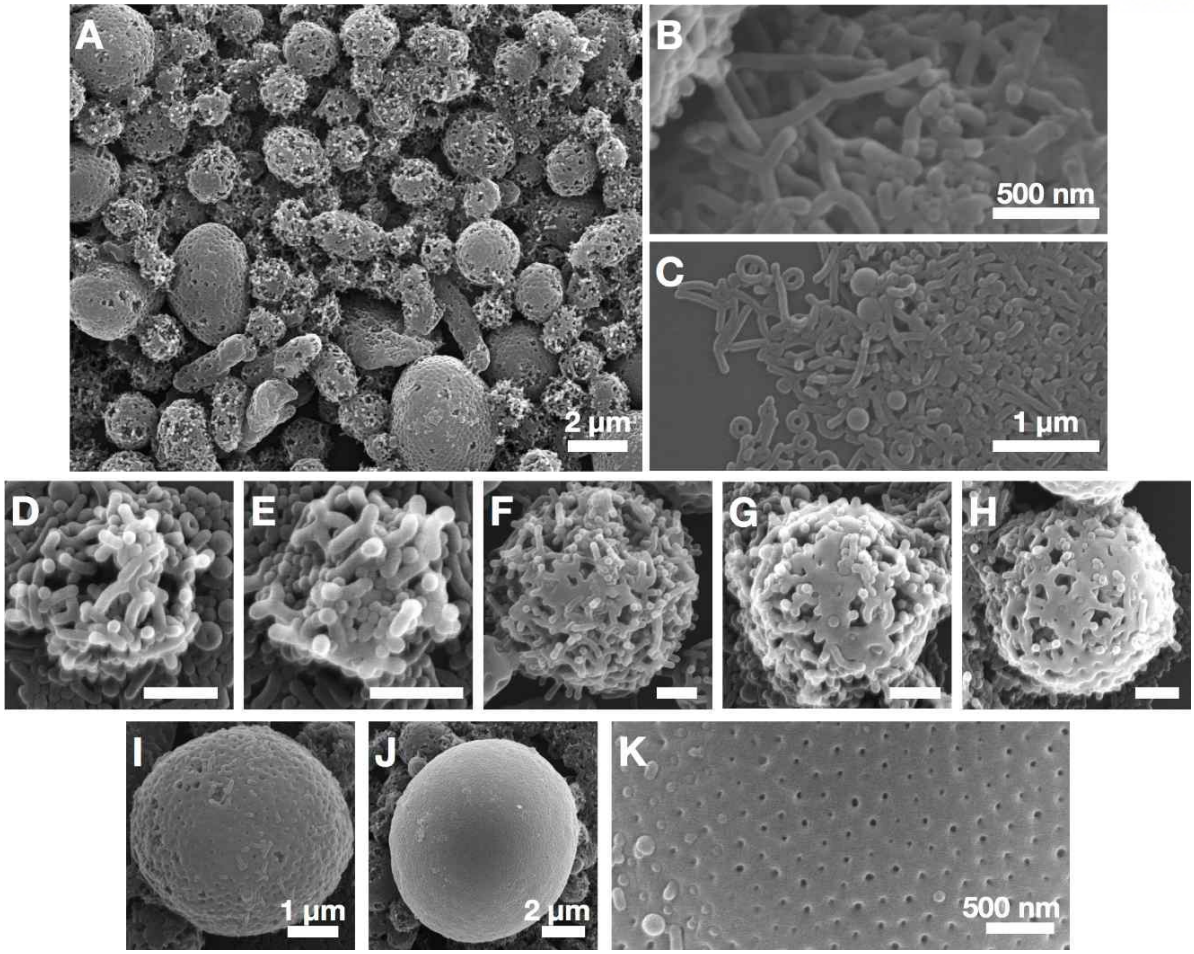

Figure 4-3. SEM images of cylindrical micelle aggregates of BCP blends of $PEG2000_3$-PS_{2030}/$PEG1000_3$-*(3,4,5)*-$(PS_{54})_3$ with composition of 80/20 w/w. Aggregates of the branched micelle existed in various state.

We used scanning electron microscopy (SEM) to further investigate the aggregate in the fraction of $PEG1000_3$-(*3,4,5*)-$(PS_{54})_3$ in binary blend exceeded 20 %. Aggregates of the branched micelle existed in various state in one solution. (Figure 4-3) From bicontinuous structures having a constant pore on the surface, we could see all the structures that are morphological transition to the cylinder and sphere according to the curvature change. (Figure 4-3D-J) We could also observed the various type of fragments from the aggregate. The number of aggregates was inversely proportional to the fraction of $PEG1000_3$-(3,4,5)-$(PS_{54})_3$, and as the fraction of $PEG1000_3$-(*3,4,5*)-$(PS_{54})_3$ increases, the amount of fragments increases. As a result, fragments were generated from the aggregates as the fraction of $PEG1000_3$-(3,4,5)-$(PS_{54})_3$ increases.

Branched cylindrical micelles

Danino[8] reported that the polymer forming bilayer structures changed to branched cylindrical micelles as the mixing ratio of surfactant with large curvature is increased due to the increase of net curvature in the binary mixture. These cylindrical micelles from the change of curvature has entropic penalty, so the defect like spherical end-cap and branched point increases in order to reduce entropic penalty. As results, it forms branched micelle structures with a Y-junction, and finally a sphere, a short-armed branched micelles, and vesicles coexist.

In the binary blended system of $PEG2000_3$-PS_{2030} and $PEG1000_3$-(3,4,5)-$(PS_{54})_3$, as the fraction of polymer with large curvature ($PEG1000_3$-(3,4,5)-$(PS_{54})_3$) increases, we could observe that the bicontinuous structures changed to branched micelles and spherical micelles.

From a range of $PEG1000_3$-(3,4,5)-$(PS_{54})_3$ fractions, we observed the mixed phase of short-armed branched micelles, various type of fragment, sphere and aggregates of branched micelles as shown in Figure 4-4. These short armed branches have almost the same number of spherical end-caps and U-junction points, and cylinder undulations were observed as shown in Figure 4-4c. This is due to the difference in the molecular weight of blending polymers, and curvature changes were mainly observed around the end cap or junction point.

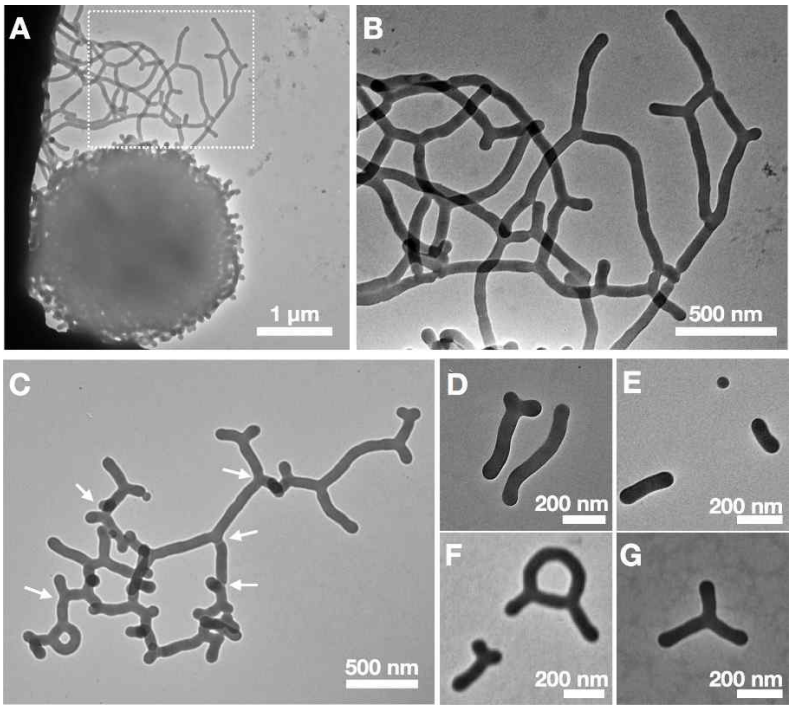

Figure 4-4. TEM images of (A-C) branched micelle structures and (D-G) fragments. (C) The arrows indicate points with cylinder undulations.

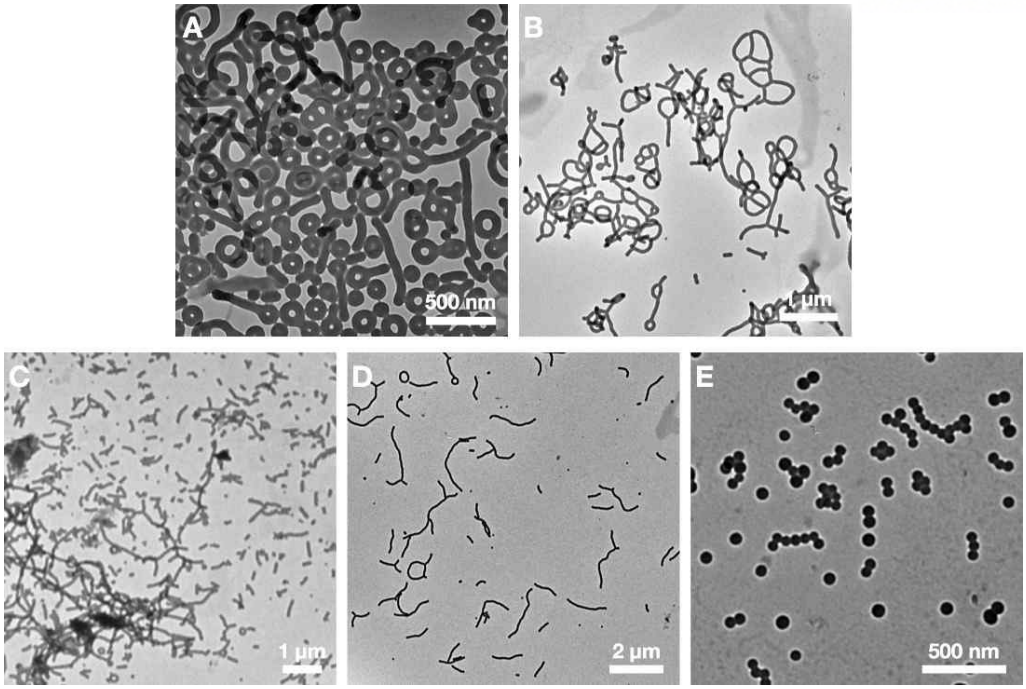

Figure 4-5. TEM images of fragments from BCP blends of $PEG2000_3$-PS_{2030}/$PEG1000_3$-*(3,4,5)*-$(PS_{54})_3$ with composition of (A) 80/20 w/w, (B) 78/22 w/w, (C) 76/24 w/w, (D) 74/26 w/w, (E) 72/28 w/w.

Shape deformation of the fragments detached from aggregate

As the fraction of $PEG1000_3$-(3,4,5)-$(PS_{54})_3$ increased, the number of fragments increased, and shape changes of fragments such as length and shape were observed. Therefore, we adjusted the ratio at a narrow interval to observe the shape change of the cylindrical micelle in detail. At Blend 20 ($PEG2000_3$-PS_{2030}: $PEG1000_3$-*(3,4,5)*-$(PS_{54})_3$ = 80:20), we observed lasso micelles or toroidal micelles that can be observed in cylinders with high molecular weight or unstable end-caps. In the case of Blend 22 ($PEG2000_3$-PS_{2030}: $PEG1000_3$-*(3,4,5)*-$(PS_{54})_3$ = 78:22), many circular networks with long-cylinders were observed. At Blend 24 ($PEG2000_3$-PS_{2030}: $PEG1000_3$-*(3,4,5)*-$(PS_{54})_3$ = 76:24), however, circular networks were hardly visible and mainly aggregate and very short-cylinders were observed. Blend 26 ($PEG2000_3$-PS_{2030}: $PEG1000_3$-*(3,4,5)*-$(PS_{54})_3$ = 74:26) was similar to blend26, but a longer type of branched micelle was mainly observed. Finally, we observed the morphological transition to spherical micelles in blend 28 ($PEG2000_3$-PS_{2030}: $PEG1000_3$-*(3,4,5)*-$(PS_{54})_3$ = 72:28). (Figure 4-5)

The shape deformation tendency of micelles is shown by the circular micelles (like lasso micelles, toroids) in blend 20 and 22 which have small fraction of $PEG1000_3$-*(3,4,5)*-$(PS_{54})_3$, while blend 24 and 24 with slightly increased ratios tend to show branched micelles. This indicates that the curvature and stability of the micelles depend on the surface area occupied by $PEG1000_3$- *(3,4,5)* - $(PS_{54})_3$. And it is

speculated that linear micelle structures may exist in Blend 24, 26 where the ratio of PEG1000$_3$- *(3,4,5)* - (PS$_{54}$) $_3$ is higher. (For the same reason, blend 22 and 26 have the longer-cylinders than blend 20 and 24) In blend 28, PEG1000$_3$- *(3,4,5)* - (PS$_{54}$) $_3$ is three times as high as the number of moles of PEG2000$_3$-PS$_{2030}$, so that the area occupied by PEG1000$_3$-*(3,4,5)*-(PS$_{54}$)$_3$ in the micelles is sufficiently wide to cover the instability of PEG2000$_3$-PS$_{2030}$ in spherical micelles.

Comparison of morphological transition according to polymer topology difference

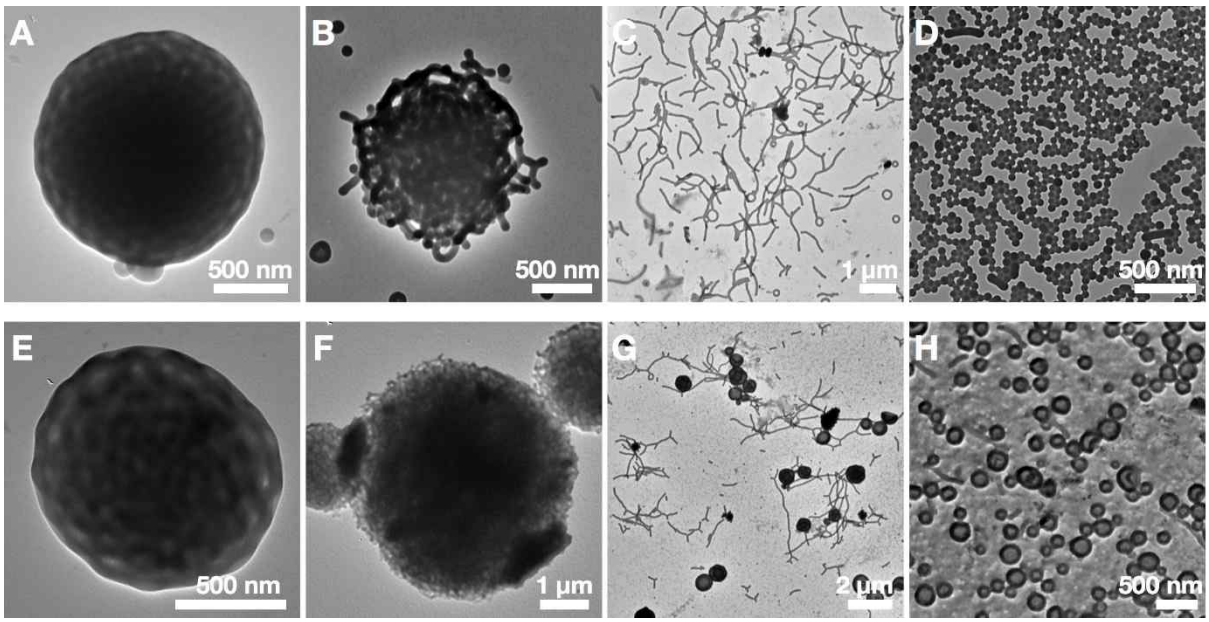

Figure 4-6. TEM images of self-assembled structures of BCP blends (A-D) PEG2000$_3$-PS$_{2030}$/ PEG1000$_3$- *(3,4,5)* - (PS$_{54}$)$_3$ with varying composition, (A) bicontinuous structures (PEG2000$_3$-PS$_{2030}$: PEG1000$_3$- *(3,4,5)* - (PS$_{54}$)$_3$ = 95:5), (B) cylindrical micelle aggregates (PEG2000$_3$-PS$_{2030}$: PEG1000$_3$- *(3,4,5)* - (PS$_{54}$)$_3$ = 80:20), (C) cylindrical micelles (PEG2000$_3$-PS$_{2030}$: PEG1000$_3$- *(3,4,5)* - (PS$_{54}$)$_3$ = 75:25), (D) spherical micelles (PEG2000$_3$-PS$_{2030}$: PEG1000$_3$- *(3,4,5)* - (PS$_{54}$)$_3$ = 70:30), (E-H) PEG2000$_3$-PS$_{2030}$: PEG1000$_3$-PS$_{118}$ with varying composition, (E) bicontinuous structures (PEG2000$_3$-PS$_{2030}$: PEG1000$_3$-PS$_{118}$ = 95:5), (F) cylindrical micelle aggregates (PEG2000$_3$-PS$_{2030}$: : PEG1000$_3$-PS$_{118}$ = 90:10), (G) cylindrical micelles and vesicles (PEG2000$_3$-PS$_{2030}$: PEG1000$_3$-PS$_{118}$ = 75:25), (H) vesicles (PEG2000$_3$-PS$_{2030}$: PEG1000$_3$-PS$_{118}$ = 50:50).

In order to investigate the cause of the morphological change which could not be seen in previous studies, we conducted a comparative experiment with a dendritic-linear BCP (PEG1000$_3$-PS$_{118}$) similar in size to PEG1000$_3$-*(3,4,5)*-(PS$_{54}$)$_3$.

In binary blend with $PEG1000_3$-*(3,4,5)*-$(PS_{54})_3$, as the fraction of $PEG1000_3$-*(3,4,5)*-$(PS_{54})_3$ increases, the structure changes in a direction changing to a sphere having a high curvature. The morphological transition of the BCP blend is as follows according to the compositional change of $PEG2000_3$-PS_{2030} : $PEG1000_3$-*(3,4,5)*-$(PS_{54})_3$; bicontinuous structures (95: 5) > cylinder aggregates (80:20) > branched cylinders (75:25) > spheres (70:30).

However, the structural change when the ratio of $PEG1000_3$-PS_{118} was increased was as follows : bicontinuous structures ($PEG2000_3$-PS_{2030} : $PEG1000_3$-PS_{118} = 95:5) > cylinder aggregates (90:10) > branched cylinders and vesicles (75:25) > vesicles (50:50). Similar to branched-branched BCPs, structural change occurred in the direction of higher curvature, but vesicles were observed differently from the bb-BCP

Comparing these two different blending series in terms of molar ratio of polymers, 20% fraction of $PEG1000_3$- *(3,4,5)* - $(PS_{54})_3$ ($PEG2000_3$-PS_{2030}: $PEG1000_3$- *(3,4,5)* - $(PS_{54})_3$ = 80:20) have $PEG2000_3$-PS_{2030}: $PEG1000_3$- *(3,4,5)* - $(PS_{54})_3$ = 1:4, 10% fraction of $PEG1000_3$- PS_{118} have $PEG2000_3$-PS_{2030}: $PEG1000_3$- PS_{118} = 1:1.

It is presumed that the blend of dendritic-linear polymer having more large curvature will change the curvature sufficiently at a lower molar ratio because of the influence of the packing shape depending on the architecture of polymer. Also, mixing phase with vesicles from exceed 25% fraction of $PEG1000_3$- PS_{118} seems to be caused by the problem of polydispersity due to the large molecular weight difference between polymers.[9]

4.4 Summary

The micelle structures by self-assembly can be used in various field such as biomedicine, cosmetic and industry. However, this applications have different results depending on their shapes and sizes. Therefore, it is important to adjust the precise shape and size to suit according to purpose. We observed unusual morphological changes caused by slow exchange of polymers and different curvature in blended system with large molecular weight differences. Mixing small molecular weight polymers with high curvatures will change the morphology from bilayer to cylinder as the ratio increases. In order to compensate for the entropy penalty resulting from that, defects (Y-junction and spherical end-cap) are increased. Eventually, all cylinders are changed to spherical micelles in the direction of increasing end-cap at a certain ratio.

4.5 Experimental

Methods. ^{1}H spectra was recorded at 400 MHz on a Agilent 400-MR DD2 spectrometer. CD_2Cl_2 was used as standard solution in ^{1}H-NMR spectra. The average molecular weights and polydispersity indices of block copolymers were measured by Agilent 1260 Infinity GPC system, comprising a PL gel 5 μm mixed D column (Agilent Technologies) and differential refractive index detectors using THF as an eluent at 35 °C with a flow rate of 1 mL min^{-1}. The polymer sample in THF was filtered by using PTFE filter before injection. For the calibration of GPC system, a PS standard (Agilent Technologies) was used.

Matrix-assisted laser desorption ionization time-of-flight mass spectroscopy (MALDI-TOF-MS) was performed using a Bruker Ultraflex III TOF-TOF mass spectrometer equipped with a nitrogen laser (335 nm). The experimental sample was prepared by mixing block copolymers dissolved in THF (5 mg mL^{-1}) and matrix solution (sinapinic acid or dithranol in THF, 30 mg ml^{-1}). The prepared sample was dropped onto the MALDI plate and dried at room temperature before measurement.

Scanning electron microscopy (SEM) was performed on Hitachi S-4300 at an acceleration voltage of 15 kV. Sample was prepared by dropping the self-assembled solution onto a slide glass and drying at room temperature. The prepared sample was coated with Pt by using Hitachi E-1030 ion sputter (20 mA, 60s).

Transmission electron microscopy (TEM) images were obtained on JEOL JEM-2100 microscope at 200 kV and Hitachi 7600 at 100 kV. Specimens were prepared by adding a drop of the suspension of self-assembled structures onto a carbon-coated Cu grid (200 mesh, EM science). After 30 min, remaining solution on a grid was removed with a filter paper, and the grid was air-dried at room temperature overnight.

Polymer synthesis. Block copolymers used in this study were synthesized as previously reported (in chapter 2).

Block copolymer of dendritic linear PEG-b-PS was prepared by ATRP of styrene initiated from PEG macro-initiator. And block copolymer of branched-branched PEG-b-PS was obtained through the Cu(Ⅰ)-catalyzed azide-alkyne click reaction. Azide end functionalized PS was clicked with the PEG dendron linked to focal benzoyl group with three propargyloxy groups.

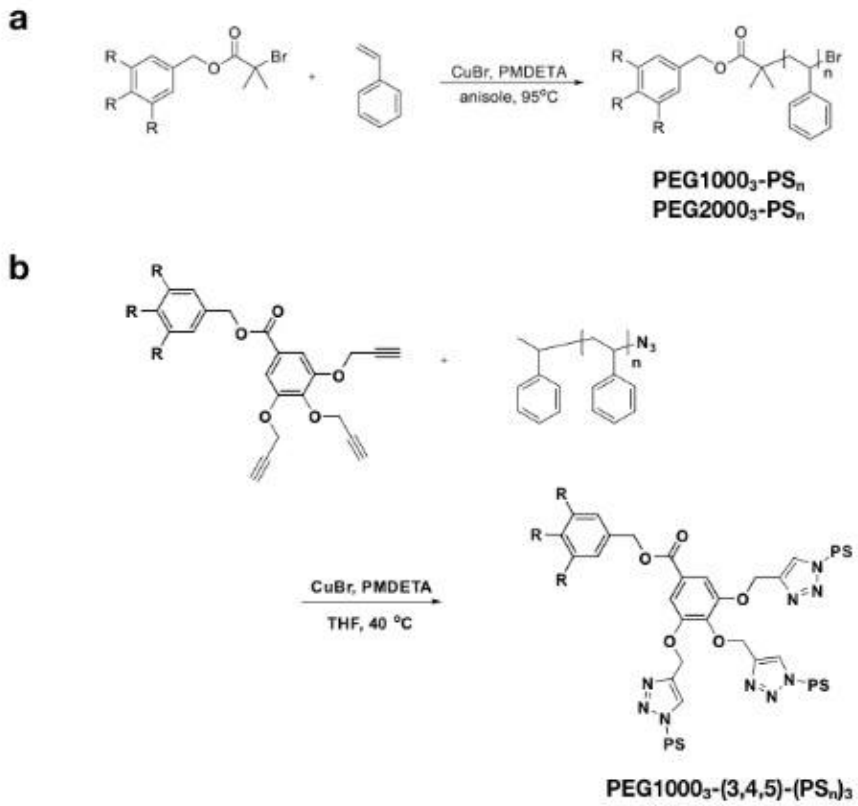

Scheme 4-1. Synthesis of (a) dendritic linear PEG-b-PS by ATRP and (b) branched-branhced PEG-b-PS by click reaction.

Table 4-1. Characterization of block copolymers.

Sample	M_n (g mol^{-1})[a]	$Đ$[a]	DP_n *(PS)*[b]	f_{PEG} (%)[c]	*Phase*[d]
PEG2000$_3$-PS$_{2030}$	176 000	1.20	2030	2.8	cubosome
PEG1000$_3$-PS$_{118}$	19 000	1.09	118	24.4	sphere
PEG1000$_3$-(*3,4,5*)-(PS$_{54}$)$_3$	22 500	1.05	162*	17.8	vesicle

[a]The number average molecular weight and molecular weight distribution determined by GPC (THF, 35 °C, 0.3 mL min^{-1} flow rate) using PS standards. [b]DP_n determined by ^{1}H NMR integration. [c]The molecular weight ratio of the PEG domain to that of the PS block. (3000 g mol^{-1} for PEG1000$_3$-PS$_n$, and 6000 g mol^{-1} for PEG2000$_{x3}$-PS$_n$). [d]Observed morphology of self-assembled structures of the suspension solution prepared from a dioxane solution of the BCP (1 wt%).

Self-assembly of binary blends. The stock solutions of two block copolymers having a concentration of 10 mg mL^{-1} in 1,4-dioxane were prepared. According to a ratio, each stock solution was added to the capped vial and the resulting solution of BCP blend (total 5 mg / 0.5 mL, 1 wt%) was stirred for 24 h at room temperature for the homogenous mixing. 0.5 mL of water was added at a constant rate (0.25 mL h^{-1}) to the solution of BCP blend using a syringe pump with vigorous stirring (600 rpm). After self-assembly, the organic solvent in the resulting suspension was removed by dialysis (molecular weight cutoff (MWCO) = 12-14 kDa, SpectraPor) against water for 1 day.

4.6 Reference

1. Blanazs, A.; Armes, S. P.; Ryan, A. J., Self-Assembled Block Copolymer Aggregates: From Micelles to Vesicles and their Biological Applications. *Macromol. Rapid Commun.* **2009**, *30*, 267-277.

2. Schacher, F. H.; Rupar, P. A.; Manners, I., Functional Block Copolymers: Nanostructured Materials with Emerging Applications. *Angew. Chem. Int. Ed.* **2012**, *51*, 7898-7921.

3. Chen, Z. Y.; Cui, H. G.; Hales, K.; Li, Z. B.; Qi, K.; Pochan, D. J.; Wooley, K. L., Unique Toroidal Morphology from Composition and Sequence Control of Triblock Copolymers. *J. Am. Chem. Soc.* **2005**, *127*, 8592-8593.

4. Thünemann, A. F.; Kubowicz, S.; von Berlepsch, H.; Möhwald, H., Two-Compartment Micellar Assemblies Obtained via Aqueous Self-Organization of Synthetic Polymer Building Blocks. *Langmuir* **2006**, *22*, 2506-2510.

5. Li, Z.; Kesselman, E.; Talmon, Y.; Hillmyer, MA. Lodge, TP., Multicompartment micelles from ABC miktoarm stars in water. *Science* **2004**, *306*, 98-101.

6. Cui, H. G.; Chen, Z. Y.; Zhong, S.; Wooley, K. L.; and Pochan, D. J., Block Copolymer Assembly via Kinetic Control. *Science* **2007**, *317*, 647-650.

7. Wang, X. S.; Guerin, G.; Wang, H.; Wang, Y. S.; Manners, I.; Winnik, M. A., Cylindrical Block Copolymer Micelles and Co-Micelles of Controlled Length and Architecture. *Science* **2007**, *317*, 644-647.

8. Dan, N.; Shimoni, K.; Pata, V.; Danino, D., Effect of Mixing on the Morphology of cylindrical Micelles. Langmuir 2006, 22, 9860-9865.

9. Jain, S.; Bates, F. S., Consequences of Nonergodicity in Aqueous Binary PEO-PB Micellar Dispersions. *Macromolecules* **2004**, *37*, 1511-1523.

Chapter 5. Specific Separation of Histidine-tagged Protein by Functionalized Polymer Cubosomes

5.1 Abstract

With the development of molecular biology, it is possible to artificially produce proteins with desired functions and properties. Therefore, researchers needed a simple method to selectively isolate desired proteins at high yield. Immobilized-Metal Affinity Chromatography (IMAC) is one of the easiest purification methods of protein. It is based on the interaction between metal ion immobilized on an insoluble matrix and specific side chain of amino acid. In this study, Ni-NTA functionalized polymer cubosome was synthesized and demonstrated to selectively immobilize and isolate histidine-tagged protein.

5.2 Introduction

Protein separation is indispensable step in the bioscience. In many ways, Metal Chelate Affinity Chromatography (MCAC) which utilizes selective affinities between transition metal ion (Co^{2+}, Ni^{2+}, Cu^{2+}, Zn^{2+}) and histidine-tagged protein has become a powerful tool for the single-step purification.[1-3] After Porath and co-worker demonstrated selective isolation of histidine-tagged protein using metal ion attached on agarose gel in 1975,[4] further research is being carried out to obtain more efficient results. Various types of substrate such as beads, nanoparticles, glass etc. have a great attention for immobilization, high loading capacity and easy separation.[5-9]

For example, Xu and coworkers synthesized magnetic nanoparticles with Ni-NTA on the surface to provide a large surface area and a method for easily separating proteins from cell debris without hassle.[9] The other way, Martin and coworker proposed a triazacyclononane (tacn)-ring-type Acbztacn ligand which stabilize the ligand-metal interactions by macrocyclic effect resulting from the tacn ring to reduce the limitations of NTA/metal/Histidine like metal leaching and protein dissociation.[10]

Self-assembly of amphiphilic block copolymers (BCPs) into inverse bicontinuous cubic (IBC) mesophases in dilute solution is emerging phenomenon.[11-15] Hereby, three-dimensionally well-defined periodic porous nanostructures consisting of the minimal surfaces are available as substrate consisting large surface area.

Recently, we reported that dendritic-linear PEG-*b*-PS BCPs preferentially self-assembled into IBC mesophases in dilute solution resulting the formation of colloidal particles and mesoporous film having the triply periodic minimal surfaces (TPMSs) of the BCP bilayer. [11-13] The TPMS surface of the BCP bilayer could be easily functionalized with desired surface functional groups through the co-assembly

of BCP and functionalized linear BCPs. Due to the presence of high molecular weight PSs as a hydrophobick block, these IBC structures of the BCPs were structurally robust under ambient conditions and these mesoporous structures were potentially useful for separation, catalyst and nanotemplating. Here, we report surface-functionalized polymer cubosomes were used to high performance materials for affinity-base separation of protein due to its large surface area.

5.3 Results and discussion

Co-assembly of bb-BCP and linear BCPs.

Self-assembly of BCP blends in solution is a facile way of creating nanostructures with the finely tuned structures, morphologies, and functions without synthesizing new BCPs. We used blends of bb-BCPs and linear BCPs having chemically identical structural units in both polymer blocks but differing architectures in the hydrophilic blocks for co-assembly into inverse mesophases in solution. The BCP blends for co-assembly in solution consisted of a bb-BCP as the major component (>90 wt%) and a BCP with a linear PEG hydrophilic block and the same block ratio as that of the major BCP as the minor component.

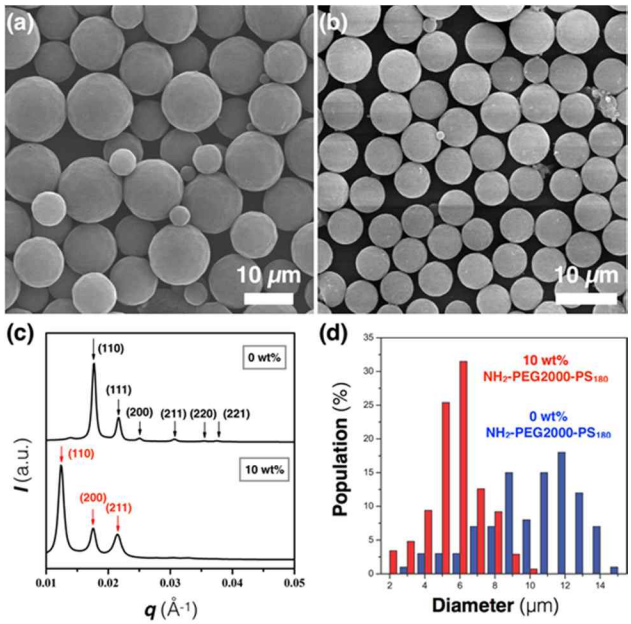

Figure 5-1. (a and b) Low magnification SEM images showing the polymer cubosomes of (a) PEG750$_3$-(3,4)-(PS$_{60}$)$_2$ and (b) the BCP blend of PEG750$_3$-(*3,4*)-(PS$_{60}$)$_2$ and NH$_2$-PEG2000-PS$_{180}$ (9:1 w/w). (c) SAXS results showing the phase transition from the D surface of PEG750$_3$-(*3,4*)-(PS$_{60}$)$_2$ (*Pn3m*, a =50.0 nm) to the P surface of the BCP blend (*Im3m*, a = 71.8 nm). (d) Distribution of the diameters of polymer cubosomes of PEG750$_3$-(*3,4*)-(PS$_{60}$)$_2$ (blue bars, average = 11 μm) and the BCP blend (red bars, average = 6 μm).

We self-assembled the BCP blend consisting of PEG750$_3$-(*3,4*)-(PS$_{60}$)$_2$ and NH$_2$-PEG2000-PS$_{180}$ (9:1 w/w) under our standard conditions. Compared with the average diameter of the polymer cubosomes of PEG750$_3$-(*3,4*)-(PS$_{60}$)$_2$ (11 μm, Figure 5-1a), the average diameter of the polymer cubosomes of the BCP blend decreased to 6 μm (Figure 5-1b and d). In addition, the linear PEG chains protruding from the surface of the bilayer of the BCP blend might lower the surface energy of the bilayer, which would cause the resulting bilayer to adopt a lattice having lower local curvature upon the formation of the inverse mesophases. The SAXS results for the dried polymer cubosomes of PEG750$_3$-(*3,4*)-(PS$_{60}$)$_2$ and its blends with NH$_2$-PEG2000-PS$_{180}$ exhibited a phase transition from the D surface (*Pn3m* symmetry, a = 50.0 nm) to the P surface (*Im3m* symmetry, a = 71.8 nm) when the weight fraction of the linear BCP in the BCP blend was increased to 10% (Figure 5-1c).

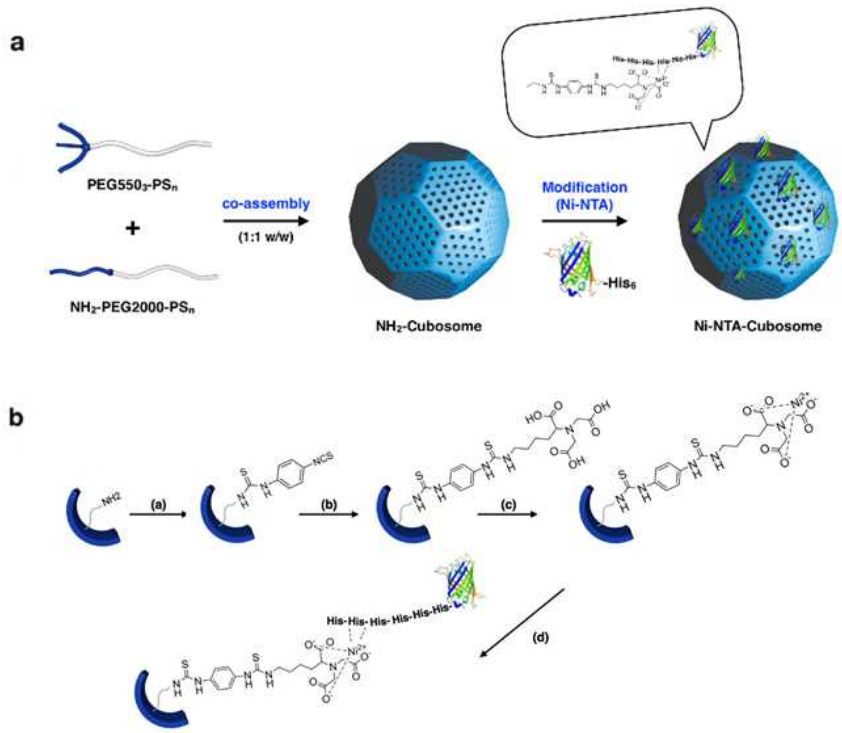

Scheme 5-1. (a) Schematic diagram of polymer cubosome formed by self-assembly of BCP blend consisting of PEG750$_3$-(*3,4*)-(PS$_{60}$)$_2$ and NH$_2$- PEG2000-PS$_{180}$ and its surface modification for specific adherence of histidine tagged proteins. (b) NTA layer addition and protein absorption of NH$_2$ functionalized polymer cubosome. (a) *p*-Phenylene diisothiocyanate, ethanol, 40 ℃. (b) N,N-bis(carboxymethyl)-L-lysine, water. (c) N,N-bis(carboxymethyl)-L-lysin, water. (d) 6xHis-GFP, PBS buffer.

Synthesis of Ni-NTA functionalized polymer cubosomes

The polymer cubosomes formed by self-assembly of the BCP blends possessed the desired functional groups throughout the surface of the TPMS of the bilayer forming the IBC mesophase. The presence of functional groups embedded within the mesoporous networks arranged in a 3-D crystalline order rendered the polymer cubosomes and monolithic films of the BCP blends attractive platforms for biochemical reactors, affinity-based separations, nanotemplating, and ultrafiltration. After confirming the presence of the surface amino groups throughout the surface of the polymer cubosomes of the BCP blend ($PEG750_3$-(*3,4*)-$(PS_{60})_2$/NH_2-PEG2000-PS_{180} (9:1 w/w)) by visualizing the surface amino groups labeled with fluorescamine using confocal laser scanning microscopy (CLSM) (Figure 2a), we introduced a Ni-NTA complex onto the surface of the polymer cubosomes of the BCP blend by reacting *N*-(5-amino-1-carboxypentyl)iminodiacetic acid with 1,4-phenylene diisothiocyanate as a linker (Scheme 5-1).[16] The introduced *N*-nitrilotriacetic acid (NTA) was complexed with $NiCl_2$ in water.

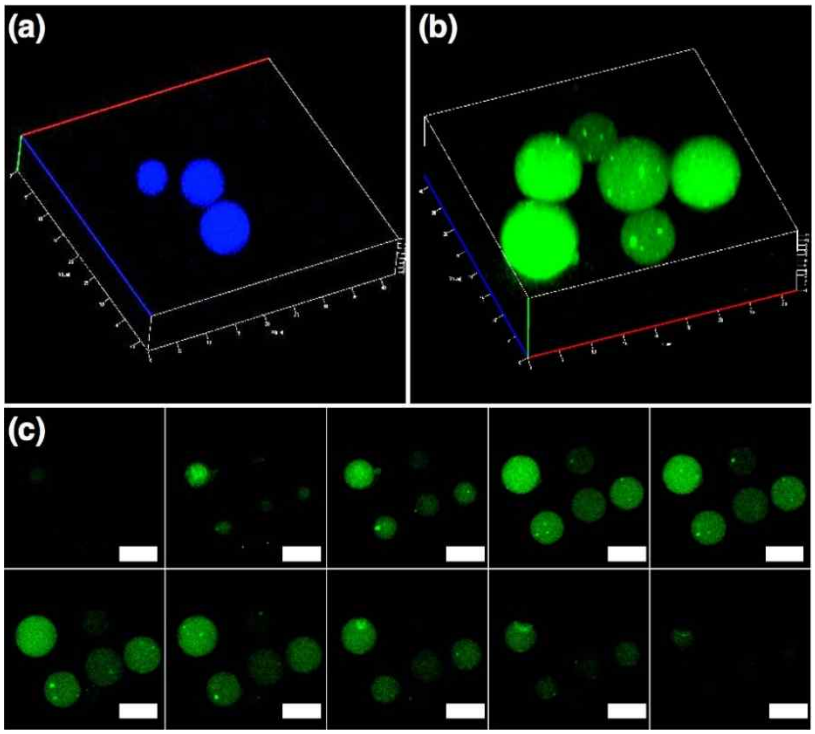

Figure 5-2. (a and b) 3-D reconstructed images of CLSM of (a)the polymer cubosomes of the BCP blend with the surface amino groups labeled by fluorescamine and (b) His-tagged GFP complexed Ni-NTA functionalized polymer cubosomes. (c) CLSM images of His-tagged GFP on the polymer cubosomes at different focal depths (each step: 0.8 μm, scale bar = 10 μm).

Immobilization and isolation of histidine-tagged protein

Utilizing the large surface area of the mesoporous water channel networks embedded within the polymer cubosomes, the Ni-NTA-functionalized polymer cubosomes were used as affinity-based separation materials for proteins by using His-tagged green fluorescent protein (GFP) as a model protein. The His-tagged GFPs readily formed complexes with the surface-bound Ni-NTAs within the water channel networks of the polymer cubosomes, which was visualized on CLSM (Figure 5-2b). The cross-sectional views of the polymer cubosomes clearly showed the internalized GFPs throughout the minimal surfaces of the polymer cubosomes (Figure 5-2c).

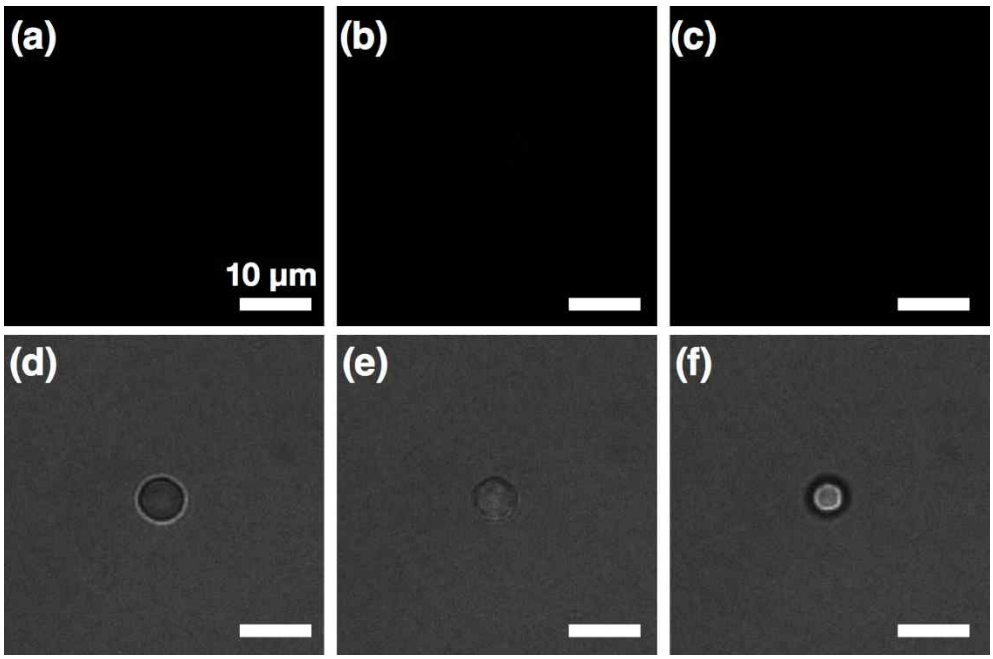

Figure 5-3. CLSM images of the polymer cubosomes after removing GFP different focal depths (each step: 2 μm, scale bar = 10 μm). (a-c) Fluorescence images and (d-f) merged images.

The complexed His-tagged GFPs could be completely recovered when the complexed polymer cubosomes were treated with imidazole (0.1 M in PBS), which is a competitive binding agent to Ni-NTA (Figure 5-3). This result indicated that external guest macromolecules could easily access the water channels of large diameters embedded in the polymer cubosomes, which makes the polymer cubosomes with functional groups throughout the entire surface promising materials for affinity-based separation of proteins and biopolymers

5.4 Summary

In summary, we used blends of bb-BCPs and functionalized linear BCPs having chemically identical structural units in both polymer blocks but differing architectures of BCPs for co-assembly into inverse mesophases in solution. By specific affinity with histidine-tagged protein, we demonstrated that Ni-NTA functionalized polymer cubosome can act as a useful substrate for selective separation of protein. This system should offer new application such as nanocatalyst, drug delivery.

5.5 Experimental

Methods. ^{1}H NMR spectra were recorded using CD_2Cl_2 as solvent on a Agilent 400-MR DD2 spectrometer. Molecular weights and weight distribution of block copolymers were measured by Agilent 1260 Infinity GPC system equipped with a PL gel 5 μm mixed D column (Agilent Technologies) and differential refractive index detectors. GPC measurements were carried out under THF as an eluent with a flow rate of 1 mL min-1 at 35 ºC and A PS standard (Agilent Technologies) was used for calibration. Before injection, the solution of polymer sample was filtered by using PTFE filter.

Scanning electron microscopy (SEM) images were obtained using Hitachi S-4800 FE SEM at an acceleration voltage of 10 kV. The samples were prepared by loading onto a conductive carbon tape and drying at room temperature and then coated with Pt by using a K575X Sputter Coater (20 mA, 60s). Transmission electron microscopy (TEM) images were obtained using a JEOL JEM-2100 microscope at 200 kV. Specimens were prepared by placing a drop of the solution on a carbon-coated Cu grid (200 mesh, EM science). After 30 min, remaining solution on a grid was removed with a filter paper, and the grid was air-dried overnight. Confocal laser scanning fluorescence microscopy (CLSM) was performed on a LSM710 Confocal Microscope (Carl Zeiss).

Synchrotron small angle X-ray scattering data were obtained on the SAXS beam line (PLS-II 6D) at Pohang acceleration laboratory (Pohang, Korea). The particle size distribution of polymer cubosomes was measured by analyzing SEM images of polymer cubosomes with ImageJ software. 300 particles were selected for the image analysis from SEM images taken from 5~10 different positions.

Polymer synthesis. Block copolymers used in this study were synthesized as previously reported. (in chapter 2,3).

Block copolymer of branched-branched PEG-*b*-PS was obtained through the Cu(Ⅰ)-catalyzed azide-alkyne click reaction between hydrophobic polymer module (PS-N3) and branched hydrophilic module ($PEG750_3$-(3,4)). Also, block copolymer of amine functionalized PEG-*b*-PS was obtained by using azide-alkyne click reaction between PEG-diazide and PS containing alkyne functionality, and then azide functionalized PEG-*b*-PS was converted to amines by Staudinger reaction.

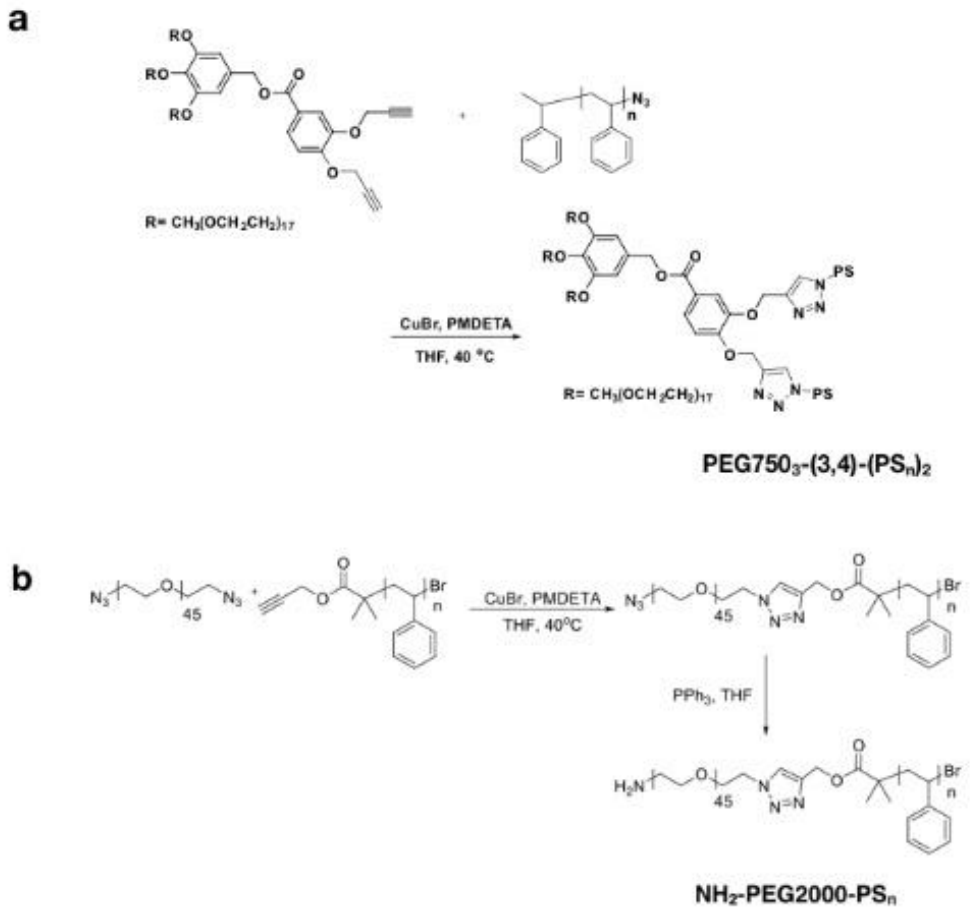

Scheme 5-2. Synthesis of bb-BCP and amine functionalized linear BCP.

Table 5-1. Characterization of block copolymers.

Sample	M_n (g mol^{-1}) [a]	$Đ$ [a]	DP_n (PS)	f_{PEG} (%) [c]
PEG750$_3$-(3,4)-(PS$_{60}$)$_2$	16110	1.04	60 [b]	18.0
NH$_2$-PEG2000-PS$_{1194}$	22000	1.09	1184 [d]	10.5

[a] The number average molecular weight and molecular weight distribution determined by GPC (THF, 35 °C, 1 mL min^{-1} flow rate) using PS standards. [b] The number average degree of polymerization of homo PS chains determined by GPC measurements. [c] The molecular weight ratio of the PEG domain to that of the PS block. (2000 g mol^{-1} for PEG$_{45}$-PS$_n$, and 2250 g mol^{-1} for 750$_3$-PS$_n$). [d] DP_n determined by ^{1}H NMR integration.

General procedure for self-assembly of block copolymers. The block copolymers was dissolved in 2 mL of 1,4-dioxane (1 wt%) in a capped vial, and the solution wes stirred for 3 h at room temperature. 2 mL of water was added at a controlled rate (1 mL h^{-1}) to the solution using a syringe pump with vigorous stirring (850 rpm). After self-assembly, the organic solvent in the resulting suspension was removed by dialysis (molecular weight cutoff (MWCO) = 12-14 kDa, SpectraPor) against water for 24 h.

Self-assembly of block copolymer blends. . Each of block copolymers was dissolved in 2 mL of 1,4-dioxane (1 wt%) in the capped vials, and the solutions were stirred for 3 h at room temperature. According to a ratio, each stock solution was added to the capped vial and the resulting solution of BCP mixture (total 20 mg / 2 mL, 1 wt%) was allowed to equilibrate for 24 h at room temperature. Water (total 2 mL) was added at a controlled rate (1 mL h^{-1}) to the solution via a syringe pump with vigorous stirring (850 rpm). The resulting suspension was dialyzed (molecular weight cutoff (MWCO) = 12-14 kDa, SpectraPor) against water for 24 h to remove the organic solvent.

Dye labeling of surface functional groups of polymer cubosomes. Polymer cubosomes (10 mg mL^{-1}, 750_3-(*3,4*)-$(PS_{60})_2$/NH_2-PEG2000-PS_{180}=90/10) in methanol were mixed with dye solution (Fluorescamine in methanol, 2000 eq. to NH_2 groups). The mixtures were incubated at room temperature for 1 day with shaking, and then transferred into the centrifugal tubes with a centrifugal filter (MWCO = 100 kDa, Amicon). The excess dyes were removed from the suspension through the repeated centrifugation.

NTA layer addition and protein absorption of surface functional groups of polymer cubosomes. Polymer cubosomes of $PEG750_3$-(*3,4*)-$(PS_{60})_2$/NH_2-PEG2000-PS_{180} (10% w/w) were prepared by the general procedure described above. The NH_2-functionalized polymer cubosomes were reacted with p-Phenylene diisothiocyanate in ethanol at 40 ℃ for 1 day. These NCS-polymer cubosomes were mixed with aqueous N,N-bis(carboxymethyl)-L-lysine solution (pH 8) for 6 hours at room temperature. Then these polymer cubosomes were incubated with aqueous $NiCl_2$ solution (pH 5) for 6 hours at room temperature. These NTA-polymer cubosomes were mixed with rGFP (Cell Biolabs, INC.) in a PBS buffer (pH 7.4) for 24 hours. In each step, the residual reagent was removed by repeated centrifugation and dilution with same solvent.

5.6 Reference

1. Gaberc-Porekar, V.; Menart, V., Perspectives of immobilized-metal affinity chromatography. *J. Biochem. Biophys. Methods* **2001**, *49*, 335–360.

2. Porath. J., Immobilized Metal Ion Affinity Chromatography. *Protein Expr Purif.* **1992**, *3*, 263-281.

3. Mitchell, D. M.; Gennis, R. B., Rapid purification of wildtype and mutant cytochrome c oxidase from *Rhodobacter sphaeroides* by Ni^{2+}-NTA affinity chromatograph. *FEBS Letters* **1995**, *368*, 148-150.

4. Porath, J.; Carlsson, I.; Olsson, I.; Belfrage, G., Metal chelate affinity chromatography, a new approach to protein fractionation. *Nature* **1975**, *258*, 598-599.

5. Bornhorst, J. A.; Falke, J. J., Purification of Proteins Using Polyhistidine Affinity Tags. *Methods Enwymol.* **2000**, *326*, 245-254.

6. Allen, T. Y. L.; Tan, H. Y.; Bianco, P. R., Advanced uses of IMAC Affinity Chromatography. *Austin Chromatogr.* **2016**, *3*, 1042.

7. Lauer, S. A.; Nolan, J. P., Development and Characterization of Ni-NTA−Bearing Microspheres. *Cytometry* **2002**, *48*, 136-145.

8. Vahidi, A. K.; Yang, Y.;Ngo, P. N.; Li, Z., Simple and Efficient Immobilization of Extracellular His-Tagged Enzyme Directly from Cell Culture Supernatant As Active and Recyclable Nanobiocatalyst: High-Performance Production of Biodiesel from Waste Grease. *ACS Catal.* **2015**, *5*, 3157-3161.

9. Xu, C.; Xu, K.; Gu, H.; Zhong, X.; Guo, Z.; Zheng, R.; Zhang, X.; Xu, B., Nitrilotriacetic Acid-Modified Magnetic Nanoparticles as a General Agent to Bind Histidine-Tagged Proteins. *J. Am. Chem. Soc.* **2004**, 12*6*, 3392-3393.

10. Johnsom, D, L.; Martin, L, L., Controlling Protein Orientation at Interfaces Using Histidine Tags: An Alternative to Ni/NTA. *J. Am. Chem. Soc.* **2005**, *127*, 2018-2019.

11. La, Y.; Park, C.; Shin, T. J.; Joo, S. H.; Kang, S.; Kim, K. T., Colloidal inverse bicontinuous cubic membranes of block copolymers with tunable surface functional groups. *Nat. Chem.* **2014**, *6*, 534−541.

12. An, T. H.; La, Y.; Cho, A.; Jeong, M. G.; Shin, T. J.; Park, C.; Kim, K. T. Solution self-assembly of block copolymers containing a branched hydrophilic block into inverse bicontinuous cubic

mesophases. *ACS Nano* **2015**, *9*, 3084−3096.

13. Park, C.; La, Y.; An, T. H.; Jeong, H. Y.; Kang, S.; Joo, S. H.; Ahn, H.; Shin, T. J.; Kim, K. T. Mesoporous Monoliths of Inverse Bicontinuous Cubic Phases of Block Copolymer Bilayers. *Nat. Commun.* **2015**, *6*, 6392.

14. Yu, H.; Qiu, X.; Nunes, S. P.; Peinemann, K. V., Biomimetic block copolymer particles with gated nanopores and ultrahigh protein sorption capacity. *Nat. Commun.* **2014**, *5*, 4110.

15. Lin, Z.; Liu, S.; Mao, W.; Tian, H.; Wang, N.; Zhang, N.; Tian, F.; Han, L.; Feng, X.; Mai, Y., Tunable Self-Assembly of Diblock Copolymers into Colloidal Particles with Triply Periodic Minimal Surfaces. *Angew. Chem.* **2017**, *129*, 7241-1246.

16. Maury, P.; Escalante, M.; Péter, M.; Reinhoudt, D. N.; Subramaniam, V.; Huskens, Creating Nanopatterns of His-Tagged Proteins on Surfaces by Nanoimprint Lithography Using Specific NiNTA-Histidine Interactions. J. *Small.* **2007**, *3*, 1584-1592.